University of Alberta

Comparative Histology of Burned Mammals Using Light Microscopy:
Examining Heat-Induced Changes in Femoral Samples of Deer, Pig and Cow.

by

Kalyna Horocholyn

A thesis submitted to the Faculty of Graduate Studies and Research in partial fulfillment of the requirements for the degree of

Master of Arts

Department of Anthropology

Fall, 2013

Edmonton, Alberta

Abstract

This study focuses on the histological comparisons between deer, pig and cow. Five femoral specimens from each species were selected and burned at 600^{o}C, 800^{o}C and 1000^{o}C. Burned and unburned control samples were thin-sectioned for light microscopic analysis. Visibility of histological structures in burned samples was reduced due to carbonization. Limitations in visible cortical areas resulted in biased sampling selections and smaller sample sizes. Quantitative analysis showed evidence of deer Haversian structures being the smallest and cow Haversian structures being the largest of the samples studied. Statistical analysis demonstrated changes in osteon dimensions of pig and cow samples at 800^{o}C and 1000^{o}C. The contraction of osteons in pig burned samples at these two temperatures led to pig osteon dimensions being similar to those of deer osteons at 800^{o}C and 1000^{o}C. This result suggests that species differentiation may be difficult to conduct on burned specimens above 600^{o}C.

Acknowledgements

I would like to thank my supervisor, Pamela Mayne Correia, for suggesting the scope of this thesis project, for all of the help she has provided me in processing and analyzing the specimens, and for guiding me in my growth as a graduate student. I would like to thank my co-supervisor, Sandra Garvie-Lok, for helping in the statistical analysis of the data presented in this study, as well as the patience and support during the application for ethics approval and the writing process. I am grateful to Harvey Friebe, Director of Labs, for allowing me access to all of the necessary laboratory facilities at the University of Alberta and for his generosity in helping prepare and analyze specimens.

A special thank-you must be given to the owner of Parkland Packers, Hermann Knupp, for his generous donation of pig and cow specimens, as well as to Samantha Stamler and Margot Pybus from the Alberta Sustainable Resource Development, Fish and Wildlife Division, for their generous donation of deer specimens. I am indebted to the University of Alberta for funding my graduate studies, and for the Government of Alberta for providing me with additional financial support.

Finally, I would like to thank my parents, Lydia and Rick Horocholyn, for all of their love and encouragement in getting to this place in my life. To my mother – thank you for introducing me to bioanthropology all those years ago. To my father – thank you for finding all of my schooling and studies fascinating, even when I haven't. And to my loving partner, Katherine, for your patience and encouragement throughout this project - I couldn't have done this without you.

Table of Contents

List of Tables

List of Figures

Chapter 1 - Introduction

In all aspects of archaeology and biological anthropology, the presence of faunal material in human contexts sheds light on the complex relationship humans share with animals. The positive identification of human remains is one of the key tasks most osteologists face in the field, either in order to reconstruct human-animal contact in archaeological populations or to establish the need for a potential police investigation through forensic analysis. The recovery of human and faunal material can be complicated when the skeletal material is fragmented and commingled. Histological analysis is one aspect in which researchers can successfully differentiate between human and faunal origins for fragmented skeletal material using metric analysis or observing contrasting qualitative characteristics of the bone tissue.

A substantial literature exists on the histological differentiation of medium-large sized mammals (Urbanová and Novotný, 2005; Martiniaková et al, 2006a; 2006b; 2007; Morris, 2007) including humans (Mulhern and Ubelaker, 2001; 2011; Owsley et al, 1985; Hillier and Bell, 2007), but more research is necessary to confirm that these techniques can be applied to burned remains.

Burned bone is a common find in archaeological sites and in forensic cases. A crucial step in studying any of these contexts is distinguishing between the physical remains of burned animals and humans. Very little research has yet been done in applying these histological techniques in differentiating fragmented skeletal material affected by extreme exposure to heat. The gross morphometric effects of heat on bone have been studied extensively, but there have been few comparative studies done to determine whether the deformation of bone due to fire will

impact histological structure. As a result, it is unclear whether these same histological examinations can be applied to fire-damaged material.

This study examined unburned and burned bone material from three contemporary medium-large sized mammals, deer, pig and cow. Previous research has already proven that histological features in burned human and non-human remains are visible under light microscopic analysis at temperatures below the critical point (700-800^{o}C), and electron microscopy has shown visibility at temperatures exceeding 1000^{o}C. It is predicted, therefore, that histological structures will be visible at all three examined temperatures, allowing for qualitative analysis in the burned samples. As well, it is hypothesized that Haversian dimensions will be distorted as a result of heat, especially in temperatures exceeding the critical point.

The information gathered by pursuing both of these questions will assist in identifying bone samples that are no longer usable for histological examination, helping researchers choose the best methods for their work.

Chapter 2 of this thesis is an overview of the literature background on histological analysis and the examination of burned skeletal material as they apply to archaeology and forensic anthropology. Topics include qualitative differentiation between human and non-human mammals, metric analysis on histological features, the impact of heat on the gross morphology of skeletal material, and the histological analysis of burned material.

Chapter 3 outlines the selection of materials for this experiment and the subsequent procedures and analysis performed for the methodology. Chapter 4 presents the results of the experiment, with digital images depicting the various histological structures observed in the samples, as well as graphical and statistical analysis of the measurements conducted. Chapter 5

discusses the findings of the experiment and addresses the problems and unexpected outcomes in performing this experiment. Chapter 6 highlights the important conclusions drawn from this research and outlines research questions that can be pursued in future studies.

Chapter 2 - Literature Review

The aim of this research is to explore the application of light microscopy in the overlap of two important areas of anthropological studies: histological determination of human and origin, and the examination of heat-induced changes in burned skeletal material. The investigation of histological changes in burned non-human material undertaken in this study is built upon previous literature, which will be discussed in this chapter.

2.1 Background to Histology

Histology in its broad definition refers to the microscopic analysis of organic tissue. In anatomy, much of the focus is on examining the organization of four different classifications of tissues (nervous, connective, epithelial and muscle) and the way these tissues come together to form organs (Junqueira and Carneiro, 2005). In anthropology, however, the scope of histological analysis is much narrower as only skeletal tissue is examined.

Bone plays multiple roles in mammalian anatomy. The robusticity of skeletal material allows bone to act as an anchorage point for muscular activity, as well as a protective shield around internal organs. In addition to protecting organs, bone is also an organ in itself, harbouring bone marrow where the critical production of red and white blood cells occurs. Bone is used as a reservoir for crucial ions such as calcium and phosphate (Junquiera and Carneiro, 2005). As a connective tissue, bone has the ability to provide researchers with important information about an individual's health and development at a molecular level. This ability is increased in comparison with other connective tissues due to the mineralization of bone, allowing bone to preserve for much longer periods of time. This preservation in turn increases the scope of material available for histological analysis; while other soft tissues must be

intentionally preserved, the high inorganic content makes bone ideal to examine under a range of conditions that would destroy other types of tissue. This allows osteological analysis to contribute to such diverse fields as evolutionary biology, forensic science, and archaeology.

Bone is composed similarly across mammals at a microscopic level. The aforementioned inorganic material, hydroxyapatite [$Ca_{10}(PO_4)_6(OH)_2$], makes up almost two-thirds of the content of bone. The remainder of bone is composed of organic collagen. The strands of collagen act as the framework around which hydroxyapatite crystals form in plate-like layers (Martini et al, 2008). This fusion creates the rigid yet flexible nature exhibited by bone.

There are three main cell types that are responsible for the development and maintenance of bone tissue. Two of the chief cells, osteoblasts and osteoclasts, work together as a Basic Multicellular Unit (BMU) (Frost, 1966) to balance to action of bone deposition and resorption during bone remodelling. Osteoclasts secrete acids that dissolve the uncalcified bony matrix (osteoid) through the exocytosis of lysosomes (Martini et al, 2008). This causes the resorption of bone material by releasing stored calcium and phosphate, as well as amino acids. While removing cortical bone, the osteoclasts create a "cutting cone" or a cavity in the direction of the mechanical strain. These cutting cones can be visible under a microscope, taking on the appearance of a valley of receding bone. Once resorption is complete, osteoclasts undergo apoptosis (cell death).

Osteoblasts secrete the uncalcified osteoid which then mineralizes ten days after deposition with the addition of calcium phosphate crystals (Stout and Crowder, 2011). After deposition, the osteoblasts either undergo apoptosis or become trapped in the bony matrix and develop into osteocytes. Osteocytes, the third type of cell, "maintain and monitor the protein and mineral

content of the surrounding matrix" (Martini et al, 2008), communicating with each other through the canaliculi to coordinate BMU responses to external stimuli.

There are two bone tissue types that can be discerned through histological analysis. Woven or immature bone is composed of collagen strands in a disorganized array. Woven bone at microscopic levels appears coarse and fibrous, and has a higher concentration of osteocytes than mature bone (White and Folkens, 2005). Woven bone is found during early embryological stages of bone development and is present at sites of injury as a 'first response' to mending damaged skeletal tissue.

The more prevalent form of bone tissue is lamellar, or mature, bone. Lamellar bone is composed of orderly layers of collagen fibres and forms through appositional growth (White and Folkens, 2005), creating a more reinforced structure as compared to the weaker woven bone. In turn, lamellar bone can be divided into two categories of bone based on means of the diffusion of nutrients and blood. Trabecular (spongy or cancellous) bone tissue is found more internally and has a very porous appearance due to the scattered nature of the trabeculae, or thin spicules, that make up the bony network (Martini et al, 2008). The interconnected spaces between trabeculae house marrow as well as blood vessels that nourish the bone.

Compact (or cortical) bone, on the other hand, is very dense and robust. This being the case, blood supply must be organized differently than in trabecular bone. Instead, concentric lamellar bone centres around a Haversian canal which acts as a tunnel through which blood and nerve fibres can be supplied to the bone. Haversian canals are linked to one another through Volkmann's canals which run perpendicular to Haversian canals. This linkage allows the osteons to communicate with the exterior through the periosteum, and interiorly with the

medullary cavity through the endosteum. These two membranous layers act as sheaths around cortical bone where osteoprogenitor cells reside, developing into osteoblasts when needed close to the site of bone remodelling (Junquiera and Carneiro, 2005).

The Haversian canal and associated concentric lamellae make up a complex which is known as a Haversian system or an osteon (Fig. 2.1). In histological cross-section, the Haversian system can be described as similar to tree rings circulating outwards from a central canal. It is this morphology on which the histological analysis depends, and it is the primary source used in this research for generating data. In between the concentric lamellar layers are small cavities called lacunae in which osteocytes reside. These lacunae are in turn connected to each other through canaliculi, allowing direct networking between osteocytes to coordinate the BMU's actions in bone remodelling and maintenance. The bony matrix between Haversian systems is occupied by interstitial lamellae. The outer circumferential lamellar layer inhabits the space between the periosteum surrounding the cortical bone and the outer rim of the field of osteons, while an inner circumferential lamellar layer occupies the area between the osteons and the endosteum connecting to the internal medullary cavity.

The appearance of the cortical structures and the organization of the Haversian systems vary between mammalian groups. These differences permit us to distinguish between species under normal circumstances either through visual analysis or by measuring the dimensions of structures.

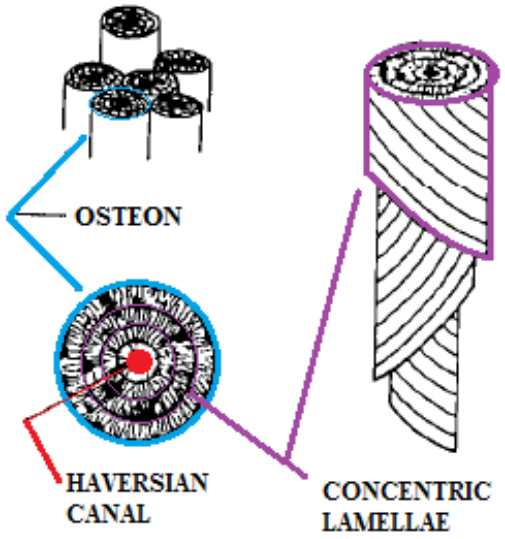

Figure 2.1 – Structure of a Haversian system (osteon) and its components. (Adapted from Cowin et al, 1983)

2.2 Histology for Species Identification

2.2.1 Qualitative Analysis

The three animals selected for this research all belong to the Order Artiodactyla and share similar bone structures, namely primary plexiform bone (Fig. 2.2), as an identifying feature. This similarity was described by Enlow and Brown (1956, 1957, 1958) in their extensive study of vertebrate histology. According to their classification of bone structures, plexiform bone appears as the layering of rectangular primary vascular canals (also called primary osteons) in a well-organized network known as a plexus (Enlow and Brown, 1956; 1958). These rectangular sections are layered in a horizontal direction (Mulhern and Ubelaker, 2001). Plexiform bone is typically cited as a form of bone structure that is indicative of non-human origin, but it is not prevalent in all non-human groups, and can occasionally occur in rapidly growing human infants and children (Enlow and Brown, 1956; Enlow and Brown, 1958; Enlow 1963; Cuijpers, 2009), so its usage in species verification must be in conjunction with other features and it should not be relied upon in isolation.

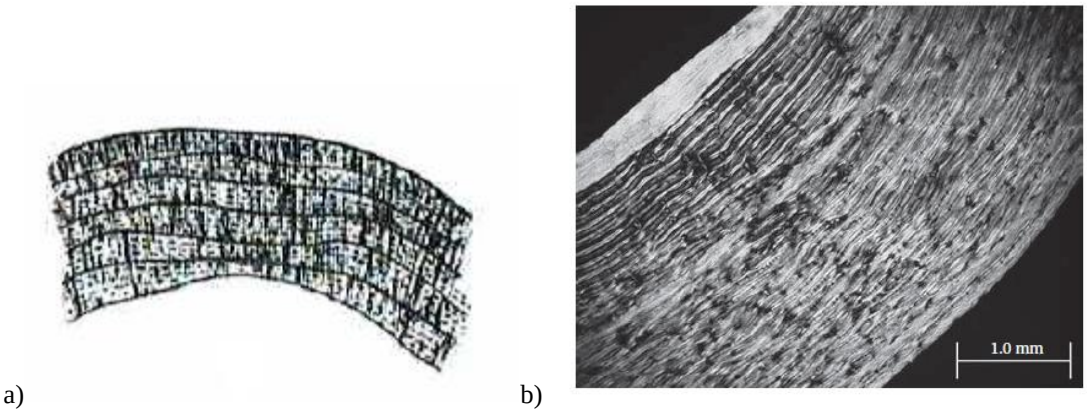

Figure 2.2 – a) Schematic outline of plexiform bone structure as outlined in Enlow and Brown (1956: 411)
b) Plexiform structure as present in a deer femoral section at 40x magnification. (Mulhern and Ubelaker, 2011. Photo credit: Crowder and Dominguez.)

Artiodactyls typically have plexiform structures forming the bulk of the compact bone, while older individuals may display scattered secondary osteons (Fig. 2.3a); these Haversian systems, however, are few in number throughout the plexiform layers. The area near the endosteum of the bone is often dense Haversian bone which is characterized by a greater concentration of Haversian systems frequently superimposing previous generations of osteons (Fig. 2.3b). The density of the secondary osteons results in reduction or absence of interstitial lamellae (Enlow and Brown, 1956).

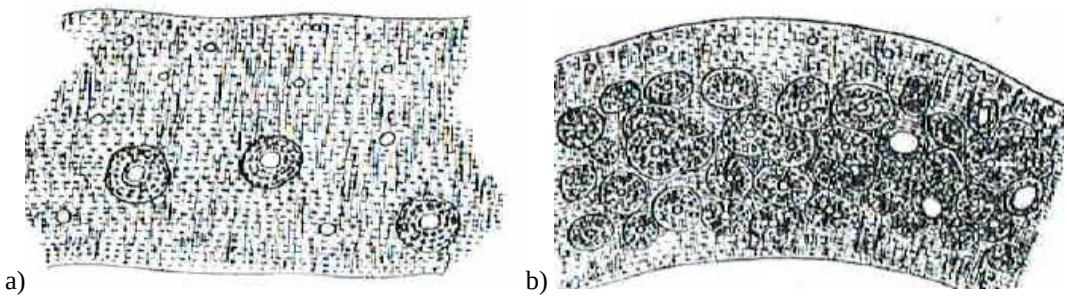

Figure 2.3 – a) Schematic diagram of scattered osteons in irregular Haversian bone.
b) Schematic diagram of densely-packed osteons in dense Haversian bone. (Enlow and Brown, 1956: 413)

As can be expected, there are still structural differences between artiodactyls. Hillier and Bell (2007) succinctly summarize the typical pattern of deer as plexiform bone originating near the periosteal surface while Haversian structures extend from the endosteal edge. Immature cervids predominantly display plexiform bone, while mature individuals have a higher proportion of dense Haversian structures, indicating that Haversian bone replaces plexiform structures throughout growth and aging. Besides plexiform bone with few secondary osteons and few interstitial lamellae (Owsley et al, 1985; Foote, 1916), deer also display primary vascular reticular bone (Singh et al, 1974), an absence of inner and outer circumferential lamellae (Singh et al, 1974) and osteon banding (Morris, 2007). The primary vascular reticular bone found in reindeer (Fig. 2.4; Singh et al, 1974) is bone with irregular and disorganized primary vascular canals (Enlow and Brown, 1956). Osteon banding, as found in the femur and humeri of white-tailed deer (Morris, 2007), is described as a "distinct row of five or more primary and/or secondary osteons" (Mulhern and Ubelaker, 2001: 221). Unfortunately, the majority of studies done on cervids (Table 2.1) lack consensus on which species to focus on, resulting in the possibility of potentially conflating histological features across species.

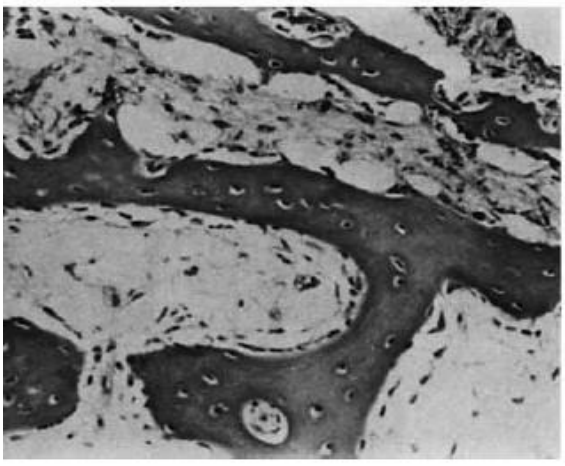

Figure 2.4 – Decalcified section of a reindeer rib displaying primary vascular reticular bone at 256x magnification. (Singh et al, 1974: 428)

Table 2.1 – Qualitative descriptions of the histological morphology of histological features in several deer (Family Cervidae) taxa according to previous literature.

Species	Bone	Description	Source
Mule deer (*Odocoileus hemionus*) Reindeer (*Rangifer tarandus*) Elk (*Cervus canadensis)*	Femur	- mostly composed of plexiform with few Haversian systems	Foote (1916)
Reindeer (*Rangifer tarandus*)	Long bones, ribs	- primary vascular (non-Haversian) reticular bone - neither inner nor outer circumferential lamellae	Singh et al (1974)
Unidentified cervid*	Humerus	- plexiform bone; primary osteons with few interstitial lamellae	Owsley et al (1985)
Rocky Mountain mule deer (*Odocoileus hemionus*)	Forearm (metacarpal, radius, humerus)	- plexiform with incompletely remodeled secondary osteons occupying 30% of mid-diaphyseal cortex	Skedros et al (2003)
White-tailed deer (*Odocoileus virginianus*)	Long bones	- dense Haversian bone - small Haversian canal diameter and low osteon density compared to other mammals of relative size	Hillier and Bell (2007)
White-tailed deer (*Odocoileus virginianus*)	Femur, humerus, rib	- plexiform present in all femora, 2/3 of humeri, and 1/6 ribs - osteon banding found in 66.7% of femora and 33.3% of humeri	Morris (2007)
Red deer (*Cervus elaphus*)	Antler	- similar to lamellar bone in appearance - uniform longitudinal orientation of osteons, in contrast to bone osteons which may be either transversely or diagonally oriented - smaller osteons than seen in bone	Paral et al (2007)

* The publication fails to identify the species of deer used in this study.

Research on the bone structures in domestic pigs (Table 2.2) confirmed the artiodactyl pattern of predominantly plexiform bone (Fig. 2.5) with few scattered secondary osteons. The compact bone is made up of dense Haversian structures (Foote, 1916; Martiniaková et al, 2006a; Martiniaková et al, 2006b), and osteon banding is present in roughly half of the specimens analyzed (Mulhern and Ubelaker, 2001; Morris, 2007; Cuijpers, 2009). A feature that is unique to domestic pigs is the presence of resorption lacunae (Fig. 2.6) found in the spaces between Haversian systems (Martiniaková et al, 2006a; Martiniaková et al, 2006b). These lacunae, housing osteocytes, indicate that pigs have a higher turnover rate of bone development compared to other artiodactyls (Martianikova et al, 2006b). However, Hillier and Bell (2007) include pigs and cows in the same category as humans based on the similar appearance of dense Haversian bone (Fig. 2.7), stressing the importance of these other features, especially plexiform bone and osteon banding, in reliably differentiating pig bones from human bones.

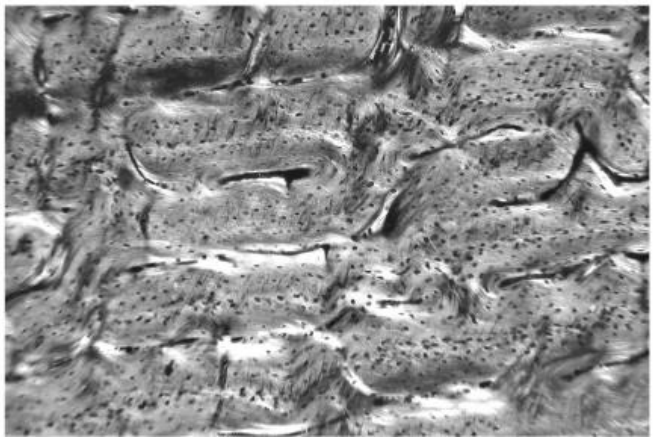

Figure 2.5 – Plexiform structures as found in a cross-section of a pig tibia. (Cuijpers, 2009: 82)

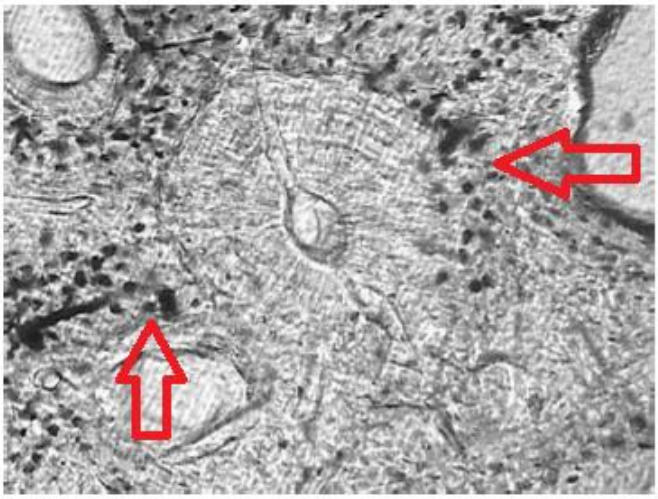

Figure 2.6 – Resorption lacunae (red arrows) surrounding an osteon in a pig femur at 200x magnification. (Martiniaková et al, 2006a: 168)

Figure 2.7 – Display of dense Haversian bone found in a pig femur at 200x magnification. (Martiniaková et al, 2006a: 169)

Table 2.2 – Qualitative descriptions of the histological morphology of bone structures in domestic pig (*Sus scrofa domesticus*) according to previous literature.

Bone	Description	Source
Femur	- predominantly plexiform structure with dense clusters of secondary osteons in posterior aspects	Foote (1916)
Long bone, Rib	- primary plexiform with few scattered secondary osteons in older individuals	Enlow & Brown (1958)
Femur	- 4 out of 6 specimens displayed osteon banding - widespread plexiform structures	Mulhern & Ubelaker (2001)

Femur	- primary vascular plexiform and dense Haversian bone - resorption lacunae between secondary osteons	Martiniaková et al (2006a)
Femur	- primary vascular plexiform, and dense Haversian bone - resorption lacunae between secondary osteons	Martiniaková et al (2006b)
Femur	- primary vascular laminar and plexiform bone - resorption lacunae between secondary osteons	Martiniaková et al (2007)
Femur, Humerus, Rib	- 100% of femora and 75% of humeri display plexiform bone (0% of ribs) - 50% of femora display osteon banding	Morris (2007)
Femur (and other long bones)	- presence of primary fibrous bone with primary osteons in the form of plexiform, reticular and laminar organization - arrangements of scattered and dense osteons	Cuijpers (2009)
Femur	- low number of lamellae and osteocytes visible - moderate amount of interstitial lamellae	Castrogiovanni et al (2011)

Domestic cattle (Table 2.3) likewise display the same artiodactyl features of primary vascular plexiform bone with few scattered secondary osteons (Fig. 2.8). The middle of the cortex contains dense Haversian structures (Enlow and Brown, 1958; Martiniaková et al, 2006a; Martiniaková et al, 2007), while the endosteal and periosteal layers house non-vascular bone (Martiniaková et al, 2006a; Cuijpers, 2006; Martiniaková et al, 2006b; Martiniaková et al, 2007) which is unique to bovids (Fig. 2.9). This histological type is characterized by concentric lamellae absent of vascular canals (Enlow and Brown, 1956).

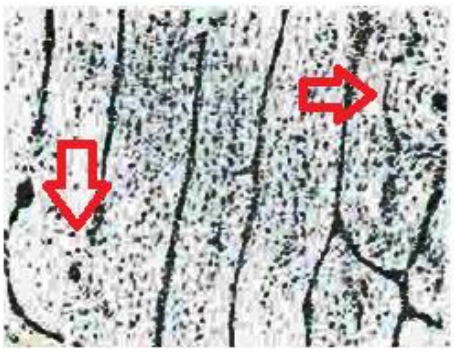

Figure 2.8 – Primary vascular plexiform bone with scattered osteons present (red arrows) in a bovid humerus. (Enlow and Brown, 1958: 211)

a)

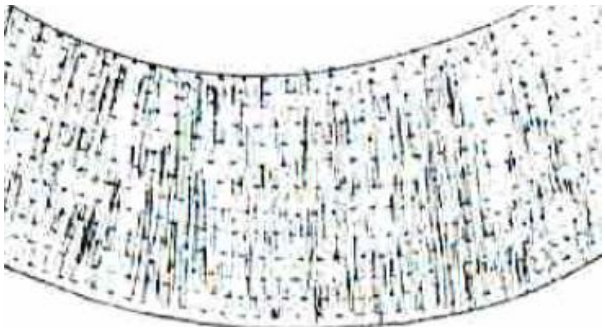

b)

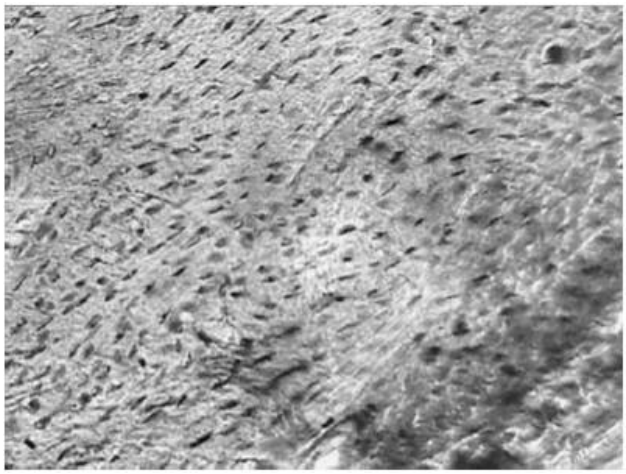

Figure 2.9 – a) Schematic diagram of non-vascular bone (Enlow and Brown, 1956: 411).
b) Example of non-vascular bone as seen in a cow femur at 200x magnification. (Martiniaková et al, 2007: 85)

In studies differentiating cow bone from horse, Cuijpers (2006) and Cuijpers and Lauwerier (2008) described the fibro-lamellar bone type in cows as being more fibrous than in horses which had a more predominant lamellar component to the same structure type. Fibro-lamellar compact bone is defined as a complex of fibrous (woven) matrix of periosteal origin mixed with deposited lamellar matrix (Francillon-Viellot et al, 1989). The lamellar matrix creates primary osteons which densely vascularize the woven bone. This shows the variability of structure types in terms both of type of deposition and type of vascularization (Francillon-Viellot et al, 1989).

Table 2.3 – Qualitative descriptions of the histological morphology of bone structures in domestic cow (*Bos taurus domesticus*) according to previous literature.

Bone	Description	Source
Long bone, Rib	- primary plexiform bone with some scattered secondary osteons - dense Haversian bone present in cortex of ribs	Enlow & Brown (1958)
Femur	- non-vascular bone present around medullary cavity with concentric lamellae and osteocytes - dense Haversian structures in mid-cortex - primary vascular plexiform bone with primary osteons found near periosteum	Martiniaková et al (2006a)
Femur	- primary lamellar non-vascular bone - reticular and plexiform with primary osteons - scattered secondary osteons with little to no organization - longitudinal and reticular Haversian canals	Cuijpers (2006)
Femur	- primary vascular plexiform - non-vascular bone at endosteal and periosteal borders	Martiniaková et al (2006b)
Femur	- primary vascular plexiform - non-vascular bone at endosteal and periosteal borders - middle of cortex housed irregular and/or dense Haversian structures	Martiniaková et al (2007)
Diaphyses of long bones (Femur, Tibia, Metatarsus, Metacarpus, Radius)	- fibrous fibro-lamellar bone complex	Cuijpers & Lauwerier (2008)
Femur, Humerus	- elliptically-shaped osteons that are irregularly scattered-vascular canals irregularly arranged longitudinally or slightly obliquely	Zedda et al (2008)
Femur	- homogenous appearance of bone with few borders between adjacent lamellae visible	Castrogiovanni et al (2011)

2.2.2 Quantitative Analysis

The study of histomorphometry, the metric analysis of histological structures, has taken two primary trajectories since Amprino (1947) first measured bone structures of various animals through microradiography. His results demonstrated a relationship between types of bone structure and growth dynamics, opening a new field of comprehension in the study of bone histology in mammals. This relationship showed how structure formation is a result of the growth rate experienced in different animals. Subsequent studies by Currey (1964), Kerley (1965) and Jowsey (1966) adopted his methodology to the measurement of the correlations

between osteon dimensions and age in human specimens. Other studies have instead taken the preliminary interspecies comparisons made by Amprino and expanded them to explore the prospect of differentiating mammalian taxa based on histological structures. The goal of these latter studies has been to determine methods for differentiating human (see Mulhern and Ubelaker, 2011 for summary of human standards) from non-human mammalian fragments which can be applicable either in archaeological studies or in forensic cases where other identification techniques are unavailable.

The majority of this research has been conducted by analyzing the dimensions of secondary osteons and Haversian canals, though a few studies have been innovative in examining other metric variables such as osteon circularity or primary vascular canal dimensions (eg. Crescimanno and Stout, 2011; Martiniaková et al, 2006a). The bone samples used in these studies have come from major long bones that undergo biomechanical stresses (eg. femur, tibia, humerus) or elementa that help support the body against gravity (eg. ribs). Most of these measurements can be done only on bone samples that display sufficient Haversian bone. With plexiform bone being the most prevalent structure type in artiodactyl elements, this may be difficult to undertake, and this limitation of quantitative analysis is acknowledged in these comparative studies. Tables outlining the relevant results of histomorphometric analysis on deer (Table 2.4), pig (Table 2.5) and cow (Table 2.6) histological parameters will be provided at the end of section 2.2.2

Jowsey (1966) elaborated on the initial studies done by Amprino (1947) by examining age-related changes in human osteons as well as in other animal groups (rat, rabbit, dog, cat, Rhesus monkey, human, cow, and two extinct pre-mammalian forms). She (Jowsey, 1966) measured the perimeters of secondary osteons and Haversian canals, and the cortical thickness of

the rib and femoral samples. Her cross-comparative results showed that cows had the largest dimensions for both osteons and Haversian canals. Humans had slightly smaller perimeters than cows and the other large groups, though the standard deviations of all four taxa overlapped. The rest of the animals followed the similar pattern of having smaller perimeters correlated with smaller body sizes. It is interesting to note, though, that animals larger than 10kg have relatively constant values, indicating that the rate of body size to osteon dimensions stabilizes after a certain body size.

Owsley and his associates (1985) used metric and morphological differences in deer and human bone structures as a way to positively identify the suspected remains of a woman in a forensic investigation. A deer humerus was examined for cortical thickness, and microsections were taken to determine the osteon density (per mm^2) and diameter of Haversian canals (Table 2.4). These results were compared with measurements taken from known elements of the deceased individual and the unknown fragments found. The values for the three criteria in the unknown specimen fell more closely within the range displayed by the known human remains. The osteon density of the deer bone was much greater than those found in the known human specimen, but the mean and minimum diameter of its Haversian canals were found to be less than in the human. The maximum diameter of deer Haversian canals, though, was found to overlap with both the known and unknown human fragments. Owsley and his collaborators noted the importance of identifying plexiform bone as a means of ruling out potential human origin in unknown fragments, stressing the necessity of examining the qualitative morphology of histological bone alongside the histomorphometric aspects.

Albu and associates (1990) processed diaphyseal sections of femora from dog, pig, cow and horse to examine the dimensions of Haversian canals. The density of Haversian canals per

square millimetre was determined in three separate layers of the cortical bone, with minimum, maximum and mean densities calculated. They found that dog had the greatest canal density throughout all layers, doubling the values present in cow sample which had the least dense spread. Pig and horse were found to be intermediate between dog and cow for canal densities.

The means of minimum, maximum and average Haversian canal diameters were recorded. Although they had the lowest mean for minimum canal diameter, dog samples displayed the largest spread of average diameters. Cow had the highest means for all three diameter values, and the second-highest range of diameters. Horse had the second largest diameter values, but pig had the smallest difference in diameter spread, suggesting a consistent precision in the diameters of Haversian canals. This led to pig having the overall smallest values in maximum and average canal diameters.

A study performed by Urbanová and Novotný (2005) examined a selection of femora and tibiae from wild and domesticated animals common in Europe. From measurements for the diameters, areas, and perimeters of Haversian canals and osteons, as well as osteon density, the non-human samples were split into four groups to compare to the values collected from human samples. Two cervid species, roe deer and red deer, and domestic pig and domestic cow were included in the non-human samples. Four classification formulae were generated from discriminant function analysis, culminating in a 94% classification accuracy for group of origin. These four formulae incorporated maximum osteon diameter, Haversian canal area and osteon density. The addition of cortical thickness to these micrometric parameters increased the accuracy to 100%.

Humans were found to have the lowest osteon density of any sample, while pig and cow had mid-range densities compared to the higher densities found in roe deer and red deer. In

using the discriminant functions, humans were found to have the widest maximum osteon diameters (mean of 236.91 µm), while cows (Group 2) and pigs (Group 3) had some overlap with the lower range of human values (means of 238.46 and 223.26 µm, respectively). Roe deer and red deer (Group 4) had maximum osteon diameters (means of 110.11 and 127.72 µm, respectively), while cows (Group 2) and pigs (Group 3) had some overlap with the lower range of human values. Roe deer and red deer (Group 4) had maximum osteon diameters that were much lower than the other three groups with no overlapping ranges (Fig. 2.10).

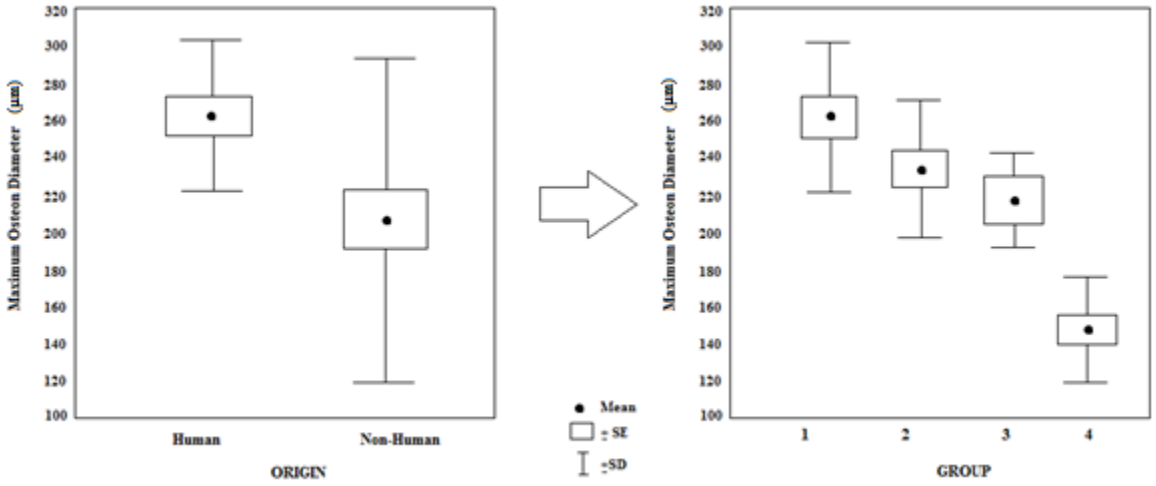

Figure 2.10 – Box-whisker plot of maximum osteon diameter values to distinguish human from non-human origin (left) and to distinguish between formed groups of taxa (right). (Adapted from Urbanová and Novotný, 2005: 84)

Overall, osteon and Haversian canal measurements were the largest in humans, and both deer species having the smallest dimensions. Pig and cow values fell closer to humans in an intermediate range between humans and deer. The results from this study also disproved the notion held in the previous literature (e.g. Sauer and Lackey, 2000) that Haversian canal diameters less than 50 µm were indicative of non-human origin, as cow and horse samples displayed maximum diameters nearing the 50 µm threshold. While no non-human samples displayed diameters larger than 50 µm in this study, later studies by Martiniaková et al (2006a, 2006b) and Zedda et al (2008) have demonstrated that upper ranges of Haversian canal diameters

in cow and horse exceed this threshold of 50 µm when including the upper ranges of one standard deviation range.

The first of three major studies done by Martiniaková and her colleagues examines the differences in microstructural features between pig and cow femoral material (2006a). The area, perimeter, and minimum-maximum diameters of secondary osteons, Haversian canals, and primary vascular canals were measured. The values for cow metrics were consistently larger than in pig, but the standard deviations for all of the parameters showed an overlap between the two species. Discriminant functions were developed for each species in an attempt to use these metrics for species identification. The function for cow led to an 80.63% success rate, while the function for pig had a success rate of 48.75%. The researchers highlighted the necessity of including qualitative analysis in species differentiation due to the overlap, which is reflected in the poor success rate for pig determination.

The second study (Martiniaková et al, 2006b) expanded on the initial study by adding sheep, rats and rabbits alongside cow and pig as non-human samples to compare with human samples. Haversian canal and secondary osteon area, perimeter and minimum-maximum diameters were measured, excluding primary vascular canals in this study. Rats were exempt from the analysis due to their lack of Haversian bone. The results confirm the patterns found in previous studies, such as Urbanová and Novotný (2005), in that humans have the largest dimensions for osteons and Haversian canals. The values for cow osteon parameters were found to be within the human 1 standard deviation ranges, while pig and sheep values reached the lower end of the human values. The values for Haversian canals distinctly separated humans from other animals, even cow and pig, indicating that this parameter is more beneficial in distinguishing human from non-human samples. Overall, the body size of non-human specimens

were related to overall histomorphometric dimensions as cow, pig and sheep (in descending order) had much larger values compared to rabbit. However, the measurements taken in Martiniaková et al (2006a, 2006b) were found to be greater than those found in Urbanová and Novotný (2005).

Using similar formulae as before (Martiniaková et al, 2006a), each species had an assigned regression coefficient to be used in the appropriate discriminant functions. These functions gave an overall success rate of 76.17%, with the combination of quantitative and qualitative features approached 100% correct identifications. Humans had a 100% success rate, followed by rabbit (86.47%), cow (78.54%), sheep (57.33%) and pig (42.67%). The poor success of pig and sheep functions is a reflection of their intermediary position between the upper range (human and cow) and the lower range (rabbit) of values.

The third study conducted by Martiniaková and a team of researchers (2007) focused on distinguishing between the non-human species examined in the previous study (Martiniaková et al, 2006b). The femora of pig, cow, sheep and rabbit were measured for area, perimeter and minimum-maximum diameters of primary vascular canals, secondary osteons, and Haversian canals. Scheffe tests were performed on pairings of animals to find significant differences between features in each species (for example, examining the area, perimeter and minimum diameter in cow versus pig). These tests determined that between pig and cow, there are no significant differences in the area of all three measured features: in the perimeter in Haversian canals and primary vascular canals; in minimum diameter of Haversian canals and osteons; in the maximum diameter of primary vascular canals.

The discriminant functions established in the two previous studies (Martiniaková et al 2006a, 2006b) led to an overall success rate of 73.83% with perimeter and minimum diameter of primary vascular canals being the two most influential variables. Again, incorporation of qualitative features increased the correct identification rate to 100%.

Morris (2007) conducted an extensive study on the quantitative and qualitative differences exhibited by the bone structures of dog, pig and white-tailed deer. She measured the cortical thickness, osteon density, and areas of osteons and Haversian canals in humeral, femoral and rib samples. Pigs were found to have the largest dimensions of the three species. The analysis for osteon density was a projected estimate due to the limited amount of Haversian structures found in the pig specimens; this was attributed to the fact that the pig specimens were mainly sub-adults, whereas the dog and deer specimens included those of adults. The lack of Haversian structures may have also contributed to biased measurements of the secondary osteons and Haversian canals as a result of non-randomization. These values, however, are consistent with previous research in showing that pigs typically display larger osteon and Haversian canal areas compared with dog and deer specimens (Albu et al, 1990). Morris also noted that the femoral samples demonstrated the largest proportion of plexiform bone out of the three elements studied. This, in combination with the age of the specimen, can impact the osteon dimensions and osteon density present in any given sample, potentially skewing any results recognized within the sample.

A closer examination of the histomorphometric differences between horse and cow bone was done by Zedda and a team of associates (2008). Previous studies by Cuijpers (2006) and Cuijpers and Lauwerier (2008) outlined the qualitative differences between the two species, while Albu et al (1990) showed their close similarity in Haversian canal dimensions. In their

study, Zedda and colleagues (2008) measured the diameter, perimeter and area of osteons and Haversian canals; these results directly contradict Albu et al (1990) with horses possessing consistently larger dimensions across all parameters, whereas the greater values were found for cows in Albu et al (1990). In general, Zedda et al (2008) showed that osteon diameters in cow were 36% smaller on average than in horses, and the average cow Haversian canal diameter was 52% of that of horses.

A number of studies have demonstrated the limitations of using quantitative measurements to discern human remains from non-human specimens, especially with the overlapping values that medium-to-large mammals share with humans for osteon and Haversian canal parameters. The problems facing researchers in properly identifying the origin of human or non-human fragments is illustrated in a set of graphs (Figs. 2.11 and 2.12) from Hillier and Bell (2007).

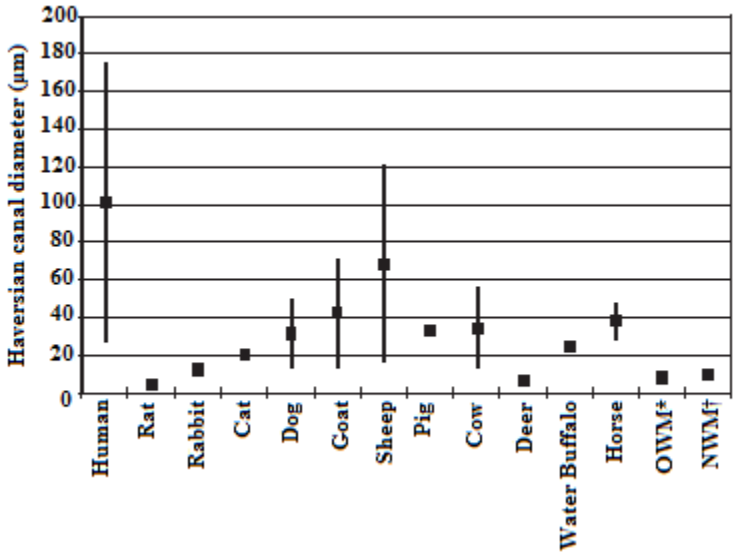

Figure 2.11 - Cumulative data on various ranges of mammalian Haversian canal diameters emphasizing the overlapping values present in a number of mammals with humans. (Taken from Hillier and Bell, 2007:254)

* OWM = Old World Monkeys † NWM = New World Monkeys

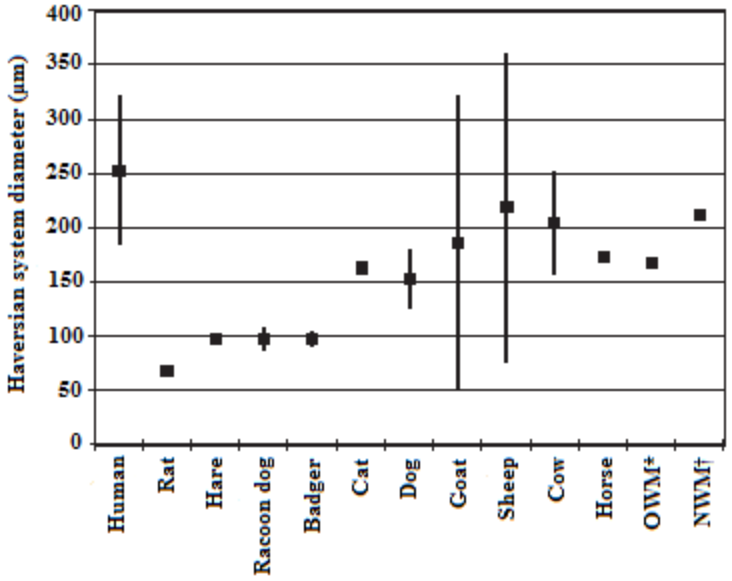

Figure 2.12 - Cumulative data on various ranges of mammalian Haversian system diameters emphasizing the overlapping values present in a number of mammals with humans. (Taken from Hillier and Bell, 2007:254)
* OWM = Old World Monkeys † NWM = New World Monkeys

Compounding these limitations is the fact that the majority of data have been compiled on a limited number of elements, namely prominent long bones and ribs, and typically with adult humans as a comparison against all non-human specimens. In an archaeological or forensic circumstance in which fragmented bones must be identified at a histological level, it is possible that the type of element will not be easily recognized. It is thus difficult to accurately use a set of values ascribed to only a subset of possible skeletal elements.

This problem was addressed by Cattaneo and her colleagues (2009) in a study that focused on the analysis of flat and subadult bones compared to values derived from long and adult bones. The non-human collection was composed of dog, cat, cow, rabbit, sheep, pig, quail chicken and turkey samples. Discriminant function analysis was performed using Haversian canal area, and minimum-maximum diameters of Haversian canals. An algorithm generated from a previous study (Cattaneo et al, 1999) on burnt material was used to verify the accuracy of

differentiating between human and non-human samples; a negative value denoted non-human origin while a positive value implied human origin.

Neither the type of element nor age played a factor in correctly identifying non-human origin, but these two variables were necessary for proper diagnosis of human samples. Metric analysis performed on adult human long bones had 70% accuracy, while adult flat bones had 28.2% accuracy. Incorrect identification was especially high in neonate remains (93.3% on long bone and 68% on flat bone). Subadult analysis also had a high failure with 56.1% of long bones incorrectly identified and 60% of flat bones incorrectly assigned.

On average, the rate of failure on any non-human bone was 0.9%, indicating that the algorithms developed show consistent results for any non-human element. On the other hand, Cattaneo and her fellow researchers concluded that their algorithm can only successfully determine human origin when using adult long bones.

Crescimanno and Stout (2011) introduced a novel method of investigating osteon dimensions for differentiating human and non-human specimens through osteon circularity. The basis for this analysis relies on the hypothesis that non-human osteons approach a perfect circle at a greater rate than human osteons. The determination of a perfect circular osteon relied on having a homogenous shape between the osteon and the Haversian canal. A potential sex-based discrimination between female and male humans was explored, but there was no significant difference found.

For this experiment, non-human samples were represented by dog, pig and deer. The most commonly researched bones (humerus, femur and rib) were examined. The human average for mean osteon circularity was 0.850 where 1.00 implies a perfect circle. Each element

examined displayed different values for circularity, with ribs consistently demonstrating higher values than humeri and femora, showing a statistically significant difference between rib osteon circularity and humerus and femur osteon circularity. These differences were present in both human and non-human group samples.

Dog samples had a mean circularity of 0.874, while deer osteons had a mean of 0.871 and pig osteons had a mean of 0.870. The averages for the non-human osteon circularities were not significantly different from each other, showing a uniformity in non-human samples (Fig. 2.13). This means that osteon circularity can only be used as a method to determine human origin through an algorithm in which negative values are of human origin and positive values indicate non-human origin. When using this method for species identification, there was a 76.5% accuracy rate.

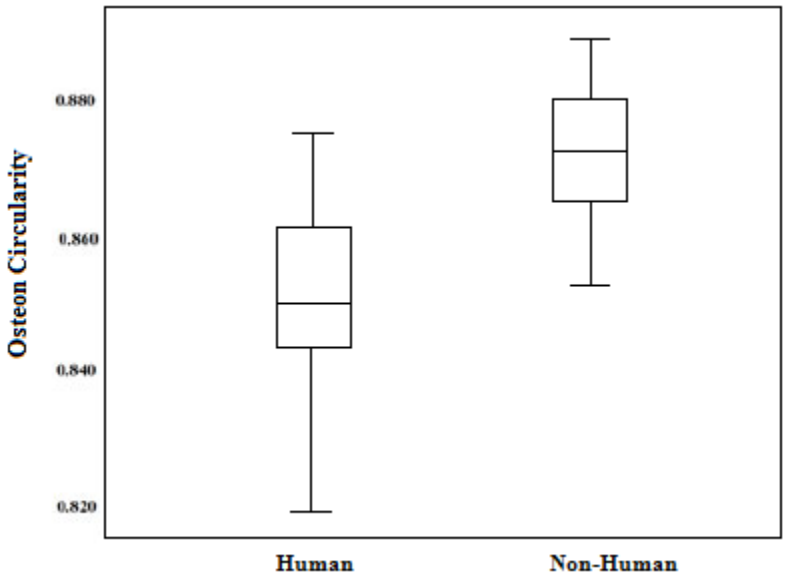

Figure 2.13 - Box chart showing the uniformity in non-human osteon circularity as being more homogenous than in human osteon circularity. (Taken from Crescimanno and Stout, 2011: 6)

Table 2.4 - Histomorphometric values from analyzing long bones from several deer (Cervidae) taxa collected from previous literature.

Study	Subcategory per study	Mean Osteon Area (μm^2)	Osteon Diameter (Min/Max) (µm)	Mean Haversian Canal Area (μm^2)	Haversian Canal Diameter (Min/Max) (µm)
Owsley et al (1985)	Specimen A Specimen B	-	-	-	31 - 250 63 - 312
Urbanová and Novotný (2005)	Red deer Roe deer	7410.84 ±357.90 9900.04 ±455.86	85.01 - 110.11 ±2.10 ±2.75 100.96 - 127.72 ±2.51 ±3.37	409.35 ±22.26 327.58 ± 23.08	17.80 - 24.97 ±0.58 ±0.74 15.13 - 23.72 ±0.63 ±0.92
Morris (2007)	Femur Humerus	13900 ±650 14700 ±600	-	387 ±205 401 ±186	-

Table 2.5 - Histomorphometric values from analyzing femora from domestic pig (*Sus scrofa domesticus*) collected from previous literature.

Study	Mean Osteon Area (μm^2)	Osteon Diameter (Min/Max) (µm)	Mean Haversian Canal Area (μm^2)	Haversian Canal Diameter (Min/Max) (µm)
Albu et al (1990)	-	-	-	28.73 - 39.85
Urbanová & Novotný (2005)	33118.87 ±3239.81	180.72 – 232.26 ±9.88 ±11.95	826.45 ±66.88	26.23 – 36.18 ±1.39 ±1.37
Martiniaková et al (2006a)	29194.63 ±9896.69	84.54 – 216.68 ±17.15 ±52.11	1009.49 ±540.84	15.53 - 40.53 ±5.27 ±14.16
Martiniaková et al (2006b)	28031.80 ±10004.39	83.15 – 211.07 ±17.24 ±55.42	1015.21 ±539.63	15.61 – 40.60
Morris (2007)	19700 ±8700	-	645 ±341	-

Table 2.6 - Histomorphometric values from analyzing femora from domestic cow (*Bos taurus domesticus*) collected from previous literature.

Study	Mean Osteon Area (μm^2)	Osteon Diameter (Min/Max) (µm)	Mean Haversian Canal Area (μm^2)	Haversian Canal Diameter (Min/Max) (µm)
Jowsey (1966)	-	250 ±40	-	-
Albu et al (1990)	-	-	-	39.81 - 70.94

Urbanová & Novotný (2005)	36067.23 ±2951.58	181.49 – 238.46 ±5.65 ±8.07	1176.37 ±79.35	30.99 - 42.56 ±1.16 ±1.38
Martiniaková et al (2006a)	31725.40 ±11246.49	77.01 – 258.45 ±15.95 ±66.06	1196.65 ±646.33	15.60 – 47.47 ±4.38 ±14.98
Martiniaková et al (2006b)	32664.98 ±1111.03	76.22 – 269.63 ±14.63 ±69.15	1224.71 ±653.33	15.58 – 48.76 ±4.32 ±15.59
Zedda et al (2008)	23576.9 ±14326.0	128.8 – 195.3 ±41.5 ±73.5	717.0 ±474.0	20.7 – 36.5 ±6.1 ±16.7

2.3 Analysis of Cremated Remains

The primary goal of many archaeologists and forensic investigators dealing with burnt material is foremost to be able to recognize it as such, whether it be through the diagnosis of heat exposure in bone (Buikstra and Swegle, 1989; Hanson and Cain, 2007; Gonçalves, 2012), or the correct identification of cremated remains as being bone (Whyte, 2001; Cattaneo et al, 1999). The majority of these research topics fall into two main categories: macroscopic analysis covering colour changes, fracture patterns, and shrinkage due to exposure to extreme heat, and microscopic analysis to examine the relationship between temperature and corresponding changes in bone microstructure.

2.3.1 Alteration of Burned Bone – Colouration & Shrinkage

A key indication for the burning of bone is the visual change in bone colouration. Colouration is dependent on a number of variables including oxygen availability, metals in the environment, temperature and duration of heating. Numerous studies have examined the relationship between temperature and the colouration of affected bone (Shipman et al, 1984; Buikstra and Swegle, 1989; Nicholson, 1993). The seminal experiment conducted by Shipman and her associates (1984) observed various categories of colour changes in sheep and goat bones over a range of 20^{o}C to 940^{o}C (Table 2.7). The first stage of burning (20-285^{o}C) produces a variety of neutral colours with a white or yellow hue. Stage 2 (285-525^{o}C) creates combinations

of red, brown and grey. At Stage 3 (525-645^{o}C) bone is black with hues of blue or reddish-yellow. Stage 4 (649-940^{o}C) sees the return of neutral white with shades of blue-grey present. The last stage (940^{o}C and up) creates calcined bones with darker greys and reddish-yellow hues. Because of overlapping colourations, it is difficult to pinpoint specific temperatures but the prevalent tones can be used to identify the stage of burning.

Table 2.7 - Categories of colours observed in burned sheep and goat bones according to temperature. (Adapted from Shipman et al, 1984)

Stage	Temperature (^{o}C)	Colour
I	20-285	Neutral white, pale yellow, yellow
II	285-525	Reddish-brown, very dark grey-brown, neutral dark grey, reddish-yellow
III	525-645	Neutral black, medium blue, some reddish-yellow
IV	645-940	Neutral white, light blue-grey, light grey
V	940+	Neutral white, medium grey, reddish-yellow

Nicholson (1993) expanded on this study by including a broader array of animals, including non-mammals, to observe these same colour categories from 200^{o}C to 900^{o}C. Her results showed variation in colour at a given temperature, suggesting that a clear correlation between colour and temperature cannot be made more accurately than $\pm$ 200^{o}C in fresh bone, while the colouration of archaeological bone will be influenced by other taphonomic processes besides heat exposure. Mayne (1990) added more evidence for the unreliability of temperature reconstruction from colouration in her observations of multiple colour categories present in the same burned sample. As a result, colouration does not seem to suggest as much about the condition of burning as about proximity to the heat source and duration of exposure to heat, with the presence of multiple colourations seen on single bones (Schwartz, 1993 in Mayne Correia, 1997).

Buikstra and Swegle (1989) minimized the colour options in their study of discerning pre-incineration bone condition by using only three categories of burning patterns: unburned (normal), smoked (black) and calcined (grey-blue, grey and white). They discovered that after cremation, fleshed and green (greasy) bones could not be distinguished based on colouration, while dry bones had very few external colour changes but greater expression of combustion within the cortex.

An issue that arises from heat is the alteration in the dimensions of bone which could potentially impact histological analysis. Buikstra and Swegle (1989) demonstrated a narrow range of shrinkage from -0.7% to -5.6%, with a maximum temperature that reached 1060^{o}C. They noted that the majority of altered bones shrank less than 3% at 700-800^{o}C. Since any changes to the dimensions of bones are too minute to affect their measurements under 800^{o}C, many archaeologists do not bother accounting for the shrinkage.

Thompson (2005) tested the extent of distortion at a similar range of temperatures (500^{o}C, 700^{o}C and 900^{o}C). He found that the percentage of shrinkage of bone was linked to the temperature as well as duration of exposure. Thompson (2005) showed that less than 9% of the bone samples studied demonstrated changes in dimension. However, in the same experiment, burning bone at 900^{o}C could account for a shrinkage of 15% to 40%, suggesting a lowered threshold of 700-1000^{o}C for potential alteration in bone dimensions. Various experiments (Buikstra and Swegle, 1989; Bradtmiller and Buikstra, 1984; Herrmann, 1977) demonstrate that unless prominent shrinkage occurs, the microstructure of bone is for the most part unaltered, allowing regular histological techniques to be applied. As well, Thompson (2005) points to the difficulty in accurately accounting for shrinkage in studies when pre-incineration dimensions are

not known, leaving only controlled experimental conditions to answer questions on the extent of shrinkage in burned remains.

2.3.2 Microscopic Analysis of Cremated Remains

In response to the predominant emphasis on examining burnt bone through macroscopic analysis, Herrmann (1972a, 1972b, 1977) used histological techniques to examine the microstructural responses of archaeological bone to extreme heat exposure. In these studies, Herrmann determined the temperatures at which the organic components of bone were completely burned, resulting in the fusion of bone mineral crystals. This "critical level" was set at 700-800^{o}C (Herrmann, 1972a), at which point the fusion of the inorganic components of bone impacts the macroscopic appearance due to shrinkage. Below this critical level is "incomplete cremation" which is characterized by darker colouration of the bone in shades of black, brown and blue-grey (Herrmann, 1972b) due to the carbonization of the organic material remaining in the bone material.

Despite the remarkable changes occurring around the critical level, the histological makeup of completely cremated bone is still identifiable using scanning electron microscopic (SEM) analysis. This type of microscopy allows for comparisons in the appearance of osteons to determine the temperature at which a bone was burned. Herrmann (1977) referred to the shrunken dimensions of osteons at higher temperatures (past the critical level). This was determined to be a result of the inorganic crystal fusion. His findings helped researchers to use histological techniques in determining age from burnt human bone.

Bradtmiller and Buikstra (1984) followed the results of Herrmann (1977) by examining the reliability of determining the age of death in cremated bone material through histological

techniques. The researchers used fleshed and recently defleshed human femora, as well as archaeological dry bone, to determine the role of flesh in insulating bone from heat damage. However, the archaeological material could not be examined microscopically due to the extent of demineralization. The technique developed by Kerley (1965) for determining age through counting secondary osteons was used, although it was deemed only possible in temperatures below the critical level. The shrinkage of bone attributed to the fusion of bone mineral crystals above 700-800^{o}C would impact the precision of Kerley's method due to distortions in the expected dimensions of osteons. The thin sections were processed for microradiography and then further examined under a light microscope to show results that contradict Herrmann's (1977) conclusions on the size of osteons after cremation. Whereas Herrmann (1977) had noted shrinkage in osteon size, Bradtmiller and Buikstra (1984) demonstrated that osteons had in fact increased in size after cremation compared to unburned bone. This disparity drew them to suggest a further re-examination of the temperature levels at which bone mineral crystal fusion occurs, as well as other approaches to analyzing bone microstructure.

In paleoanthropological and archaeological studies, there is a crucial emphasis on being able to identify evidence of controlled exposure to fire in fossilized remains or bone material that has undergone millennia of taphonomic processes. This allows the development of human-made fires to be investigated with more reliable methods, expanding an anthropological understanding of human fire use for dietary or ritualistic purposes. Hanson and Cain (2007) investigated fire-induced histological changes by comparing faunal remains burnt under controlled conditions to burnt and unburnt archaeological samples from two sites. Adult sheep humeri and femora were defleshed in preparation for burning, with a couple of specimens further boiled to remove grease, allowing comparison with the unboiled greasy specimens. The specimens were cremated using a

hardwood firepit, and the temperatures of the flames were measured at set intervals. The maximum temperature reached was around 700^{o}C, while the minimum recorded temperature was 270^{o}C at the time of adding the specimen into the fire. According to the levels found by Herrmann (1972a, 1977) and others, this indicates that the majority of the bone samples were not completely incinerated and would retain much of their organic material. Categories were established from the burnt samples by intensity of heat rather than solely by temperature due to the dual impact of duration and temperature on the characteristics of burnt bone; this was also accounted for by noting the proximity of the sample to the source of the heat (Table 2.8; Hanson and Cain, 2007).

The final conclusions drawn from this experiment showed that the samples from the two sites displayed similar characteristics to the experimentally burned remains. The same impact on histological structures could be found when using either closed ovens or open firepits. However, differences noted between greasy and non-greasy bones through direct observation of the duration and intensity of heat were related to differences in histological appearances. No direct inferences can be made, though, on whether fire-damaged bone is a result of human-made fires, leaving this question perhaps unanswerable in paleoanthropological studies.

Table 2.8 – Descriptions of histological conditions at different heating levels on experimentally burned sheep limbs. (Modified from Hanson and Cain, 2007)

Experimental Samples	Temperature (^{o}C)	Location on fire	Heating Level	Histological condition
M1 (Fleshed)	270	Coals, at edge	None/Low	Light tan/white All features are clear No carbon deposition No cracking
M2 (Fleshed)	400	Coals, at edge	None/Low	Light tan/white All features are clear No carbon deposition No cracking
M3 (Non-greasy)	462	Coals, in centre	High	Centre is black or white White edges with lost histological structures

				Carbon deposition Wide and prevalent cracks
M4 (Non-greasy)	620	Coals, in centre	Medium-High	Black or brown Edges are black or white (disappeared histological structures if white) Carbon extensive Radiating cracks
M5 (Greasy)	482	Coals, at edge	Medium	Deep red or brown Darker edges Carbon is visible Cracks beginning to show
M6 (Greasy)	482	Coals, in centre	Medium-High	Black or brown Edges are black or white (disappeared histological structures if white) Carbon extensive Radiating cracks
M7 (Greasy)	590	Coals, at edge	Low-Medium	Deep tan, yellow, pale orange/red Carbon minimal around edges No cracking
M8 (Greasy)	705	Coals, in centre	High	Centre is black or white White edges with lost histological structures Carbon deposition Wide and prevalent cracks
M9 (Greasy)	470	Flames, 10cm from centre	None/Low	Light tan/white All features are clear No carbon deposition No cracking
M10 (Greasy)	380	Flames, 20cm from centre	Medium	Deep red or brown Darker edges Carbon is visible Cracks beginning to show
M11 (Unheated)	-	-	None/Low	Light tan/white All features are clear No carbon deposition No cracking
M12 (Unheated)	-	-	None/Low	Light tan/white All features are clear No carbon deposition No cracking

With technological advancements, new methods are available to use in identifying cremated remains. Many of these new technologies require expensive equipment, like DNA analysis (Cattaneo et al, 1999; Gonçalves, 2012), X-ray (Shipman et al, 1984; Hiller et al, 2003; Piga et al, 2008; Beckett et al, 2011), infrared spectroscopy (Stiner et al, 1995; Thompson et al, 2009; Squires et al, 2011), and albumin protein identification (Cattaneo et al, 1999).

The study done by Cattaneo and colleagues (1999) compared more traditional histological techniques with DNA analysis through polymerase chain reaction (PCR) and immunological methods to detect the human protein albumin in order to determine which methodology was best suited for differentiating faunal material from human material at a microstructural level. The samples came from human cadavers, modern cemetery burials, and butchered remains from cows, horses, sheep and pigs. Samples were burned at temperatures within the 800-1200^{o}C range, exceeding the point at which organic material would be present. Digital images of the thin sections were taken after examination under transmission light microscopy. Various quantitative parameters were measured, including the areas of the Haversian canals and osteons, and the minimum and maximum diameters of Haversian canals and osteons. Statistical analysis through the Mann-Whitney U test showed a distinct difference between faunal and human material, and discriminant functions were created to predict correct taxonomic origin for 79% of the samples. Comparatively, genetic material was not detected in any of the burnt material, and less than half of the human subjects retained detectable albumin after cremation. With these results, Cattaneo and colleagues demonstrated the validity and necessity of histological techniques in archaeological and forensic cases where bone material has been burned.

The advent of x-ray technologies has made it possible to examine the effects fire causes in bone at a much more detailed molecular level compared to other methods. Its inclusion to examine burnt material by Shipman and her colleagues (1984) alongside other methods showed how each technique can be used to identify burning temperatures from the appearance of bone. Their research demonstrated a major change in the bone mineral crystalline structure around 645^{o}C, while the crystals themselves begin increasing in size starting between 525^{o}C and 645^{o}C.

To follow-up on these results, Piga and his team (2008) examined the changes in the crystalline structure of fragmented bone from 200^{o}C to 1000^{o}C, with an emphasis on observing the step-by-step process undergone within this 'crucial' temperature range at 650^{o}C, 750^{o}C, 775^{o}C, 825^{o}C and 850^{o}C. This research used a new x-ray calibration technique that directly evaluated the average size of crystals from the breakdown of the bone mineral lattice organization in order to replace other methods that rely on an arbitrarily assigned index of crystallinity (Shipman et al, 1984; Stiner et al, 1995; Thompson et al, 2009; Beckett et al, 2011). This index is determined based on 'splitting factors' (SF): "an average of the heights of the two peaks … divided by the height of the low point between them" (Stiner et al, 1995: 228; Weiner and Bar-Yosef, 1990). Larger SF values are indicators of a more ordered lattice of crystals, thus leading to the arbitrary border between normal and elevated crystallinity indices (Stiner et al, 1995).

As well, their experiment included three different times (0, 18, and 60 minutes) to observe the intersecting effects of duration and temperature on changes in bone microstructure. In general, it was determined that exposure to a given temperature for 60 minutes had the same appearance as bone exposed to temperatures 100^{o}C higher at 0 minutes (Piga et al, 2008). This distinction is important to account for when reconstructing thermal treatment at the initial time of cremation.

The overall findings from Piga and colleagues' work (2008) on crystalline structure were in accordance with those put forth by previous researchers (Shipman et al, 1984; Hiller et al, 2003) in that crystals expanded in size in correlation with temperature, though significant changes were not observed until 700^{o}C, and pronounced differences occurred between 750-850^{o}C. The fastest rate of crystal expansion occurred between 750-1000^{o}C, whereas afterwards it was difficult to

assess the relative size of crystals due to limitations imposed by the equipment. Piga and his colleagues (2008) link the accelerated growth of the crystals to the destruction of the organic components in bone.

Hiller and colleagues (2003) put forth the use of a complementary x-ray technique known as small-angle x-ray scattering (SAXS) in an attempt to determine whether this method is better suited to detect changes in crystal structure at lower temperatures than x-ray diffraction (XRD) techniques. Until 1000^{o}C (Hiller et al, 2003), there is a continual trend in crystalline perfection in which the hydroxyapatite ions become more homogenous and the growing size of the hydroxyapatite crystals lead to a decrease in lattice disorder (Beckett et al, 2011). This process of developing a more cohesive lattice is known as recrystallization.

The ability for SAXS to be used at a range of lower temperatures relies on the technique examining the size, shape and orientation of bone mineral crystals directly. This is in comparison with other x-ray methods that require the analysis of lattice cohesion in order to indirectly measure the crystals (Shipman et al, 1984; Piga et al, 2008; Beckett et al, 2011). The researchers for this study (Hiller et al, 2003) heated cortical bone of recently defleshed sheep for either 15 or 45 minutes at temperatures of 500^{o}C, 700^{o}C or 900^{o}C. At 500^{o}C (15 minutes), the average crystal size increased to 15nm, threefold from the original measurement of 5nm, while at 900^{o}C (45 minutes), this average crystal size further doubled to 30nm.

Time also plays a factor in the rate of crystal expansion. Hiller and colleagues (2003) observed that initial changes in the crystal shape occurred after 15 minutes. At 45 minutes, the thickness of the crystals continued growing without any impact on the shape of the crystals. This indicates a thermal stabilization point where an optimal crystal shape is obtained with little heat

exposure, while expansion of the crystals continues according to "specific heating regimens" (Hiller et al, 2003: 5096). These subtle changes are not visible with XRD techniques due to the indirect assessment of crystal appearance, but can be seen using the more precise analysis through SAXS.

Beckett and her colleagues (2011) investigated the potential applications of XRD and similar technology in differentiating burnt human bone from burnt faunal material. They found that the variation in histological features present between species after heating was similar to the variation before heating. Different mineral phases and stages of recrystallization specific to different species were observed at the burning temperatures 600^{o}C and 1400^{o}C. Human bone demonstrated recrystallization at 600^{o}C, while few to no animal bones displayed these same characteristics at 600^{o}C. At this temperature, human bone possessed relatively larger lattice parameter values than found in animal bones, yet the animal bones showed a decrease in lattice parameter values when compared to unheated controls. At 1400^{o}C, recrystallization and further decreased lattice parameter values were present in all samples.

However, the development of new mineral phases occurred differently between animal groups. Most species exhibited calcium oxide (CaO) and magnesium oxide (MgO) as replacements for hydroxyapatite as the dominant mineral present at 1400^{o}C. At 600^{o}C, a small number of animal species already had MgO minerals present, but no CaO was found to be present until 1400^{o}C. However other studies (Hiller et al, 2003) show that CaO can form at 700^{o}C, indicating that other conditions are in play with the formation of CaO in certain species, and that observing only two temperatures may not be sufficient for species differentiation. Overall, Beckett and her colleagues (2011) noted that there was greater interspecies variation

than intraspecies variation, and that the additional characteristics seen in burnt bone make XRD a viable option for distinguishing burnt human remains from burnt faunal remains.

Infrared spectroscopy (IRS) has been employed as a complementary method in relation to x-ray diffraction (XRD) analysis (Stiner et al, 1995; Thompson et al, 2009). This type of technology relies on the vibrations of molecular bonds caused by infrared radiation. These vibrations are measured by examining the wavelength at which radiation is absorbed (Thompson et al, 2009). Analyzing these changes at an atomic level allows a wider range of samples to be used, making it an option for fragmented cremated remains.

One of the earlier studies using IRS on burnt remains comes from Stiner and her colleagues (1995), who investigated the relationship between macroscopic changes of bone (assessed through colour and mechanical properties) and microscopic appearances at various temperatures and degrees of insulation from soil. The degree of crystallinity was determined by the separation between the absorption peaks at 603 and 565 cm^{-1}. In samples with higher splitting factors (SF), the crystals were more ordered and carbonate levels were decreased. The carbonate levels reflect the degree of calcination due to the replacement of carbonate by hydroxyapatite during recrystallization (Stiner et al, 1995). Heat ranges on buried bones were determined through colour changes, SF values, and carbonate levels. The SF and carbonate values in the lower thermal ranges were found to correspond to burned samples that were directly exposed to fire. However, researchers noted that non-fire diagenetic processes (like weathering) could also be responsible for the increasing SF values detected through IRS can lead to reduced bone matrix content. As well, there were no significant differences in carbonate values between burnt and unburned bone. The researchers of this study thus suggest that IRS, and by extension, XRD analysis are not effective at determining thermal range of burnt bones,

contradicting the results from Shipman and colleagues' study (1984). Instead, Stiner et al. (1995) suggest examination of the internal colour changes on bone to be a more viable method. Other studies (Nicholson, 1993; Mayne, 1990; Mayne Correia, 1997), though, have questioned the reliability of colour changes in bone, placing the conclusions from this study in doubt.

As a means to determine how well the crystallinity index compares against other quantifiable measurements, Thompson and his colleagues (2009) did a study investigating two types of Fourier Transform Infrared Spectroscopy (FTIR) techniques and the ratios of carbonate - phosphate (C/P), and carbonyl – carbonate (C/C) on a series of sheep samples. The first FTIR technique uses potassium bromide as a support medium (FTIR-KBr). The comparative FTIR technique has an infrared beam directed at an optically dense crystal in order to measure the internal reflection of the beam, known as "attenuated total reflection" (FTIR-ATR). When conducting blind tests to predict the burning temperature through CI values through both FTIR techniques, almost all predictions were consistently below the actual burning temperature. As well, the differences in CI values determined through each technique show that the same samples will have vastly different readings, impacting the ability for comparisons between and within studies unless the exact same techniques are used. The results of this study show that while both FTIR techniques are viable, the researchers recommend using FTIR-ATR due to its efficiency and speed over FTIR-KBr which had slightly less accurate values.

The ratio of carbonyl to carbonate is used to determine the proportion of inorganic (hydroxyapatite mineral) to organic (collagen) components in bone. This value is only viable until 700^{o}C, beyond which the organic material is completely extinguished. Both FTIR techniques produce similar carbonate:phosphate ratios, and a trend of decreasing C/P values corresponding to increasing temperatures is consistent with other studies observing carbonate

reduction at higher temperatures (Shipman et al, 1984; Stiner et al, 1995), albeit through other methods of analysis.

For further testing on the reliability of infrared-based technology, Squires and her team of researchers (2011) compared FTIR analysis and histomorphometric analysis to determine the temperatures of Anglo-Saxon cremations found in England. The conclusions of Thompson and his colleagues (2009) led to only FTIR-ATR being used in this study (Squires et al, 2011), while a polarizing microscope was employed to examine the histological structures of the burnt bone. Standards taken from Bhayro (2003) gave comparative values at three temperatures (300^{o}C, 600^{o}C and 900^{o}C).

The infrared analysis demonstrated that roughly half of the Anglo-Saxon cremations occurred around 900^{o}C based on the complete absence of organic components and the fusion of hydroxyapatite crystals. The collective appearance of these features is found above 800^{o}C (Mayne Correia, 1997). Microscopic investigations confirmed these observations, and showed that osteocyte lacunae had disappeared, and the size of Haversian canals had increased.

The appearance of osteons in the remaining samples indicated that heat was applied between 600^{o}C and 900^{o}C. The incomplete status of these cremated remains was also confirmed through the observation that the endosteal surface and inner cortical bone were not as burnt as the outer cortical bone and periosteal surface. This in turn suggests that these bodies were exposed to fire for shorter durations than those who displayed features of complete cremations.

Squires and her team (2011) were able to suggest differential cremation practices based on social status due to the variation in temperatures and exposure times exhibited in the samples These variations could be determined through the presence or absence of complete cremation.

For example, more expensive fuel was used for individuals of higher social status, thus higher temperatures and longer heat exposure would be indicative of more influential members of society.

Analysis through scanning electron microscopy (SEM) is another approach which is commonly employed with skeletal material. Shipman and her team (1984) included this technique in the research examining burnt material ranging from 185^{o}C to 940^{o}C. They determined that magnification below 1000x was incapable of detecting any diagnostic traits in their burnt samples, with the best range at 1000x to 10,000x. For comparison, they noted that light microscopy was insufficient in reconstructing cremation temperatures in that only fractures could be observed, which alone do not identify heat damage in bone material. Shipman and her colleagues (1984) observed five different stages of morphological changes through SEM examination (Table 2.9), describing a progression from a normal appearance (Stage I) to irregular surface texture (Stage II), glassiness (Stage III), to increasing bubbling in the later stages (Stages IV and V).

Table 2.9 – Heating stages in bone structures through scanning electron microscopy (summarized from Shipman et al, 1984).

Stage	Temperature (^{o}C)	Microscopic morphological changes
I	20-185	Unaltered
II	185-285	Increased surface roughness
III	285-440	Glassy, very smooth
IV	440-800	Frothy or fleecy
V	800-940	Smooth-surfaced globules

The results from Holden, Phakey and Clement (1995) confirm previous research (Herrmann, 1972a, 1972b, 1977; Shipman et al, 1984) regarding the temperatures at which recrystallization and mineral phases occur, and are validated by later research (Thompson, 2005; Mayne Correia, 1997; Beckett et al, 2011; Piga et al, 2008; Castillo et al, 2013). However,

partial fusion was observed at 1000°C and total fusion occurred by 1400°C which contradicts previous studies that note fusion (Herrmann, 1972a, 1972b, 1977) or the total loss of organic components (Shipman et al, 1984) occurring around 700-800°C. As well, the results from Holden and colleagues (1995) suggest that age determination is not feasible in samples exposed to temperatures above 600°C due to shrinkage and fusion.

Whereas Shipman and her research team (1984) observed the morphology of bone surfaces at various stages of heat, Holden and colleagues (1995) directly examined the shapes and sizes of the bone mineral crystals formed in different heating stages. Human femoral samples were burned at 200°C to 1600°C for durations of 2, 12, 18 and 24 hours, and analyzed through SEM.

In the initial stage (200-600°C), it was found that the structural features of bone were unaltered. However, at 200°C, the endosteum had begun disintegration. Partial endosteal disintegration occurred at 400°C after 12 hours; by 24 hours, there was no endosteum left.

At 600°C (2 hours), the initial crystals formed in spherical shapes with an average size of 0.064±0.040um. These crystals indicated the initiation of recrystallization, and could be observed at magnifications from 30x to 100,000x. The improvement of hexagonal crystal morphology could be observed at prolonged exposures to 600°C heat without any increase in size. The research of Hiller and team (2003) found consistent results with Holden and colleagues (1995).

At the beginning of the next stage, the formation of hexagonal crystals could be seen at 800°C. These hexagonal crystals existed alongside spherical crystals. Both crystal types increased in size at higher temperatures: hexagonal crystals grew from 0.3±0.05 μm at 800°C to 1.2±0.10 μm at 1200°C, while spherical crystals increased from 0.070±0.01 μm at 800°C to

0.200±0.05 µm at 1200°C. At 800°C, the lamellar structure is destroyed by the growth of crystals.

The fusion of hexagonal crystals occurred in localized areas, namely the walls of Haversian canals, over the range 1000-1400°C. In this same thermal range, new rhombohedral, rosette and platelet crystals appear. As well, by 1400°C, Haversian canals and osteocyte lacunae are no longer identifiable. All histological features are completely destroyed by 1600°C due to the melting of hydroxyapatite and recrystallization.

Simple light microscopy is a more accessible technology for most laboratories, yet fewer studies have used this approach in analyzing burnt remains. In recognition of this, Castillo and his fellow researchers (2013) investigated the histological appearance of human iliac bone from 100°C to 1100°C. In the first range of temperatures (100-300°C), the deformation of collagen fibres was observed. The second range (400-600°C) produced the degradation of collagen and beginnings of crystallization. Heterogenous crystalline structures were present within the third range (700-800°C), and the last stage (900-1100°C) showed a compact bone surface made up of irregular microcrystals. These results are comparable to other studies focused on crystalline appearance (Shipman et al, 1984; Holden et al, 1995; Hiller et al, 2003; Piga et al, 2008), yet do not address any of the factors in using light microscopy for identification purposes similar to those in Beckett et al (2011). This demonstrates the necessity of testing whether light microscopy is a valid technique in differentiating human and faunal material after cremation.

2.4 Case Studies

The applications of histological analysis in examining burned remains or in differentiating human origin of bone material have already been covered in numerous

publications. This thesis is rooted in the very real demand for more verification of the extent that histological techniques can be beneficial in future forensic and archaeological investigations.

2.4.1 Forensic Cases

One of the most important publications regarding histological analysis in a police case comes from Owsley and his team (1985). This article outlines the case of the partially disarticulated remains of a white female found in southeastern Louisiana. The severely decomposed body had been hit by at least two shotgun blasts, resulting in the fragmentation of the cranium and humerus. After identification of the female was determined, investigators sought to connect bone fragments found in the vehicle of the main suspect to the identified remains. The suspect claimed that the fragments originated from a deer he had poached. Owsley and his fellow researchers determined that the fragments found in the suspect's vehicle had human origin and were later matched to the victim's remains. The investigators compared the dimensions of secondary osteons and Haversian canals of the unknown fragments to the identified human remains and deer remains. The unknown dimensions matched those of the human remains and did not display any histological features that would rule out a human origin (i.e. plexiform bone).

Mayne Correia and Beattie (2001) briefly outlined forensic cases from northern Alberta that involved cremated human remains. One of these cases dealt with a train collision that led to the death of 23 individuals. Proper identification of the individuals was made difficult due to the condition of the remains as a result of severe cremation and extensive commingling. These were successful in confirming human origin of the individuals involved. Light microscopy was used

to confirm that suspicious spongy material was not bone due to the lack of any histological features.

2.4.2 Archaeological Studies - Ritual

Iregren (1995) conducted a study to examine the ritual significance attached to the purposeful interment of animal remains in human burial grounds in Iron Age Sweden. The author examined the differences in proportions of animals found in settlements versus animals found in burial contexts. Animal percentages were counted by the number of fragments and weight, and identification was based on gross morphological visualization. Domesticated animals were quite common, with cows representing 30% to 55% of the settlement fragments. Sheep/goat, horse, pig and dog were also commonly found in settlement sites. These remains represent the type of economy and diet present in these populations. The presence of animals with unique human relationships (horses and dogs) in burial grounds suggests companionship or ritual offerings, while animals associated with hunting (birds of prey or wild game) denoted a very high social status linked to an individual's hunting prowess.

The presence and frequency of animal remains commingled with human cremations marked certain Iron Age periods, suggesting shifting cultural trends regarding the inclusion of animal sacrifices in religious rites. Iregren (1995) suggests that later periods marked by a distinct absence of animal remains could be linked to a growing Christian influence, while earlier periods reflect tribute to pagan deities of fertility (domestic animals) and war (hunting animals).

Bond (1996) similarly examined the presence of animal bones in funerary deposits in Anglo-Saxon cemeteries. Amongst seven Anglo-Saxon sites examined, 18-43% of human cremations had animals included, with horse and sheep/goat being the two most prevalent

species represented. Pig, cow, red deer, bear, small domesticated birds and wild animals were also noted at these sites. Often, human and animal remains were kept in separate urns, strongly indicating a ritual significance to the inclusion of animals in funerary practices. Bond emphasizes the importance of having trained zooarchaeologists examine animal remains in cremation contexts; despite the abundance of animals present in cremations, there is still a limited understanding of these cultural customs.

McCormick (1985/1986) examined the presence of animals in prehistoric Irish burials as a response to the poor results set by the initial excavations. The deliberate placement of animal remains alongside human burials is demonstrated either by the animals appearing intact within the burials or by their appearing in augmented forms such as accessories to the deceased. As well, evidence of butchered and subsequently consumed animal remains in some burials suggest the inclusion of offering from a feast in honour of the recently deceased. Many cases of animals present at burial sites have been ruled out as intentionally placed due to different stratigraphic levels during excavation. However, it is interesting to note that certain sites have been identified as animal-only ritual sites because of the absence of connected human burials.

A study by Greenlee and Dunnell (2010) used histological techniques in identifying the origin of numerous bone fragments and artifacts found in Pacific Island archaeological sites. Preservation of bone tissue in Pacific sites is typically too poor to use DNA analysis, leading the authors to turn to traditional histological methods. Analysis was done using the histomorphological appearance and measured Haversian canal areas of human, pig and dog specimens; these results were then used as comparative standards for the unknown bone artifacts in order to identify species of the tools and other bone material. Though many of the fragments were unidentifiable, many of the commingled human and animal remains were able to be sorted,

though broader questions on how these results impact cultural analysis of Pacific Islanders remain unanswered.

2.4.3 Archaeological Studies –Diet

Two studies examining the burned remains at the Donner Campsite at Alder Creek, California through histological analysis (Robbins and Gray, 2011; Dixon et al, 2010). This campsite is the second of two sites occupied by the Donner families, emigrants from Illinois, and other migrating Americans seeking a more prosperous life in California in 1864. The infamy stemming from these collective groups comes as a desperate response to unexpected winter storms in the Sierra Nevada. The group of caravans split into two parties; the larger party camped near Donner Lake while the smaller group numbering 20 people camped at Alder Creek (Dixon et al, 2010). While written records and extensive excavations from Donner Lake indicate the practice of cannibalizing the dead in the midst of winter-borne starvation, the short existence of the Donner families at Alder Creek has made it difficult to find similar archaeological evidence of their camp (Dixon et al, 2010).

A broader historical background is given by Dixon and her associates (2010) , relating that the Alder Creek occupants were stranded for four months in dire and frigid conditions, yet very little was recorded by the witnesses. Ambiguous diary entries from outside sources record the descent into cannibalization, though it is important to note that the majority of the Alder Creek diet was made up of cattle and wild game. Expected species include domesticated animals that travelled in the Donner caravan (cattle, horse, and dogs) and wild animals native to the Sierra Nevada area.

Both studies (Robbins and Gray, 2011; Dixon et al, 2010) set out to identify the species of 85 burned fragments uncovered at the Alder Creek. Initial classification was determined through visual analysis based on size. Fragments were thus separated into six animal class sizes, though problems such as potential shrinkage due to cremation and heavy fragmentation made this difficult. As a result, only 13% of the fragmented material could be identified by element type. The overwhelming majority (over 2000) of the bone fragments were sorted as Class V mammals (deer-, human- and bear-sized) (Robbins and Gray, 2011).

Histomorphometric and qualitative analyses were performed to determine if any Class V fragments had human origin. A minimum number of 104 fragments from Class IV and V were necessary in order to determine whether or not human remains could be detected. This was calculated from the statistical likelihood that human remains would compose 1% of the bone refuse due to the duration of suspected cannibalism at the Alder Creek occupation. Unfortunately, only 85 fragments from Classes IV, V and VI were preserved well enough to undergo histological processing (Robbins and Gray, 2011; Dixon et al, 2010), equalling only 0.005% of the total assemblage at Alder Creek (Robbins and Gray, 2011).

Human bones were identified according to five criteria: a) lack of plexiform bone, b) substantial secondary osteon remodelling, c) Haversian canal diameters between 50um and 100um, d) osteon diameters of 240um to 500um, and e) an osteon density of 1 or 2 osteons per mm^2. Non-human specimens were identified into the categories cervids, bovids, and equids. Based on their results, Robbins and Gray (2011) identified 12 horse, 29 deer and 32 cow fragments.

The breadth of non-human species identified matched those expected according to the historical accounts. The fragments were found with evidence of heavy processing, and further determination of age and number of individuals was impossible (Dixon et al, 2010). Around 95% of the remains had calcined parts, and signs of pot polish abrasion indicate that the animal remains were cooked in cast iron pots (Dixon et al, 2010).

No human fragments could be positively determined from their collection, though the very low representation of the collected fragments suggests that this study cannot definitely rule out the possibility of human remains in the Alder Creek assemblage (Robbins and Gray, 2011; Dixon et al, 2010).

2.5 Research Questions

The analysis of cremated mammalian bones and the effectiveness of using histological methods in determining species origin have already been extensively studied over the past half-century. The necessity for these types of examinations has been demonstrated in a wide variety of forensic and archaeological examples, thus the incorporation of these techniques in bioanthropological and zooarchaeological studies as something routine in any investigation is encouraged. Yet, the crux of assessing these histological features falls into the availability and accessibility of typically expensive and/or specialized equipment.

The validity of using light microscopy is explored in this thesis as a remedy to the problem of limited resources, as this form of microscopy is a staple of most laboratories. The first issue to be addressed is whether histological morphologies are recognizable under light microscopy. Many studies have confirmed the importance of qualitative appearance of histological structures in attempts to distinguish human from non-human origin. The second

component to this thesis is to examine any changes to the dimensions of Haversian structures over increasing temperature exposure. Contradictory results have already been put forth by previous studies in how heat affects the shape and size of osteons. This dissent inhibits the ability to account for these distortions in studies involving cremated remains at unknown temperatures. An attempt to determine when, or if, any significant changes occur in skewing species differentiation will be made by examining heat exposure over three different temperatures.

Chapter 3 – Materials and Methodology

Femoral shafts from deer, pig and cow were prepared for cremation at three temperatures: 600^{o}C, 800^{o}C, and 1000^{o}C. Burned samples, along with unburned controls of the same individuals, were embedded in an epoxy resin and thin-sectioned for analysis. The thin sections were ground down before being mounted onto glass slides. Digital images of the slides were taken using a light microscope with a mounted camera. Histological structures were observed for qualitative analysis. Secondary osteons and Haversian canals were measured for quantitative analysis. Statistical analysis was performed using unpaired *t*-tests to determine whether changes in Haversian dimensions occurred between temperatures.

The processing of all the samples for this experiment was done in the Physical Anthropology laboratory facilities at the University of Alberta under the supervision of Pamela Mayne Correia and Harvey Friebe.

3.1 Materials

3.1.1 Selection of Materials

The selection of mammals for this research depended on the species' abundance in human-related sites, the availability of data from previous studies for comparative analysis, and the relative size of elements to human elements. The white-tailed deer (*Odocoileus virginianus*), the domestic pig (*Sus scrofus domesticus*) and the domestic cow (*Bos taurus domesticus*) were selected on these bases. The presence of domesticated animals in sites associated with humans is well-established across the Old and New World in both archaeological and forensic-focused sites. Other domesticates, such as dog (*Canis familiaris*), horse (*Equus ferus caballus*) and sheep (*Ovis aries*), were also potential species for investigation, but size discrepancies between these

animals and humans made them less preferable to those selected. Despite not being domesticated animals, deer have also been found in numerous human sites, either as a reflection of hunting practices or due to their proximity to human habitation.

Although a number of other mammals have been extensively studied in archaeological and forensic studies, these three were specifically selected for this experiment because the robustness of their skeletal elements will likely survive cremation more readily than those of smaller mammals. Skeletal elements of larger mammals would endure cremation, but in most cases the fragmented bones could be distinguished from human material based on morphology alone. Using mammals of comparative size to humans will test whether pre-established histological techniques can still be applied to cremated remains in cases where other methods of differentiation are eliminated (i.e., size and morphology of fragments would not be applicable in an actual examination).

Each species examined was represented by five individuals, one element per individual, for a total of five femora. The pig and cow specimens came from a local butcher, and the deer specimens were generously donated by the Alberta Sustainable Resource Development Fish and Wildlife Division. None of the animals used in this experiment died of pathological causes; the pig and cow specimens were presumably healthy enough to pass inspection for processing and consumption, whereas the deer had been collected from hunters or vehicular collisions.

Due to this difference in origin, the freshness of the pig and cow bones were not comparable to the deer specimens, some of which had been collected and processed over twenty years prior to this experiment. Thus, the deer specimens have been categorized as dry while the pig and cow bones are classified as fresh (Table 3.1). The amount of organic material acting as

an accelerant impacts the nature of burning characteristics on bone. Differences in grease and fat content between these two categories were noted while observing the cremation procedure.

In examining the relationship between locomotion and bone microstructure in primates, Schaffler and Burr (1984) were able to demonstrate that the biomechanical load placed on bone influences the patterns of osteon shapes and sizes that can be differentiated between species. For this reason, only femoral specimens were used. The femur is the most robust bone in the mammalian body, reflecting its function as a key weight-bearing site in the skeleton. As discussed in chapter 2, other limb bones and ribs have been examined for histological differentiation. However, the femur is noted as having the highest percentage of unique non-human histological features such as plexiform bone and osteon banding compared to other long bones (Morris, 2007). The physical size of the femur would allow sufficient bone samples for further processing post-cremation. As well, the robusticity of the femur makes it a more suitable candidate for examination in archaeological studies as it stands a greater chance of being preserved when compared to smaller, more gracile elements.

When possible, elements were sided either by using provided records of the specimens or by using visual morphological features. The limitations in the availability of donated specimens prevented the possibility of using elements all from the same side. This is not considered a problem since the elements all come from different individuals, and I am unaware of any evidence suggesting disparities in histological structures between sides in quadrupeds.

Table 3.1 - List of specimens used in experiment.

Specimen	Species	Common	Sex	Age Group	Side	Condition
D1	*Odocoileus virginianus*	White-tailed deer	Unknown	Juvenile	L	Dry
D2	*Odocoileus virginianus*	White-tailed deer	Male	Adult	R	Dry
D3	*Odocoileus virginianus*	White-tailed deer	Unknown	Adult	R	Dry
D4	*Odocoileus virginianus*	White-tailed deer	Male	Juvenile	L	Dry
D5	*Odocoileus virginianus*	White-tailed deer	Female	Adult	L	Dry
P1	*Sus scrofa domesticus*	Pig	Unknown	Unknown	L	Fresh
P2	*Sus scrofa domesticus*	Pig	Unknown	Unknown	R	Fresh
P3	*Sus scrofa domesticus*	Pig	Unknown	Unknown	Unknown	Fresh
P4	*Sus scrofa domesticus*	Pig	Unknown	Unknown	R	Fresh
P5	*Sus scrofa domesticus*	Pig	Unknown	Unknown	L	Fresh
C1	*Bos taurus domesticus*	Cow	Unknown	Juvenile	L	Fresh
C2	*Bos taurus domesticus*	Cow	Unknown	Juvenile	R	Fresh
C3	*Bos taurus domesticus*	Cow	Unknown	Adult	R	Fresh
C4	*Bos taurus domesticus*	Cow	Unknown	Adult	L	Fresh
C5	*Bos taurus domesticus*	Cow	Unknown	Adult	L	Fresh

Disparities based on biological sex have been pursued in human studies (Mulhern and Van Gerven, 1997; Burr et al, 1990) but the underlying reason for the histological sexual dimorphism is presently unknown. No extensive studies on a sexually-dependent difference in other mammalian groups have been found by the author, thus sex will not be considered a factor in the analysis of these specimens.

Age, however, typically plays a role in the appearance of histological features. As mentioned in Enlow and Brown (1956), older artiodactyl individuals display more scattered secondary osteons amongst the plexiform tissue. This can be commonly referred to as a 'replacement' of plexiform bone by dense Haversian tissue. The appearance of additional generations of Haversian systems is correlated with age, forming the basic foundation of histological determination of age in humans (Jowsey, 1966; Currey, 1964; Kersey, 1965). Age in humans is linked to decreases in osteon dimensions but increases in Haversian canal dimensions and osteon density (Hiller and Bell, 2007).

The samples used in this research are a combination of juvenile and adult individuals, with age determination performed by examining the status of epiphyseal closure when present. The individuals selected are arguably representative of the range of ages present in animals found at human-related sites, and since the primary goal is to identify histological structures, age is not considered a factor in these results as well.

3.1.2 Preparation of Specimens

The five deer specimens had been collected from either automobile collisions or hunting expeditions in northern Alberta. The femoral samples had been processed for the removal of soft tissue prior to their donation. Records provided by the Alberta Sustainable Resource

Development Fish and Wildlife Division indicate that the femora were first boiled in laboratory conditions for a few hours in order to loosen the soft tissue. Structural changes in heated bone do not occur until around 285^{o}C (Shipman et al, 1984), and the lower temperatures achieved by boiling are not suspected of impacting the samples. Any remaining soft tissue was then removed through manual processing using scalpels and similar instruments. Once obtained, the deer specimens were stored in laboratory freezers set at -18^{o}C until the experimental procedure could commence.

The pig and cow specimens both came from the same butcher, where substantial meat had been removed prior to donation. Following a similar practice to that used on the deer bone, the pig and cow elements were first stored in the same freezer conditions (-18^{o}C) before thawing overnight in anticipation of maceration. A large boiler was employed to house all elements at the same time to boil initially at ~120^{o}C for twenty minutes, followed by another hour of boiling around 95^{o}C. Any soft tissue left after this process was removed using scalpel and tweezers. The samples were allowed to dry for several days prior to cremation

3.2 Methodology

3.2.1 Labelling Samples

Once each specimen was given a label in accordance to the species of the individual and a sequential number, each element was then segmented into four parts: a control that was unaltered (i.e. unburned), and three equal-sized sections corresponding to each temperature selected for cremation. These thermally-dependent qualifiers were in turn added to the label as a suffix. For example, the sample from Pig 2 burned at 800^{o}C was labelled as P2-2. (Table 3.2). All of the samples were taken from the mid-diaphysis because the cortex is thickest here and this

is the main site for biomechanical strains. The diaphyses of each specimen were cut into four sections 2 cm thick using a handheld reciprocating fine-toothed saw.

3.2.2 Cremation of Samples

Once all material was thawed and ready for processing, controls were set aside while all other samples were burned at their designated temperatures. The oven was pre-heated to the desired temperature, and each sample was placed singly within the oven in a ceramic crucible for 15 minutes. Any fluctuations in the oven temperature were monitored and attributed to heat loss from the door being opened or from combustion of grease (See Appendix A). During a series of burns, each sample was not placed in the oven until the set temperature had been achieved, creating a consistent temperature at which samples were exposed.

The three temperatures used were 600^{o}C, 800^{o}C and 1000^{o}C (Table 3.2). Thompson (2005) states that bone begins undergoing significant morphological changes around 600^{o}C, including fracture formation and pronounced colour changes (Herrmann, 1972b, Shipman et al, 1984). At 800^{o}C, the complete removal of organic material occurs alongside recrystallization (Herrmann, 1972a), and 1000^{o}C is above the temperature at which bone becomes calcined. Two ovens were required for this experiment as one oven was unable to reach 1000^{o}C, even though it was expected to. A Barnstead-Thermolyne Type F62700 Furnace was used for samples burned at 600^{o}C and 800^{o}C, and a Fisher IsoTemp Muffle Furnace was used for 1000^{o}C. Samples were photographed and allowed to cool naturally after removal from furnace. Samples were then embedded.

Table 3.2 – Designations of samples based on temperatures.

Temperature (^{o}C)	Label Suffix
Unburned	C
600	1
800	2
1000	3

3.2.3 Post-Cremation Processing: Embedding, Thin-Sectioning and Grinding

Bone samples were embedded in an epoxy resin using Buehler Epo-Thin Resin and Buehler Epo-Thin Hardener. Smaller samples, namely the deer specimens, were embedded in 3.75 cm disposable plastic mounting cups, while the other samples were embedded in 5 cm disposable plastic mounting cups or 150 mL plastic cups. Due to the large size of the cow sections, even after burning, incomplete sections had to be used in order to fit into mounting cups for embedding.

After the resin had settled, the epoxy pucks were removed from the mounting cups and sectioned using a Buehler Isomet 11-1180 Low Speed Saw and a diamond-tipped Isomet Wafering Blade. Smaller and regular-sized pucks were cut transversely with final sections being between 0.3 – 0.9 mm. Larger pucks were cut first sagittally, and one half was sectioned again transversely to procure a final section between 0.3 – 0.9 mm. Final sections were then glued to glass microslides using cyanoacrylate glue, and ground to a thickness of 60 - 100 μm using a Buehler Ecomet III Polisher/Grinder after the adhesive had dried. Due to the extensive build-up of carbon on the burned samples, coarser Buehler Ultra-Prep Diamond Grinding Discs of 15 and 9 um were used to remove carbon to a sufficient degree for light microscopy.

3.2.4 Microscopy, Photography and Analysis

Processed microslides were examined under a digital light microscope (Leitz Laborlux 12 POL S) at 100x magnification. Images were taken using a Nikon CoolPix 995 3.34MPX, and prominent features were measured using an ocular scale to be later calculated for digital analysis. The computer software program ImageJ was used to measure the areas, perimeters, and minimum/maximum diameters of Haversian canals and secondary osteons (Haversian systems). The scales of the images were set individually by using the converted measurements from the ocular scale. The oval and elliptical selections were used to outline the areas and perimeters of both Haversian canals and secondary osteons. Straight line selections were used to determine the minimum and maximum diameters of Haversian canals and secondary osteons. Measurements could only be accurate to 0.1 μm.

Multiple photographs were taken of representative areas from three sections of the slide: periosteal edge, mid-cortical region, and endosteal edge. Histomorphological features were examined by identifying the type of bone tissue present (or absent, if expected according to previous literature), and its location within the transverse section. When possible, equal numbers of photographs were taken of each region of the cortex for a fair distribution of sampled images. In samples with less visibility, representative images were taken of any visible section of cortical bone.

Slides were included in statistical analysis if multiple Haversian systems were visible. All measurements were made on the digital images. A percentage of slides that did have any observable Haversian systems were calculated to indicate the feasibility of analysing burned material. A minimum of 30 osteons and Haversian canals for each species per temperature were

measured to meet the requirements for adequate sample sizes. Haversian canals were selected if they were found inside osteons that were included in the analysis or had clearly defined outlines. Haversian systems were not selected if the elliptical shape was skewed from an angular sectioning, or if the secondary osteon was partially absorbed. This eliminated many osteons from the study that were present but would be difficult to properly measure for area and diameters.

This thesis measured the areas and the minimum and maximum diameters of secondary osteons and Haversian canals. These parameters were selected for their overall frequency as parameters used in previous literature, as well as having multiple sources relating to the species examined in this study. Other parameters that have been researched by previous studies were not included either because of the scope of this current project, or because certain techniques are useful only for distinguishing between human and non-human individuals.

The measurements from all possible samples were compared using the unpaired *t*-test methods outlined in Ruxton (2006) which assumes unequal variances (otherwise known as Welch's *t*-test). Larger sample sizes ($n \geq 30$) are typically considered to yield greater statistical power and increased precision when estimating unknown parameters of a population. However, small samples sizes ($5 \leq n \leq 15$) were included in the statistical analysis (de Winter, 2013). De Winter (2013) demonstrated the statistical power of Welch's *t*-test for unequal sample sizes and unequal variances when the larger sample is drawn from the population with a higher standard deviation. This assumption was met for all statistical comparisons of small sample sizes ($n \leq 15$). However, caution should be applied to the interpretation of these results as the inclusion of small sample sizes is a relatively recently explored application.

The mean values for samples burned at 600^{o}C, 800^{o}C and 1000^{o}C were compared to each respective species control to determine significant differences associated with temperature within species. Statistical analysis was also performed between species using unpaired *t*-tests to compare the mean values at each temperature.

3.2.5 Classification of Histological Structures

The identification of histological tissue features was based on descriptions provided by Enlow and Brown (1956, 1958) and outlined in Chapter 2 of this thesis. Images and descriptions of histological types detailed in previous literature were also used to corroborate the presence of tissue structures in the examined samples. For histological types that did not match those found in other studies, descriptions from Enlow and Brown (1956) and Francillon-Viellot et al (1989) were used to verify the diagnosis of these new and/or unexpected tissue classifications.

Plexiform bone was identified as the occurrence of multiple layers of brick-like structures that appeared consistently within the image. Other primary vascular tissue forms that appeared in the studied samples also included reticular bone, and laminar bone. Reticular bone was recognizable by irregularly undulated thick bands in primary vascular tissue. Laminar bone (Figure 3.1) was not found in any previous studies looking at pig, cattle and/or deer, and diagnosis of this structure type was based on the classification system of Enlow and Brown (1956). This primary vascular tissue form is defined as broad circumferential lamellae with obvious primary vascular canals. Laminar bone is different than plexiform bone in that there are no brick-like structures present.

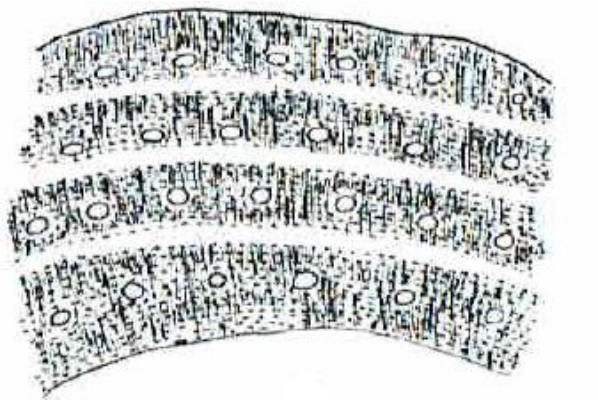

Figure 3.1 – Schematic diagram of laminar bone as outlined in Enlow and Brown (1956: 411).

The category of Haversian tissue is a culmination of the appearance of secondary osteons, whether in scattered or dense forms. Scattered Haversian tissue was defined within this study as the appearance of five or fewer osteons, with each osteon found in relative isolation from other osteons present in the image. Dense Haversian tissue consisted of four or more osteons densely clustered, or exceeding six osteons in total per image. The arbitrary divide between scattered and dense Haversian systems led to a joint category for the ease of identification.

Combination of tissue structures were described if at least 20% of the image displayed examples of a structure type. Tallies of present tissue structures were taken as a means of determining the frequency of structure types, both in combination and in isolated examples.

Chapter 4 – Results

The following chapter will systematically outline the results of the experiment. The qualitative observations on the types of histological structures found at each temperature per species will first be explored. The metric values from histomorphometric analysis and the subsequent statistical analysis from these measurements will be provided alongside tables and graphical representations of the data.

4.1 Processing Samples

4.1.1 Impact of Different Organic Components on Burning Procedure

The initial cremation procedure was carefully observed for any differences caused by extra organic material present in pig and cow samples as opposed to the relatively dry deer samples. The presence of fat and grease in pig and cow samples was associated with a spike in maximum temperatures achieved. Pigs reached maximum temperatures $25^{o}C – 40^{o}C$ above the temperature of exposure at $600^{o}C$, and cows had maximum peaks $10^{o}C$-$30^{o}C$ higher than $600^{o}C$. In comparison, deer samples did not experience any maximum temperatures beyond $612^{o}C$. In all three species, there were negligible differences in the maximum temperatures achieved at the $800^{o}C$ setting.

4.1.2 Gross Morphological Appearances

The external appearances of the samples (Table 4.1) before and after burning were noted, as much of the histological analysis was dependent on the actual preservation and colouration of the burned specimens. The appearance associated with specific temperatures will be discussed in the descriptions below.

Table 4.1 – Gross morphological changes associated with each temperature.

Temperature (^{o}C)	Description
Unburned	- Yellowish-white colour - various degrees of grease and fat present
600	- Blackened - Charred texture
800	- White exterior with blackened interior - chalky texture - fracture lines
1000	- White with a few samples displaying pink or orange discolourations in interior - broken pieces exhibit black cortex - ceramic-like texture - easily breakable with frequent fracturing

4.2 Visibility of Histological Structures at Each Temperature

When viewed under a light microscope under the same conditions, the majority (32/40) of the burned samples could be visualized well enough to identify which classes of histological structures were present in the unburned control samples. In certain areas of the slides, carbonization was too heavy to allow clear visualization of structures. In 20% of the slides, this carbonization was too extensive to allow histological structures to be visualized in any part of the slide (Table 4.2). As detailed below, this varied with treatment temperature.

Table 4.2 – Burned samples that had reduced visibility of histological structures as a result of carbonization.

Temperature (^{o}C)	Deer	Pig	Cow
600	-	P1, P2, P5	C4, C5
800	-	P4	-
1000	-	P2	-

The total loss of these samples to further analysis, as well as the biases presented by the loss of the majority of the surface areas of all burned samples, result in a skewed representation of the histological structures visible. Any measurements dependent on the structures that are

visible must be acknowledged to be based on a skewed sample. The impact of this problem will be further explored in Chapter 5.

As a consequence of the consistent inability to identify histological structures in comparative processed samples, one cow and four pig samples were not processed for thin-sectioning (Table 4.3). After most of the cow and pig sections at 600°C and 800°C were thin-sectioned with limited useful data generated, it was decided that further sectioning of the few remaining samples for those species and temperatures would not increase data output. This decision was made by comparing the external appearance of the uncut samples to the appearance of those already cut. Similar extensive carbonization made these samples very unlikely to yield useful results if further pursued.

Table 4.3 – List of unsectioned burned samples.

Temperature (°C)	Deer	Pig	Cow
600	-	P3, P4	-
800	-	P2	C5
1000	-	P2	-

In each of the following sections outlining the qualitative results of species at different temperatures, an emphasis is placed on whether histological structures appear in combinations or in isolation. This distinction is made in order to address the importance of analyzing non-human mammalian samples in their entirety because uniform structure types cannot be assumed in any given segment of the sample area. The high frequency of mixed structures reported below is an indication of the diversity and complexity of the artiodactyl bone structure types examined in this study.

4.2.1 Changes at 600^{o}C

The gross morphology of all samples from the three species burned at 600^{o}C followed the appearance outlined by previous literature. The bone was blackened extensively and had a light weight and flaky texture. On a histological level, this blackening appeared as a nearly impenetrable coating of carbonization which obscured most of the cortical region (Fig. 4.1).

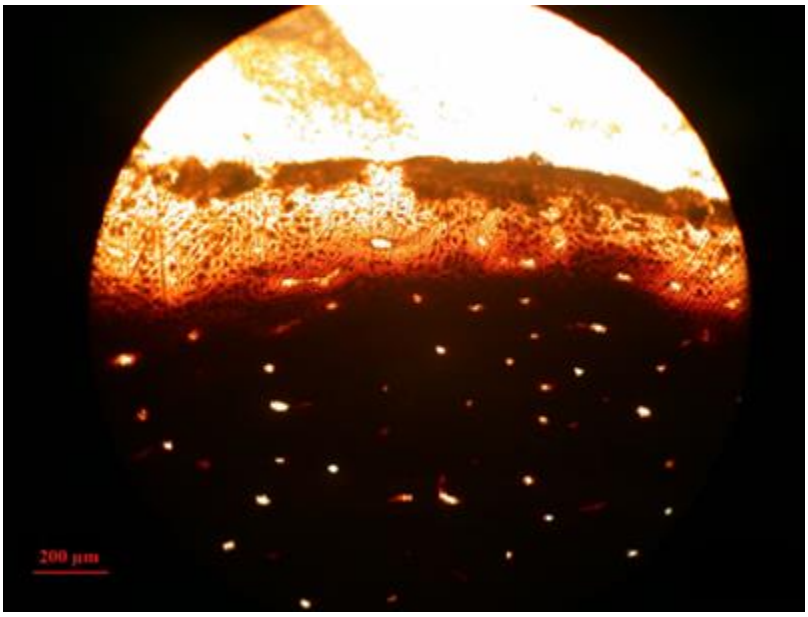

Figure 4.1 – Endosteal region of cow individual (C2) burned at 600^{o}C. Note the predominance of the impenetrable carbonization below in the mid-cortical region. Differences in structure thickness created overexposure of certain areas during microscopic analysis. White areas are patches of overexposure reflecting either empty holes or thin patches of tissue.

The areas where visibility was sufficient for qualitative and quantitative analysis, appeared as pockets of reduced carbonization along the periosteal and endosteal edges. Larger samples, especially in cow and pig, had fracture lines present as a result of cremation. These fracture lines resulted in pockets of visibility, allowing glimpses into the histology of the mid-cortical region of bone which otherwise would be buried under thick carbonization. Despite these adequately exposed areas, the samples at 600^{o}C proved to be the most difficult to process. Five out of the 12 samples were ruled unusable for analysis due to the build-up of carbonization.

Any excessive attempt to grind through the black build-up in these five sections proved to be damaging and resulted in the loss of large portions of the sample.

4.2.2 Changes at 800°C

Similar problems to those encountered at 600°C were posed by the carbonization in the mid-cortical and endosteal areas, leaving visibility open only on the very edges of the endosteal region or surrounding the prevalent fracture lines. At 800°C, the burned samples are heavier than those burned at 600oC, and have a chalky exterior. The white periosteal edge was either more translucent, allowing the observation of histological structures, or had a cloudy effect. This cloudy effect allowed for faint outlines of bone structure to be observed (Fig. 4.2), but the reliability of these outlines for quantitative dimensions could not be assumed. There is a potential to use these cloudy outlines to verify the presence of bone structure types, though it is not preferable if more visible sections are available.

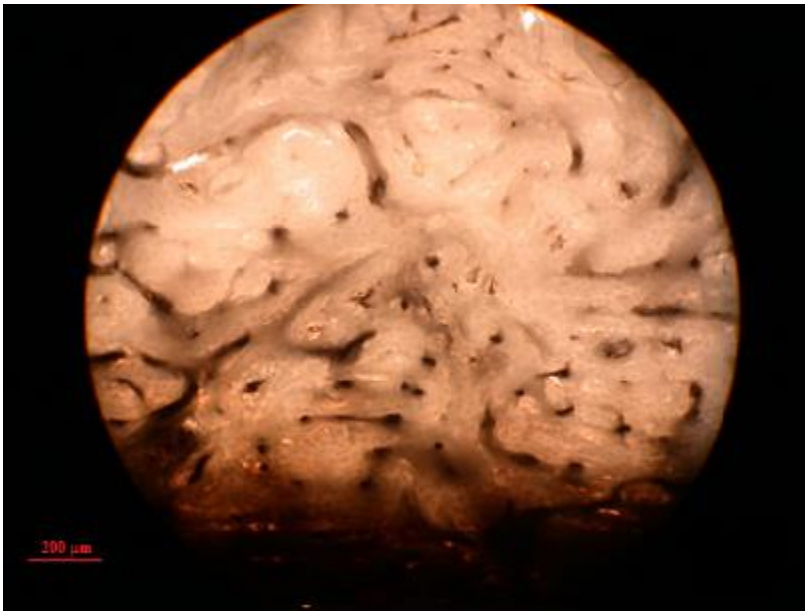

Figure 4.2 - Periosteal region of deer specimen (D1) burned at 800°C. Note the cloudy appearance throughout this slide, though the outlines of reticular bone are still visible.

4.2.3 Changes at 1000°C

Gross morphological appearances of bone burned at 1000°C were consistent with the previous literature. Similar to samples at 800°C, the external colouration was white, while cortical layers appeared black if broken post-cremation; otherwise, all edges were white. Other colours were present besides white; pink was present on the periosteal surfaces of pig bone, while orange-yellow splotches were detected on the endosteal surfaces of deer bone. No significant colours were observed on cow bone. In contrast to those burned at 600°C, the 1000°C samples were dense and ceramic-like in texture rather than light and flaky.

Breakage and fracturing were commonplace amongst the samples burned at 1000°C. Several samples fragmented into multiple pieces during cremation. Others had cracks that were present upon removal yet remained intact. These cracks either expanded during cooling and resulted in multiple fragments, or did not cause further damage to the sample. For the slides composed of multiple pieces, more histological structures were made visible around the exposed edges surrounding these fractures. The area surrounding fractures, and the edges of cortical bone, had better visibility because of the reduced carbonization. This carbonization reduction was a combination of organic material being burned away at the edges, and the increased exposure during grinding. This pattern and the colouration were similar to those at 800°C, and allowed for a surprising amount of bone surface to be visible for analysis (Fig. 4.3). As well, the duration of grinding to remove excess carbonization seemed diminished compared to samples at 600°C.

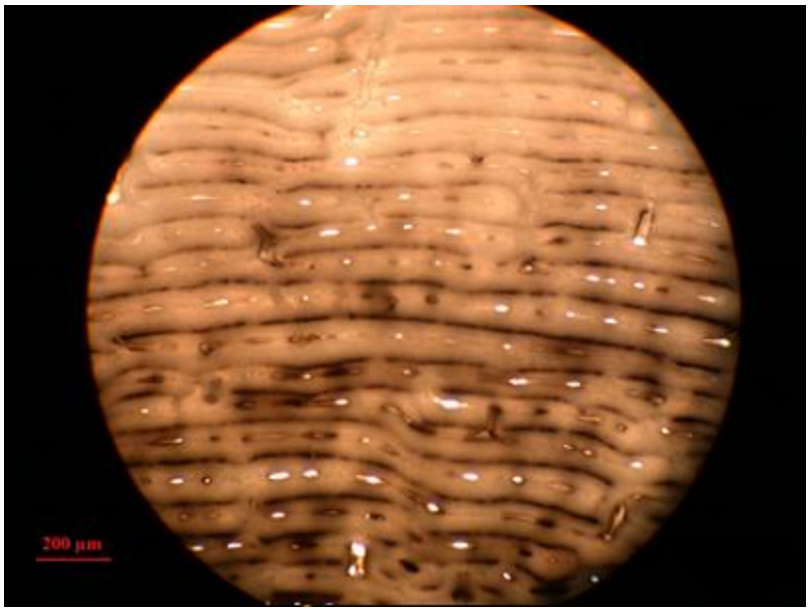

Figure 4.3 - Periosteal region of pig individual (P2) burned at 1000^{o}C, clearly displaying plexiform structure despite slight cloudiness. Note that the white areas are patches of overexposure indicating empty holes or thin patches of tissue.

4.3 Description of Histological Structure Types by Species

4.3.1 Deer

4.3.1.1 Control

Five specimens of deer were analyzed as controls, with 28 representative images taken cumulatively. Two dominant bone structure types were present throughout the deer samples: plexiform structure and Haversian structure. Plexiform structure was present in 18 of the 28 images, though it only appeared in isolation eight times (Fig. 4.4). Ten images displayed a blend of plexiform and Haversian structure (Fig 4.5), while eight showed exclusively Haversian structure (Fig. 4.6). A different structure type, reticular bone, was also observed in two images found in the specimen D4 (Fig. 4.7); this structure was found in conjunction with either plexiform or Haversian structure rather than occurring alone.

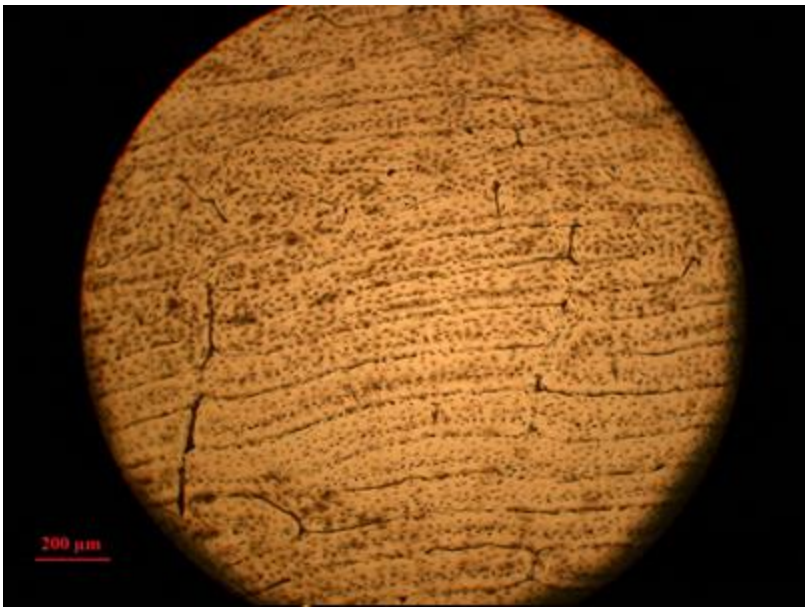

Figure 4.4 – Plexiform structures present in mid-cortical region of unburned deer specimen (D1).

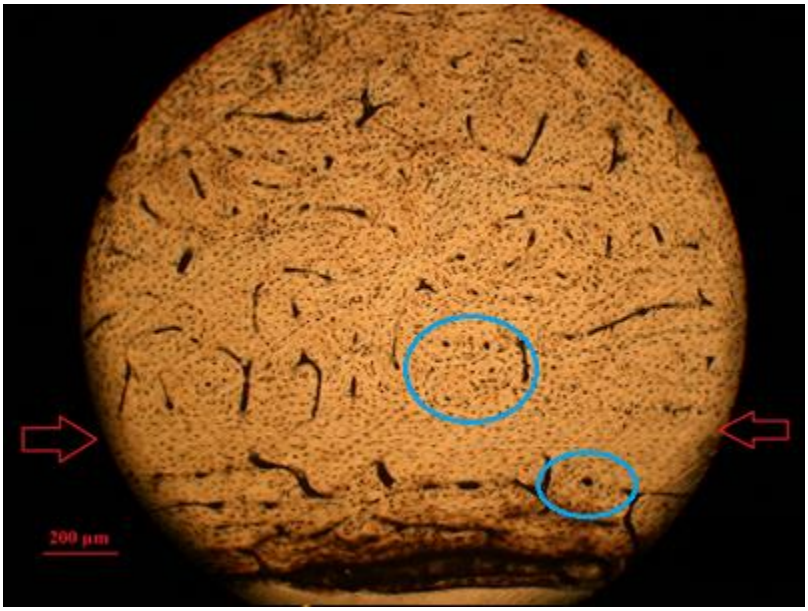

Figure 4.5 – Blend of plexiform (indicated by red arrows) and Haversian structures (blue circles) present in unburned deer specimen (D4) in the mid-cortical area.

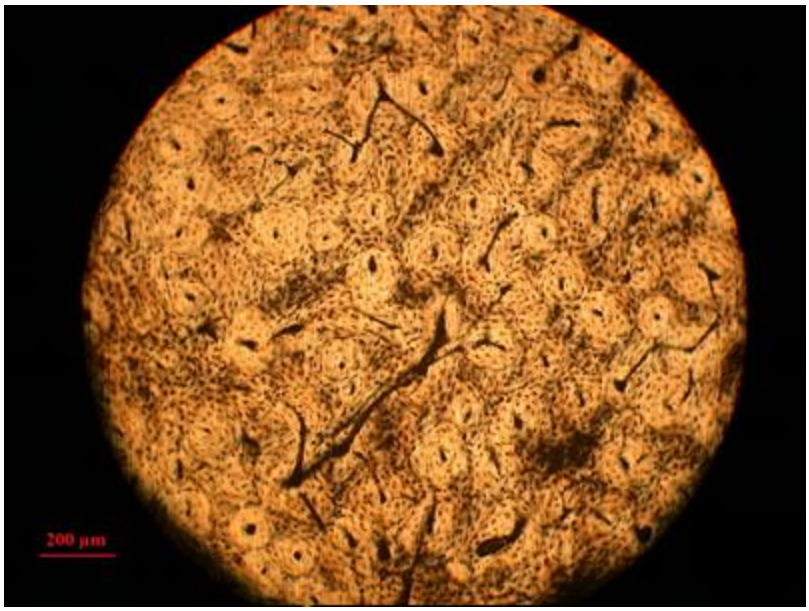

Figure 4.6 – Dense Haversian structures present in the mid-cortical region of unburned deer individual (D5).

Figure 4.7 – Presence of reticular (R) structure in conjunction with Haversian (H) structures in the mid-cortical region of unburned deer individual (D4).

Each sample was analyzed in three divisions: periosteal area, mid-cortical region, and endosteal area. Most of the periosteal area was made up of plexiform structures. The other two areas showed mixtures of plexiform and Haversian structure, though the frequencies differed.

The mid-cortical region had predominantly Haversian structure, while the endosteal edges had equal distribution of plexiform and Haversian structure.

4.3.1.2 600°C

The visibility of histological structures in the controls stands in stark contrast to the samples burned at 600°C due to the extensive carbonization present over the exposed surface area of the sample slides. As a result, the majority of the images taken for the 600°C treatment were confined to the periosteal area of the bone. Given the patterned distribution of structure types noted above, this limited the structure types available for analysis. As outlined, below, this problem was not restricted only to this temperature or to deer samples, and it raises the question of the validity of using burned material for statistical analysis given that random sampling of structures cannot occur as it would under normal conditions.

Of the 24 images taken, 12 are in the exposed periosteal region. Overall, plexiform structure is the predominant form seen at 600°C. However, because observations made on the controls show that this is the dominant type in the periosteal region, this predominance is likely due to the restricted fields of vision.

Ten of the 24 images show osteons in combination with plexiform or primary vascular structure, and reticular structure is seen at 600°C in the same individual that displays it in the control. However, the rest of the comparisons to the control group show discrepancies. Only one image has Haversian structure in isolation at 600°C while the control of the same specimen had predominantly Haversian structure. This is likely because only five images taken at 600°C display structure from the mid-cortical region of bone, where more diversity in structure types is typically found.

The reduced clarity imposed by the carbonization led to confusion in proper classification of primary vascular structure, under which plexiform and reticular bone are categorized. Twelve images were identifiable only as primary vascular structure without any distinguishing features to differentiate between reticular or plexiform bone. Secondary osteons may appear sporadically or not at all in primary vascular structure (Enlow and Brown, 1956).

Of these 12 images, three were alternatively labelled as laminar bone (Fig. 4.8, Enlow and Brown, 1956), and laminar structure also appears in conjunction with the other primary vascular structure forms (i.e. plexiform and reticular) in two images. Since laminar structure was not identified in the controls, this may reflect a misleading appearance where another type of primary vascular structure takes on the appearance of laminar bone due to interference of carbonization.

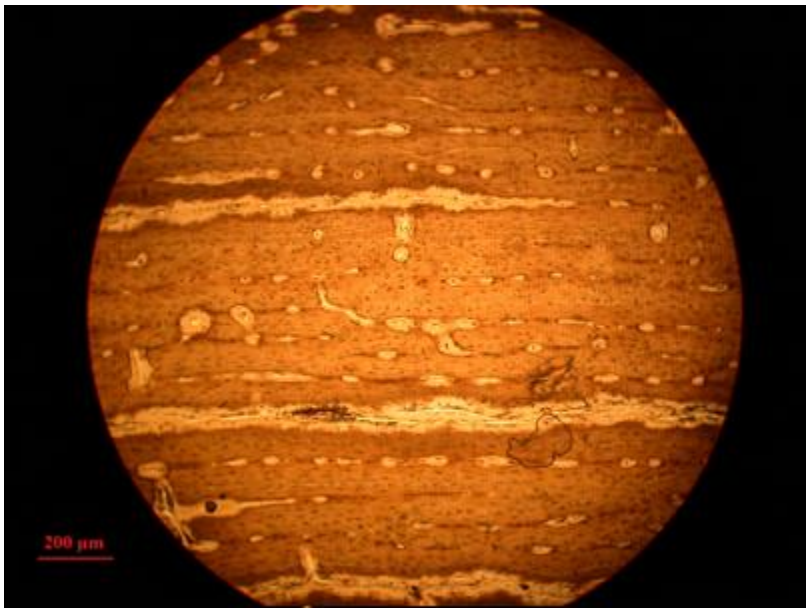

Figure 4.8 – Laminar-like bone as detected in the mid-cortical region of deer individual (D3) at 600^{o}C.

4.3.1.3 800°C

The frequencies of Haversian structure and plexiform structure observed at 800°C were evenly split at 19 and 20 images respectively out of 32 images analyzed. Only seven out of 32 images displayed mixed structure types, which stands in contrast to samples at lower temperatures which had higher ratios of combined plexiform and Haversian structure. As well, only plexiform or Haversian structures were detected; no reticular bone was visible (as in controls), nor any other derivative of primary vascular canal structure (as described at 600°C).

The carbonization present at this temperature restricted visibility in the mid-cortical region to only two images, while another ten images were taken of the mid-cortical area alongside the periosteal or the endosteal edges. Thirteen images were taken from the endosteal region, while the majority came from the exposed areas at the periosteal edge. By a slight majority, most structures present in the endosteal region are plexiform. Periosteal structures were evenly split between the 17 images taken. Ten images showed plexiform and 10 images also displayed Haversian structure; some slides showed evidence of both structures. The distribution of structure types followed the pattern outlined in the controls, though the limitations in the mid-cortical region affect the proportion of structures.

4.3.1.4 1000°C

At the highest temperature, the lowest ratio of mixed plexiform and Haversian structure was present at only six out of 26 images. Otherwise, the distribution of structure types is similar to those displayed at lower temperatures: plexiform structure is still the most prominent, seen in 18 out of 26 images, while Haversian structure appeared in 14 out of 26 images.

Interestingly, the samples at 1000°C bore a resemblance to those at 600°C in the apparent presence of laminar bone in the same specimen that displayed it at the lower temperature, D2 (Fig 4.9). However, no laminar structure is visible in D2 at 800°C or in the control sample for D2.

In contrast to the samples at 800°C, laminar structure was the only other primary vascular structure besides plexiform identifiable at 1000°C. Again, the problem of carbonization arises, presenting the challenge of discerning between legitimate laminar bone and misidentifications caused by misconstruing the canals of Haversian systems for primary vascular canals or the layered outline of plexiform bricks for the concentric beams seen in laminar bone.

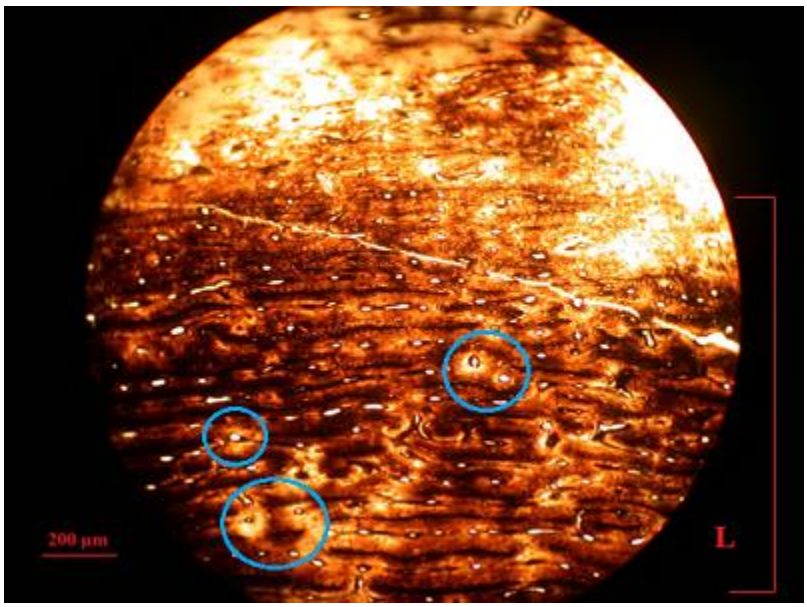

Figure 4.9 – Laminar-like structures (L) with scattered Haversian structures (blue circles) as detected in the mid-cortical and endosteal regions of deer specimen (D2) at 1000°C. The white areas are patches of overexposure resulting from empty holes or thin patches of tissue.

Carbonization continued to impact the visibility of histological structures at 1000°C. As mentioned previously, the bone segments still retain the blackened interior representative of cremated bone while the white edges from calcination are broader at 1000°C. This extended area

of translucency made it possible to examine broader swaths of mid-cortical region. As a result, images taken from the mid-cortical area were not underrepresented at this temperature, unlike the situation seen at 600 and 800^{o}C. Twelve images out of 26 were taken of the mid-cortical region. Of these, one was not in conjunction with an overlapping area from the periosteal edge and five were not in conjunction with overlapping areas from the endosteal edges. This greater visibility contributed to a more representative overview of the proportion of structure types at the three levels of cortical bone.

4.3.2 Pig

4.3.2.1 Control

Although the sampling protocol provided five control specimens, the first specimen, P1, was initially damaged during the thin-sectioning stage. Thus only four unburned pig specimens were processed for microscopic analysis. Fortunately, sufficient data were gleaned from these four to show representative structure from pig.

The most prevalent structure type found was a combination of plexiform and Haversian structures, seen in 16 out of the 31 images taken. Isolated structure types were the least common, with a cumulative total of six out of 31 images. Of these six, three images showed Haversian structures, two plexiform structures, and one reticular structure (Fig. 4.10). Reticular bone was found in combination with Haversian structure in two images, and alongside plexiform bone in five images. Trabecular bone was present in two of the specimens examined, though their inclusion did not impact any further analysis.

All three structure types in pig were found within the three regions of cortical bone, indicating that no structure type is contained in one area. Reticular bone was most common in periosteal areas (six out of eight images); the other two examples were found in the endosteal

and mid-cortical areas. The majority of the endosteal areas were composed of a combination of plexiform and Haversian structures. The mid-cortical region contained a similar distribution of mixed structures (primarily combined plexiform and Haversian structures).

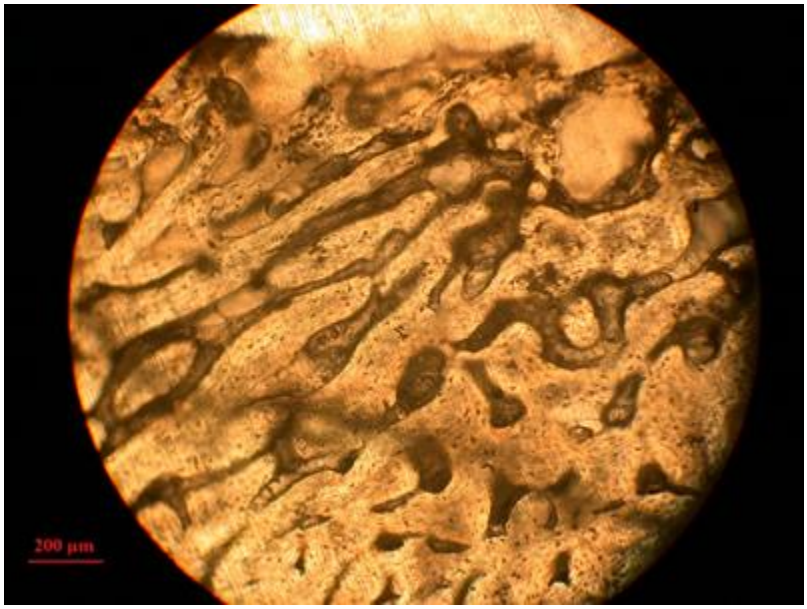

Figure 4.10 - Isolated reticular structure as found in the periosteal region of unburned pig individual (P2).

4.3.2.2 600^{o}C

As described above, only three specimens of pig (P1, P2 and P5) were analyzed at this temperature due to problems in identifying histological structures obscured by extensive carbonization. Any attempts at reducing the carbonization in P1, P2 and P5 were unsuccessful, due either to inability to penetrate the carbon accumulation or destruction of any remaining bone structure by the grinding procedure. As a result, only nine images were procured.

Even in the small patches of visibility, confident identification of histological structures was not achieved (Fig. 4.11). Three images were tentatively identified as showing Haversian structure based on the presence of possible Haversian canals. Another two images suggested possible reticular structure, but again these classifications should be considered tentative. It was

thus concluded that at 600°C, any attempt at histological analysis of the pig samples would prove to be unsuccessful.

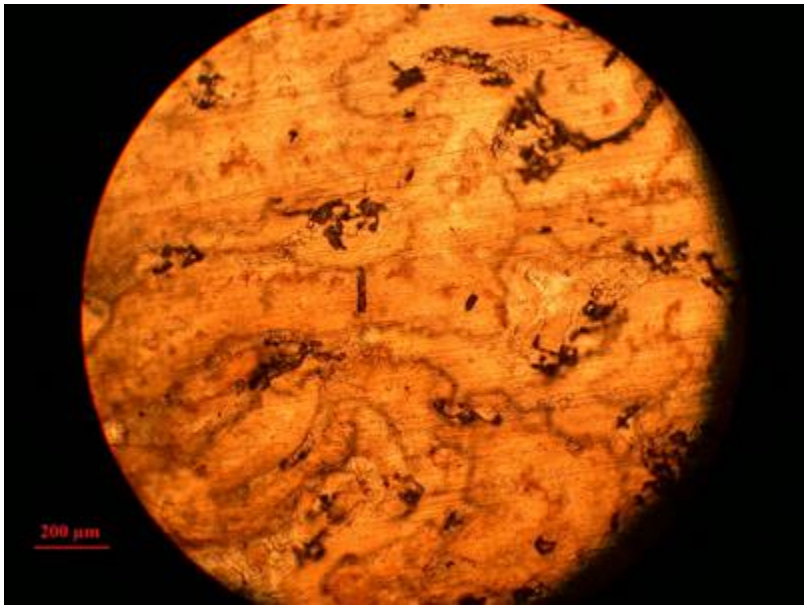

Figure 4.11 - Mid-cortical area of pig individual (P5) burned at 600°C. Note that even after carbonization has been reduced, no histological structures are recognizable.

4.3.2.3 800°C

As outlined above, only four samples (P2 through P5) were processed and analyzed at 800°C. Porosity posed a further problem in four of the images taken, with the result that one entire sample (P4) could only be described in terms of the presence or absence of Haversian systems (Fig. 4.12).

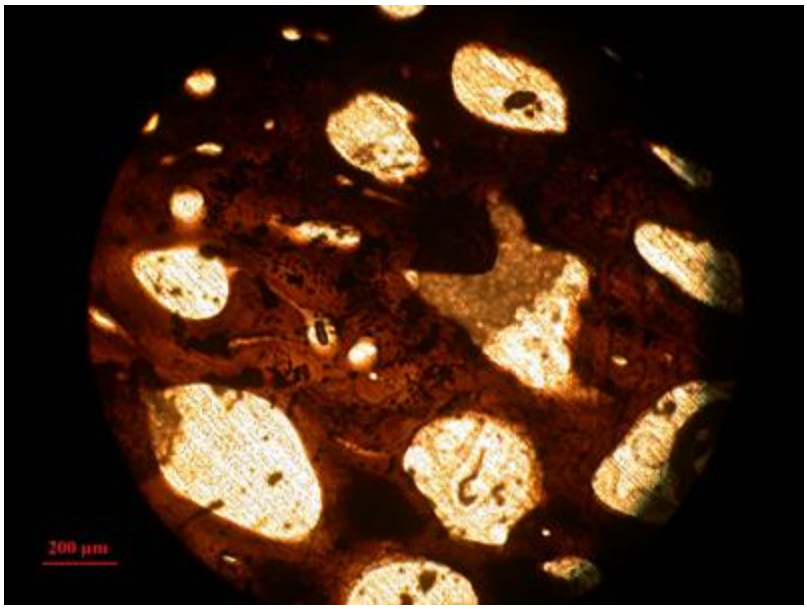

Figure 4.12 - Extensive porosity in the endosteal region of pig individual (P4) at 800°C. Because of the interference of the empty spaces, histological structures could be described only in terms of the presence of Haversian systems.

At this temperature, plexiform bone in isolation occurred rarely, being seen in only two out of 23 images. In combination with reticular structure, plexiform was present in an additional four images. Reticular bone appeared in a total of seven images, with only one of these showing it in isolation. Haversian structure was detected in 17 images: nine in isolation, four with reticular structure, and four with plexiform bone.

The three regions of cortical bone were equally represented amongst the images, and all structure groupings were distributed evenly throughout the three regions, showing no specificity in appearance in any one area. Despite the limitations imposed by carbonization, the patterns of structure distribution were consistent with those expressed in the controls.

4.3.2.4 1000°C

All five specimens of pig were analyzed at the highest temperature. Forty-four images were taken, though carbonization made it difficult to discern in detail the difference between plexiform and Haversian structure. In a number of images, the pattern of remnant carbonization vaguely resembles the network of plexiform bricks, although the frequent presence of Haversian systems undermines the confidence in identifying these as areas of plexiform structure (Fig. 4.13).

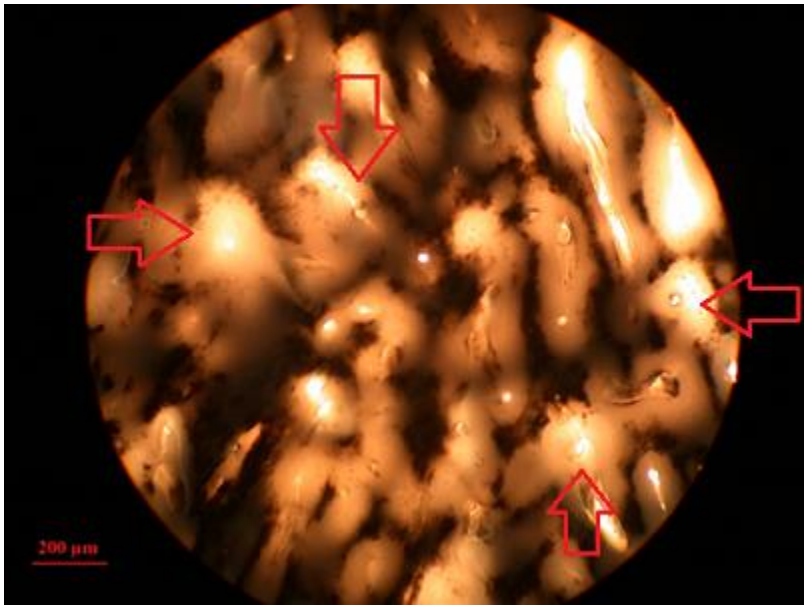

Figure 4.13 - Carbonization (black) and melted hydroxyapatite (grey) obstruction of the detail of histological structure features in pig individual (P2) at 1000°C. This particular image was categorized as Haversian structures, although the carbonization and melting prevent visualization of other structure types. The white areas are patches of overexposure either from empty holes or thin patches of tissue.

Besides the difficulties in visualization that can be attributed to carbonization, the porosity of bone at this temperature also made it difficult to identify structure types in a few images (three out of 44). This did not pose any problems in the other two species examined in this thesis, so can be considered a unique difficulty of cremated pig bone in this study (Fig. 4.14).

Despite these two issues, all 44 images underwent structure classification to the extent possible. Half of these images featured a combination of plexiform and Haversian structure. Fourteen out of the 44 images demonstrated Haversian structure only, while plexiform structure appeared in isolation in eight images. No reticular structure was detected, though this may be in part due to the obstruction imposed by carbonization.

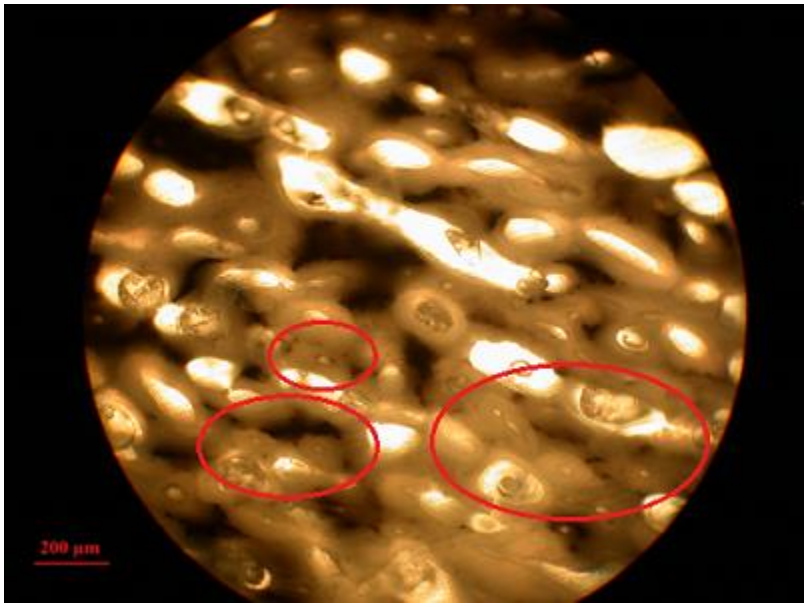

Figure 4.14 - Porosity present in pig bone (P5) burned at 1000^{o}C. This image was identified as showing Haversian structure due to the recognition of Haversian systems, though the porosity may have obscured plexiform or reticular structure.

4.3.3 Cow

4.3.3.1 Control

The physical size of the cow samples made it possible to produce images from a greater area. In each of the five samples examined, equal proportions of the three cortical regions were photographed for a good representation of the structure types available in cow.

Three structure types were described in the unburned cow samples analyzed: plexiform structure, Haversian structure, and non-vascular structure. This latter structure was found only in cow specimens (Fig. 4.15), a finding that is consistent with previous literature. Out of the 40 images taken, 22 images showed Haversian structure exclusively. Only four images were of isolated plexiform structure, and three images showed only non-vascular structure. The most prevalent combination was plexiform and Haversian structure (seven images), followed by non-vascular and Haversian structure (four images). No combinations of plexiform and non-vascular structure were found.

No non-vascular structures occurred in the mid-cortical region. The majority of non-vascular structure occurred in the endosteal area (five images), though it was present in periosteal regions as well (two images). Only one image taken in the endosteal region had any plexiform present, and it was admittedly a very small area in comparison to the Haversian structure present in the same location. Plexiform bone was thus split evenly between the periosteal and mid-cortical regions, with five appearances in each. Haversian structure was distributed throughout all three zones.

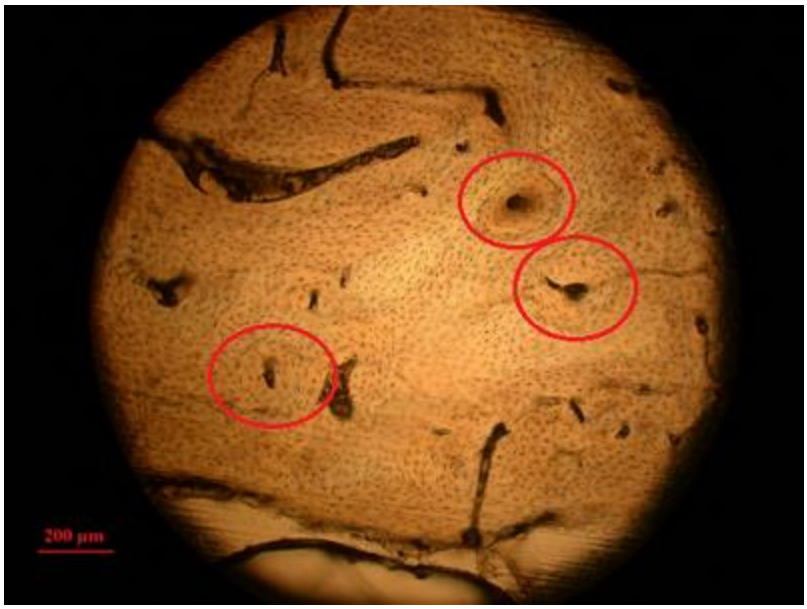

Figure 4.15 - Non-vascular structure present in unburned cow individual (C4). Note the appearance of a few scattered osteons (red circles), which can occur in non-vascularized bone structure.

4.3.3.2 600^{o}C

As described above, five specimens were processed at 600^{o}C for analysis, but two samples, C4 and C5, were too obscured by carbonization to allow definitive results to be produced for structure identification. Only three images were taken from these two samples. The remaining three samples produced 22 images. Qualitative analysis will only be reported from these 22 images.

Plexiform bone in isolation was exceedingly rare in the samples burned at 600^{o}C with only two images out of 22. The bulk of the images contained Haversian structure: 13 out of 22 images showed exclusively Haversian structure, while another nine images contained Haversian structure in combination with plexiform. Seven of these nine instances occurred in one sample, C1 (Fig. 4.16), and this proved to be the only type of structure present in C1. Plexiform structure was predominantly found in the periosteal area, while Haversian structure was more prevalent in

the mid-cortical and endosteal regions. No non-vascular structures were found at this temperature.

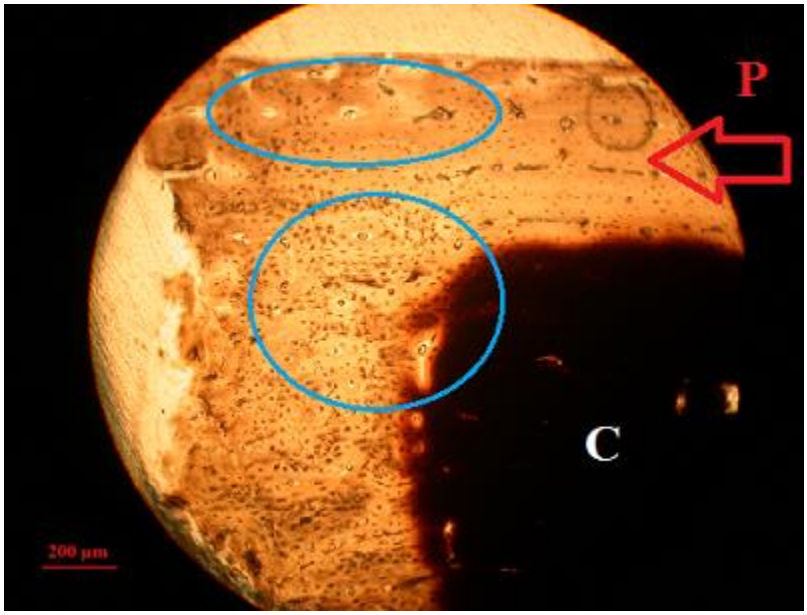

Figure 4.16 – Commingled plexiform (red arrow) and Haversian structures (blue circles) present in the periosteal region of cow sample (C1) at 600°C. The blackened section in the bottom-right shows an impenetrable area of carbonization (C).

4.3.3.3 800°C

Four samples (C5 excluded) were processed at this temperature. Visibility at this temperature was markedly better than at 600°C, though large swaths of carbon still covered much of the mid-cortical zone.

The distribution of structures varied for each sample. The sample C1-2 had plexiform present in eight out of nine of its images, though only two images were exclusively plexiform; the bulk of this sample (five images) was a combination of plexiform and Haversian structure. Sample C2-2 was the reverse, with only one image displaying plexiform structure in conjunction with Haversian structure. The remaining four images were exclusively Haversian structure. Yet again, C3-2 was different, with all four images being exclusively plexiform. This specimen at

600°C and 1000°C was composed almost entirely of Haversian structure, and its control displayed an array of structures, including non-vascular structure. No explanation can be given for the complete reversal of the structure type prevalent at 800°C compared to the other three C3 samples beyond the possibility of Haversian structure being hidden by carbon, though the extent of the plexiform structure (not all of which was photographed) is certainly perplexing.

The sample C4-2 demonstrated only Haversian structure, though this trait is consistent at 1000°C and in the unburned control. This specimen at 600°C was unobservable, thus no comparison can be made between these two temperatures.

Very little of the endosteal region could be analyzed with light microscopy, and only two images were produced. The other two zones both demonstrated similar distributions of Haversian structure and combined structure, though exclusive plexiform structure could only be seen in periosteal areas.

4.3.3.4 1000°C

Of the five samples examined at this temperature, plexiform structure could only be seen in two samples (excluding a sole image from a third sample that was otherwise entirely made up of Haversian structure). This means that out of 32 images, only eight images contained plexiform; of those eight, only three were plexiform in isolation. The majority of plexiform structure was found in the periosteal region; two images contain a combination of plexiform and Haversian structure in the endosteal region, while one other image of the two mixed structures came from the mid-cortex.

The overwhelming majority of images were of exclusive Haversian structure: 24 out of 32 images. With the aforementioned exception of one image, three samples were composed

wholly of Haversian structure. Though the predominance of Haversian structure in cow samples has been established, the absolute exclusion of plexiform structure at 1000^{o}C is surprising.

4.4 Comparisons of Histological Structures between Species

4.4.1 Plexiform Structure

This structure type occurs prominently in all three species examined, but the appearance of the neatly stacked bricks is unique and identifiable to each species.

The plexiform in deer bone is the most distinct of the three. The brick-like cells in deer are narrow and tightly-compressed with very little interstitial space between rectangular rows and individual bricks (Fig. 4.17). Secondary osteons may be present, but are typically contained within the plexus (i.e. the osteons do not disrupt the neat stacked rows of the bricks).

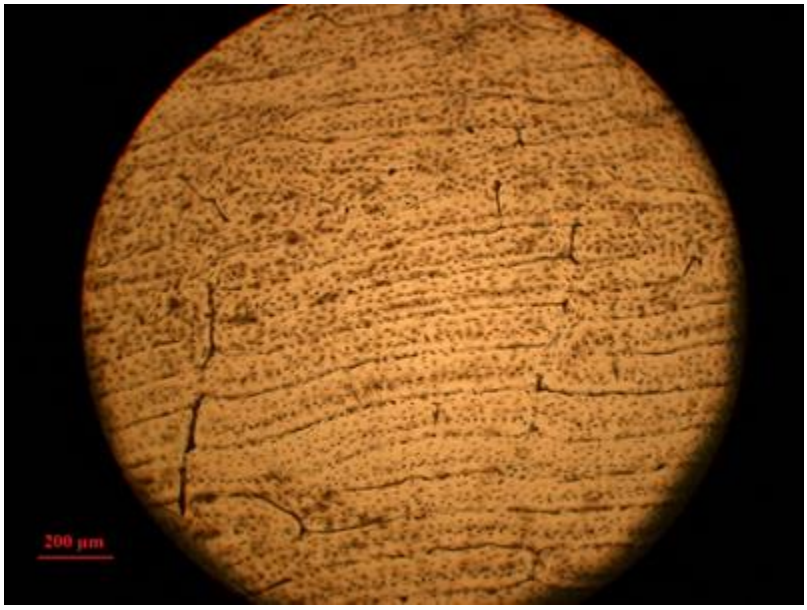

Figure 4.17 – An example of plexiform bone from unburned deer individual (D1). Note how tightly compacted all of the rows of bricks are, with little disruption from osteons.

Pig, on the other hand, is characterized by rounded ‘bricks’ that are commonly found to twist and swerve out of the linear rows typically found in deer. As well, cow plexiform forms are characterized as rounded brick. The spaces between rows are thick and lead to a chaotic organization of stacked ‘worms’ (Fig. 4.18). The clearly defined interstitial spaces can help differentiate pig plexiform structure from cow plexiform structure (Fig. 4.19), which otherwise is very similar in appearance. Secondary osteons occur more frequently in pig or cow than in deer and are more disruptive.

Figure 4.18 – Plexiform bone as found in unburned pig individual (P2). Note the disorganized array of the rows of ‘bricks’ which are rounded and more divided.

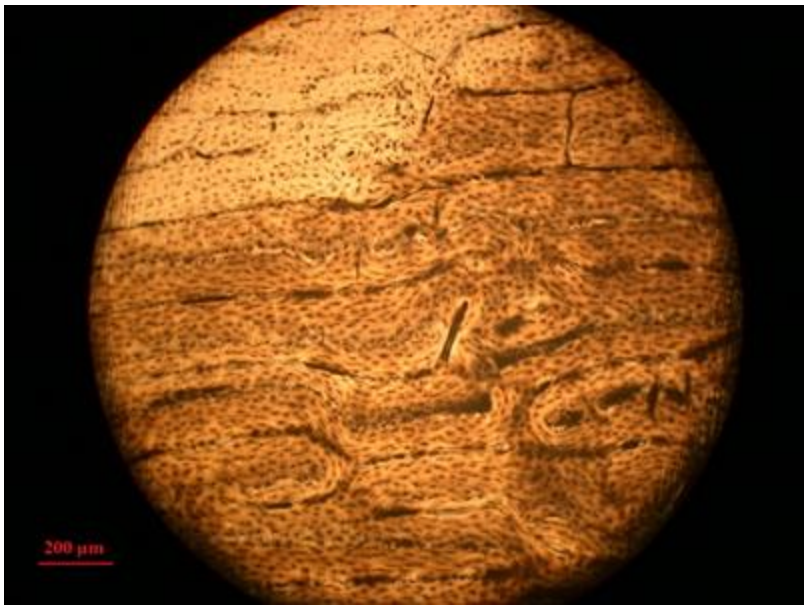

Figure 4.19 – Sample of plexiform structure from unburned cow individual (C5). Note the less defined spaces between rows.

4.4.2 Haversian Structure

Qualitatively, it may be more difficult to differentiate the appearance of secondary osteons between the three species. Deer osteons are the smallest of the three species (Fig. 4.20), and do not have a tendency to overlap (i.e. there is substantial interstitial space). Pig osteons, especially in the control samples, rarely occur separately from plexiform or reticular bone (Fig. 4.21). The interstitial space between pig osteons appears to be the narrowest of the three species, and the relative proportions between the Haversian canals and the Haversian systems seem to be larger, giving the appearance of larger canals than deer osteons of similar dimensions. Cow osteons are the largest and take on an inflated appearance due to their size and relative circularity (Fig. 4.22). However, the biggest differences lie in the metric analysis of the osteons of these species, which will be explored in the next section.

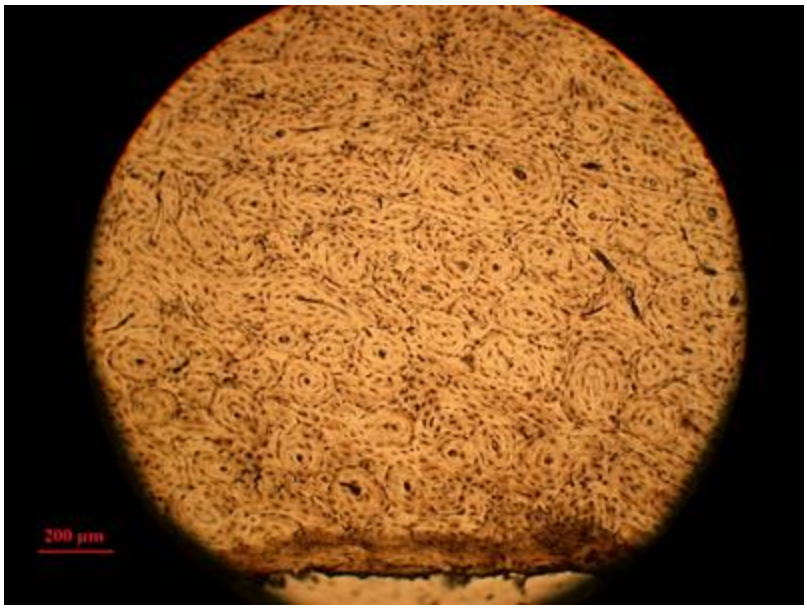

Fig. 4.20 – An example of Haversian structures as seen in unburned deer individual (D2).

Figure 4.21 – An example of Haversian structures alongside plexiform structure in unburned pig individual (P5).

Figure 4.22 – An example of Haversian structures present in unburned cow individual (C4).

4.5 Quantitative Analysis

4.5.1 Selection of Haversian Structures

In any histological section displaying Haversian structures, there will be a large number of secondary osteons and Haversian canals present. For the purposes of histomorphometric analysis, a representative selection of these Haversian structures is necessary to understand any patterns related to changes in temperature. The digital images and any subsequently present Haversian structures that were selected for metric analysis were chosen from the limited visible areas in the burned samples. As mentioned in section 3.2.4, the selection of osteons and Haversian canals for measurement depended on the amount of resorption present in the osteons, and whether or not the associated Haversian canals were distorted based on the angle of sectioning.

Under ideal circumstances, the selection of osteons and Haversian canals in this study would have been more rigorous than currently presented. A checkerboard grid system is a potential approach to equally distribute the selection of osteons and Haversian canals. A fraction of the available squares in the grid would be selected equidistant from each other. A pre-determined number of Haversian structures would be counted within each marked square. This approach was not used because of the restrictions introduced by burning the samples.

Upon thin-sectioning, it became apparent that extensive carbonization would negate any possibility of using a grid layout successfully when the presence of Haversian structures within any marked square could not be guaranteed, thus rendering the spatial selection meaningless. As well, the prevalent occurrence of mixed structure types made it difficult to guarantee equal representation within marked squares. The limitations imposed in the burned samples led to the decision to randomly select osteons and Haversian canals within the control samples in a similar scattered fashion to keep the selected Haversian populations consistent within the study.

Unfortunately, there is no consistent approach in the literature to selecting which osteons and Haversian canals are suitable for measurement. Certain studies chose to measure every possible Haversian system available (Martiniaková et al, 2006b; Urbanová and Novotný, 2005), while others had a set number of osteons selected per slide (Morris, 2007; Crescimanno and Stout, 2011; Cattaneo et al, 2009). Other studies did not detail how osteon selection occurred (Martiniaková et al, 2006a; Zedda et al, 2008; Bradtmiller and Buikstra, 1989). This inconsistency raises the question of whether valid comparisons can be made between the metric values generated by this study and those generated by other studies. Although some comparisons to literature values will be drawn in the discussion, it is important to acknowledge potential

inconsistencies between this thesis and prior studies (and between prior studies) due to varying sampling strategies.

It is acknowledged that any statistical conclusions drawn from the biased metric data generated by this thesis may not be suitable for any future comparative studies examining histomorphometric data. Any inherent bias in the results presented below should be kept in mind in examining the data.

4.5.2 Histomorphometric Analysis

The prevalence of Haversian structures visible for measurement can be determined as a percentage of the total images taken. Out of 55 total samples used in this experiment, 44 samples displayed Haversian structures. This suggests that a clear majority (80%) of the samples can be included in metric analysis. A total of 334 digital images were taken. From these images, nearly 60% displayed Haversian structures. An additional 60% of Haversian structures visible in images of Haversian bone were appropriate for measurements based on the criteria established above. This means that overall, only 35% of the images taken were incorporated in metric analysis. Considering how vital histomorphometric analysis is to species differentiation, these low results suggest that performing these comparisons may not be feasible in burned material.

4.5.3 Deer

A total of 17 deer samples displayed Haversian structures, with 98 osteons and 112 Haversian canals being measured from 36 images. The mean and standard deviation (S.D.) of each histological parameter examined per temperature are summarized in Tables 4.4 and 4.5.

Table 4.4 – Mean values for the dimensions of deer osteons at each temperature level.

Temperature (°C)	Area (µm²)		Minimum Diameter (µm)		Maximum Diameter (µm)		Number of Osteons (*n*)
	Mean	S.D.	Mean	S.D.	Mean	S.D.	
Control	15683.7	4210.5	121.9	17.3	157.1	26.4	35
600	14454.4	3427.3	130.0	16.3	141. 7	27.3	5
800	16711.3	6136.7	124.0	24.9	161.9	31.9	27
1000	13750.1	5609.0	113.6	27.1	148.4	29.3	31

Table 4.5 – Mean values for the dimensions of deer Haversian canals at each temperature level.

Temperature (°C)	Area (µm²)		Minimum Diameter (µm)		Maximum Diameter (µm)		Number of Haversian canals (*n*)
	Mean	S.D.	Mean	S.D.	Mean	S.D.	
Control	332.6	144.0	16.8	3.8	22.9	5.7	35
600	258.2	66.2	14.9	2.9	19.3	2.3	10
800	302.0	149.7	15.9	4.5	22.1	6.7	36
1000	356.9	181. 5	17.7	4.8	24.1	6.3	31

When compared to the other three temperatures, the mean values at 600°C have smaller standard deviations (see Tables 4.4 and 4.5, as well as Figs. 4.23 and 4.24). However, this may reflect the limited number of measureable Haversian structures at 600°C. These graphs demonstrate similar mean values for both the measured osteons and Haversian canals in deer at all temperatures, with substantial overlap in one standard deviation ranges.

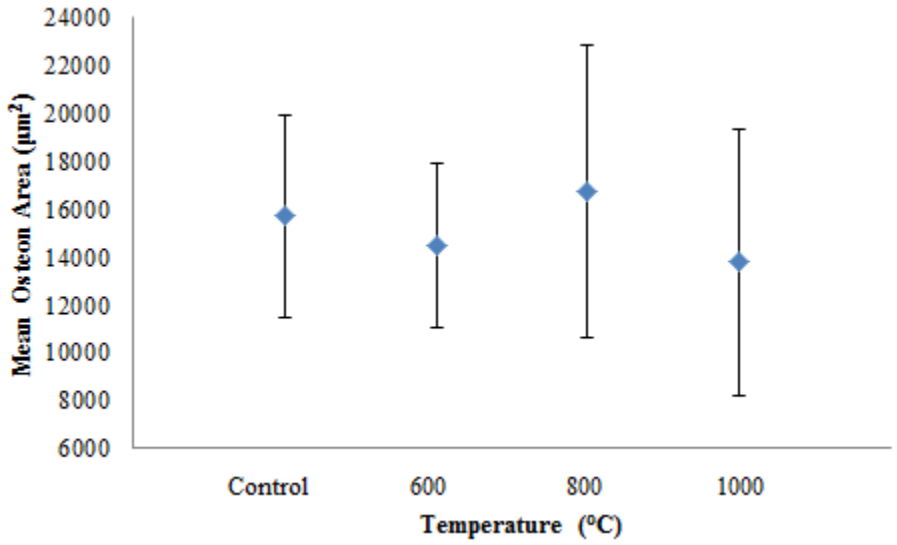

Figure 4.23 – Mean values for deer osteon areas with one standard deviation.

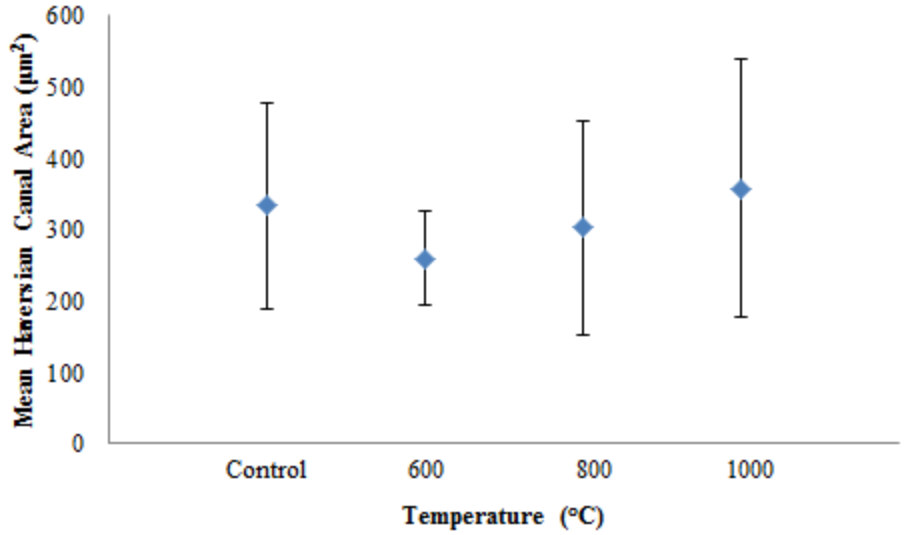

Figure 4.24 – Mean values for deer Haversian canal areas with one standard deviation.

None of the *t*-tests conducted showed any statistically significant differences in the osteon dimensions between any of the temperatures (Table 4.6). Significant differences were found in the maximum Haversian canal diameters involving all *t*-tests with 600°C. Significant differences were also found in the mean Haversian canal areas between control samples and 600°C, and between 600°C and 800°C.

Table 4.6 – P-values for each unpaired *t*-test performed using histological parameters for deer bone between the control samples, 800°C and 1000°C.

Histological Parameter	**Control vs 600°C**	**Control vs 800°C**	**Control vs 1000°C**	**600°C vs 800°C**	**600°C vs 1000°C**	**800°C vs 1000°C**
Osteon Area	0.256	0.437	0.123	0.110	0.694	0.052
Osteon Min. Diameter	0.347	0.696	0.147	0.504	0.097	0.119
Osteon Max. Diameter	0.287	0.512	0.212	0.185	0.632	0.088
Haversian Canal Area	0.027*	0.371	0.552	0.175	0.015*	0.178
Hav. Canal Min. Diameter	0.134	0.387	0.376	0.409	0.042*	0.113
Hav. Canal Max Diameter	5.40×10^{-3}*	0.562	0.454	0.037*	1.323×10^{-3}*	0.213

* - significant values ($\alpha < 0.05$)

4.5.4 Pig

Sixteen pig samples displayed Haversian structures which produced a total of 69 digital images. Fourteen of the samples were used for metric analysis, resulting in 51 osteons and 83 Haversian canals observed from only 29 digital images. At each temperature grade, the mean of each histological parameter was calculated (Tables 4.7 and 4.8), along with each respective standard deviation. Note that no Haversian structures were measured in any of the 600°C samples due to poor visibility.

Table 4.7 – Mean values for the dimensions of pig osteons at each temperature level.

Temperature (°C)	**Area (µm²)**		**Minimum Diameter (µm)**		**Maximum Diameter (µm)**		**Number of Osteons (*n*)**
	Mean	**S.D.**	**Mean**	**S.D.**	**Mean**	**S.D.**	
Control	21318.6	8297.8	143.1	27.1	178.0	37.2	37
600	N/A	N/A	N/A	N/A	N/A	N/A	0
800	15831.7	3909.9	123.7	17.9	157.0	20.0	5
1000	15871.5	5179.5	120.2	21.4	168.1	34.1	9

Table 4.8 – Mean values for the dimensions of pig Haversian canals at each temperature level.

Temperature (°C)	**Area (µm²)**		**Minimum Diameter (µm)**		**Maximum Diameter (µm)**		**Number of Haversian Canals (*n*)**
	Mean	**S.D.**	**Mean**	**S.D.**	**Mean**	**S.D.**	
Control	481.3	332.4	19.8	6.4	27.9	8.6	37
600	N/A	N/A	N/A	N/A	N/A	N/A	0
800	431.5	172.1	19.2	7.0	25.6	5.9	16
1000	408.4	266.2	18.4	5.3	27.7	7.8	30

As seen in Figures 4.25 and 4.26, an apparent pattern can be seen in the mean osteon areas of the control samples and the 800°C and 1000°C samples: the mean osteon area of the control samples was larger than the two mean values seen at 800°C and 1000°C. In contrast, the graphical representation of the mean Haversian canal areas shows no apparent differences between the three temperatures.

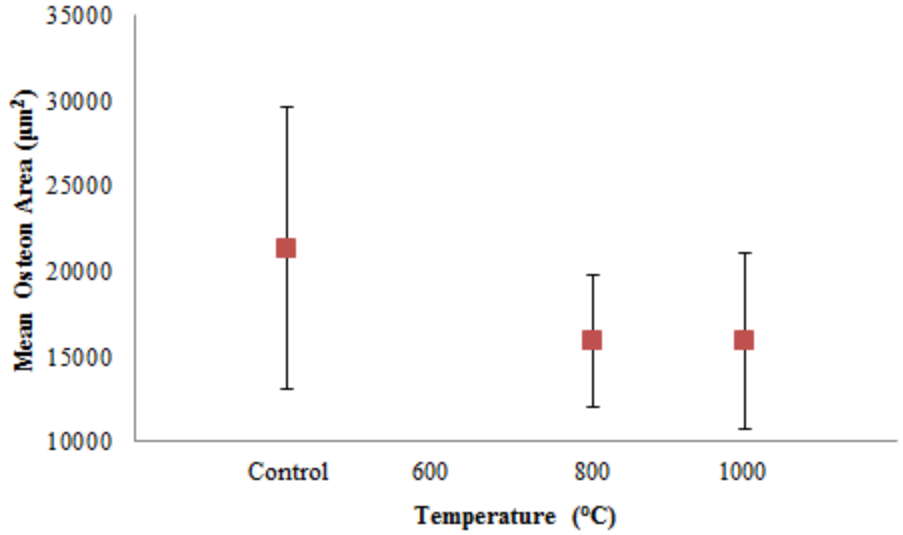

Figure 4.25 – Mean values for pig osteon areas with one standard deviation.

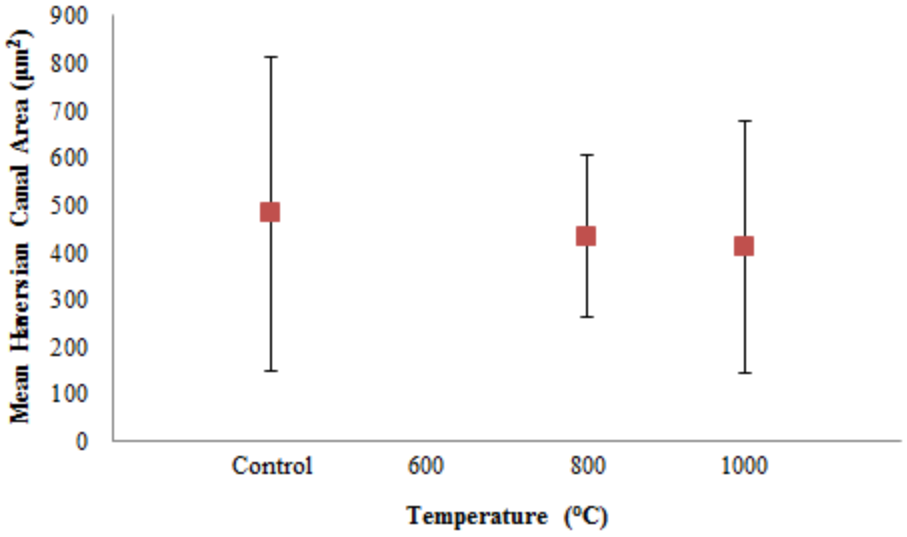

Figure 4.26 - Mean values for pig Haversian canal areas with one standard deviation.

Small sample sizes were collected at 800°C and 1000°C to allow unpaired *t*-tests to be performed for all pig Haversian measurements (Table 4.9). There were significant differences in the mean osteon areas between control and 800°C, and between control and 1000°C. There were only significant differences found between the maximum osteon diameters in the control samples and the samples at 1000°C; there were no significant differences in minimum osteon diameters

for any temperatures. Statistical analysis on pig Haversian canals determined that there were no significant differences of Haversian canal dimensions between any of the temperatures.

Table 4.9 – P-values for each unpaired *t*-test performed using histological parameters for pig bone at all temperatures excluding 600°C.

Histological Parameter	Control vs 800°C	Control vs 1000°C	800°C vs 1000°C
Osteon Area	0.033*	0.023*	0.987
Osteon Min. Diameter	0.074	0.016*	0.746
Osteon Max. Diameter	0.087	0.459	0.458
Haversian Canal Area	0.487	0.326	0.728
Haversian Canal Min. Diameter	0.792	0.341	0.691
Haversian Canal Max Diameter	0.276	0.913	0.322

* - significant values ($\alpha < 0.05$)

4.5.5 Cow

Sixteen cow samples had histological structures available to measure. Out of the 119 digital images taken of cow samples, 99 displayed Haversian structures. All measurements performed on osteons and Haversian canals came from 54 images which amounted to 161 osteons and 177 Haversian canals included for analysis. The mean and standard deviation for each examined parameter are presented in Tables 4.10 and 4.11.

Table 4.10 – Mean values for the dimensions of cow osteons at each temperature level.

Temperature (°C)	Area (µm²)		Minimum Diameter (µm)		Maximum Diameter (µm)		Number of Osteons (*n*)
	Mean	S.D.	Mean	S.D.	Mean	S.D.	
Control	32454.5	1346.7	180.9	35.8	215.8	46.9	43
600	32613.0	11264.0	178.8	34.6	229.0	38.0	32
800	26410.0	10565.6	160.5	33.1	200.3	47.5	37
1000	26131.6	11524.0	161. 4	40.4	199.0	42.1	49

Table 4.11 – Mean values for the dimensions of cow Haversian canals at each temperature level.

Temperature (°C)	Area (µm²)		Minimum Diameter (µm)		Maximum Diameter (µm)		Number of Haversian Canals (*n*)
	Mean	S.D.	Mean	S.D.	Mean	S.D.	
Control	737.7	444.4	25.5	7.2	33.7	11.0	43

600	757.9	305.1	26.6	5.9	36.4	8.1	44
800	633.4	383.5	24.4	9.7	31.4	9.7	41
1000	679.9	355.1	24.3	7.3	33.6	9.3	49

A pattern emerges when examining the graphical representation of the mean areas for cow osteons (Fig. 4.27). It is apparent that the means of the control samples and the samples at 600°C are very similar to each other, while the samples at 800°C and 1000°C have very similar mean values. Although there is still an overlap amongst all four temperatures, the maximum areas for the control and 600°C exceed those at 800°C and 1000°C, and the minimum areas of 800°C and 1000°C are below those at the lower temperatures. This suggests a change in osteon dimensions in conditions found after 600°C.

The differences between the mean Haversian canal areas were less apparent (4.28). There is a slight decrease in mean values in 800°C and 1000°C as compared to control and 600°C, but not to the same degree as seen in the osteon values.

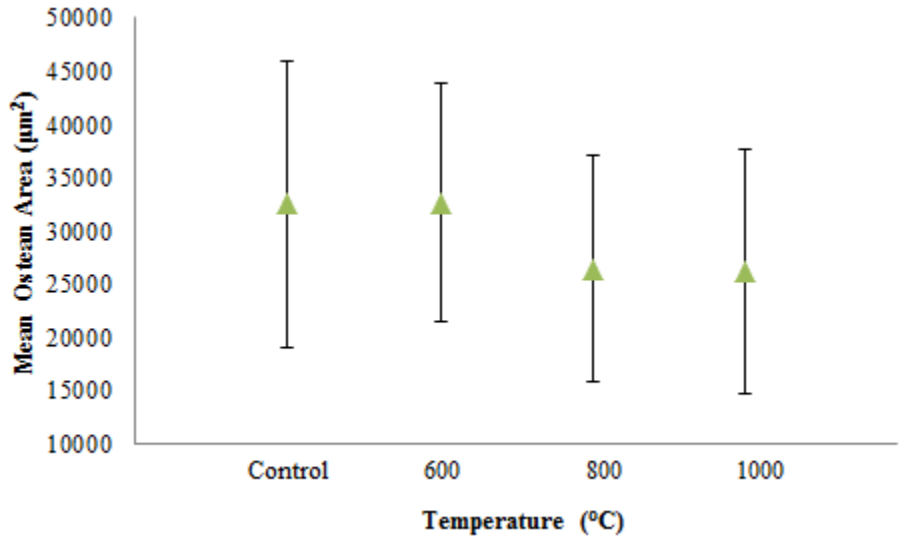

Figure 4.27 – Mean values for cow osteon areas with one standard deviation.

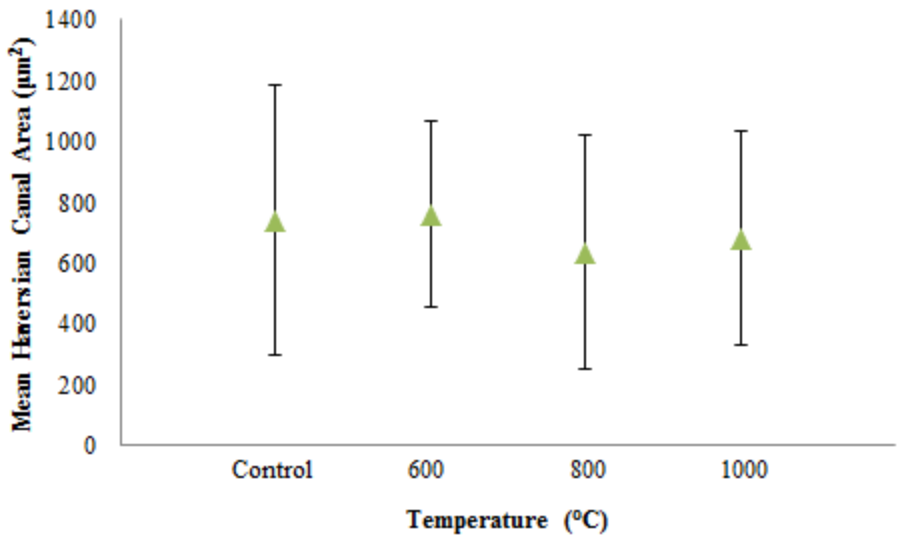

Figure 4.28 – Mean values for cow Haversian canal areas with one standard deviation.

The increased dimensions of cow femora made it possible to observe a large number of Haversian structures, and the minimum of 30 osteons and Haversian canals per temperature was exceeded in all four temperatures. This resulted in *t*-tests performed for all temperatures (Table 4.12). The *P*-values determined in the various *t*-tests indicate a significant difference occurring in all three osteon dimensions after 600°C. On the other hand, Haversian canal dimensions did not show any significant changes between any temperatures except in one case: a *P*-value of 0.012 was found between 600°C and 800°C for the maximum diameters of Haversian canals. An examination of the mean values for maximum Haversian canal diameter at all temperatures indicates that the mean value at 600°C is the highest of the four, while 800°C had the lowest mean.

Table 4.12 – P-values for each unpaired *t*-test performed using histological parameters for cow bone.

Histological Parameter	**Control vs. 600°C**	**Control vs. 800°C**	**Control vs 1000°C**	**600°C vs 800°C**	**600°C vs 1000°C**	**800°C vs 1000°C**
Osteon Area	0.956	0.027*	0.019*	0.022*	0.015*	0.908
Osteon Min. Diameter	0.798	9.680×10^{-3}*	0.016*	0.029*	0.042*	0.910
Osteon Max. Diameter	0.181	0.148	0.076	6.92×10^{-3}*	0.014*	0.894
Haversian Canal Area	0.807	0.252	0.497	0.105	0.260	0.554

Hav. Canal Min. Diameter	0.442	0.531	0.437	0.173	0.099	0.948
Hav. Canal Max Diameter	0.198	0.304	0.950	0.012	0.122	0.278

***** - significant values ($\alpha < 0.05$)

4.6 Statistical Differences between Species

The mean values of osteon (Fig. 4.29) and Haversian canal areas (Fig. 4.30) from each species per temperature were compared amongst all three species in an attempt to visualize the range of areas and to note any overlap in area values. The mean areas of cow Haversian structures were consistently higher than deer and pig values at all temperatures. The mean areas of pig Haversian structures were larger than the deer values at all temperatures, although an overlap between these two species can be seen in the one standard deviation ranges.

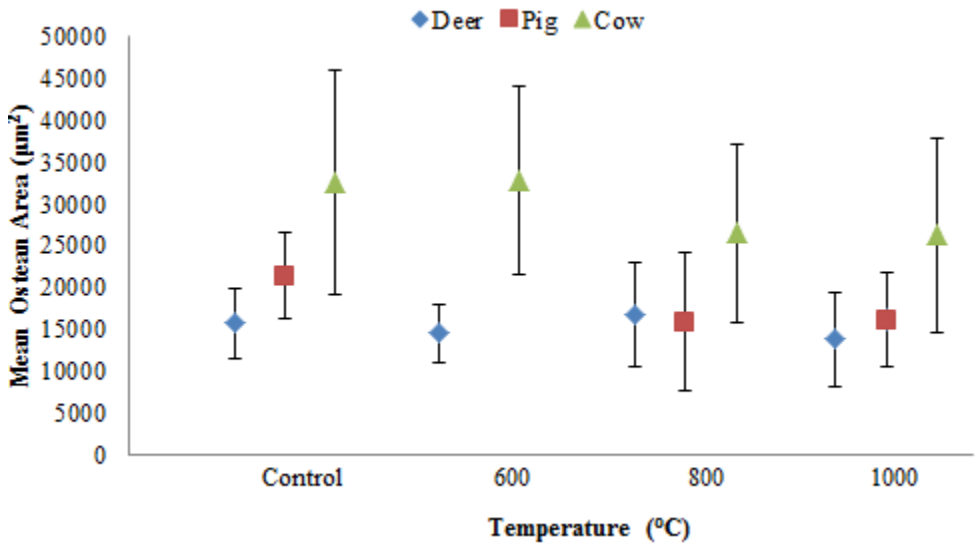

Figure 4.29 – Mean values for osteon areas with one standard deviation for deer, pig and cow samples at all temperatures.

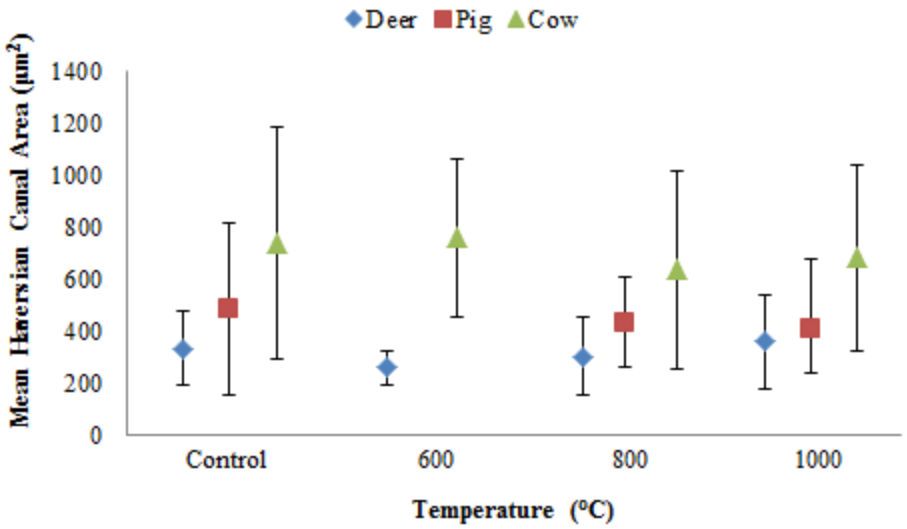

Figure 4.30 – Mean values for Haversian canal areas with one standard deviation for deer, pig and cow samples at all temperatures.

Unpaired *t*-tests were performed between two species at each temperature to determine if there were any statistically significant differences for each Haversian structure parameter examined.

4.6.1 Deer vs Pig

The lack of measured Haversian structures in pig samples at 600°C precluded any statistical analysis at this temperature. The small sample sizes of pig osteons at 800°C and 1000°C allowed for *t*-tests at these temperatures (Table 4.13). For all six parameters, there were statistically significant differences in the control samples, but at 800°C and 1000°C, there were no significant differences. This may be related to the constricted osteon dimensions present in pig samples at 800°C and 1000°C

Table 4.13 – P-values for each unpaired *t*-test performed using histological parameters between the samples for deer and pig bone with the exclusion of 600°C.

Histological Parameter	**Control *P*-value**	**800°C *P*-value**	**1000°C *P*-value**
Osteon Area	5.686×10^{-4}*	0.682	0.307

Osteon Min. Diameter	1.904×10^{-4}*	0.976	0.456
Osteon Max. Diameter	7.558×10^{-3}*	0.659	0.142
Haversian Canal Area	1.762×10^{-2}*	0.017*	0.383
Haversian Canal Min. Diameter	1.840×10^{-2}*	0.106	0.605
Haversian Canal Max Diameter	5.407×10^{-3}*	0.067	0.050

***** - significant values ($\alpha < 0.05$)

4.6.2 Deer vs Cow

The unpaired *t*-tests performed at all temperatures for all six histological parameters demonstrated significant differences between deer and cow samples (Table 4.14).

Table 4.14 – P-values for each unpaired *t*-test performed using histological parameters between the samples for deer and cow bone at all temperature levels.

Histological Parameter	**Control** ***P*-value**	**600°C** ***P*-value**	**800°C** ***P*-value**	**1000°C** ***P*-value**
Osteon Area	3.696×10^{-10}*	3.971×10^{-7}*	1.512×10^{-5}*	1.182×10^{-8}*
Osteon Min. Diameter	7.535×10^{-14}*	3.444×10^{-4}*	2.151×10^{-6}*	5.582×10^{-13}*
Osteon Max. Diameter	1.638×10^{-9}*	4.970×10^{-4}*	1.911×10^{-4}*	1.475×10^{-8}*
Haversian Canal Area	7.268×10^{-7}*	2.637×10^{-13}*	4.104×10^{-6}*	8.864×10^{-7}*
Haversian Canal Min. Diameter	3.111×10^{-9}*	5.402×10^{-9}*	2.653×10^{-9}*	5.243×10^{-6}*
Haversian Canal Max Diameter	4.627×10^{-7}*	2.069×10^{-15}*	3.731×10^{-6}*	5.526×10^{-7}*

* - significant values ($\alpha < 0.05$)

4.6.3 Pig vs Cow

The complete lack of Haversian structures observable at 600°C in pig samples precluded any statistical analysis at this temperature. All *t*-tests that were performed between pig and cow values showed statistically significant differences for all histological parameters (Table 4.15).

Table 4.15 – P-values for each unpaired *t*-test performed using histological parameters between the samples for pig and cow bone with the exclusion of 600°C.

Histological Parameter	**Control** ***P*-value**	**800°C** ***P*-value**	**1000°C** ***P*-value**
Osteon Area	2.440×10^{-5}*	7.17×10^{-4}*	2.18×10^{-4}*
Osteon Min. Diameter	8.197×10^{-7}*	4.93×10^{-3}*	2.13×10^{-4}*
Osteon Max. Diameter	1.362×10^{-4}*	3.47×10^{-3}*	3.22×10^{-2}*
Haversian Canal Area	4.486×10^{-3}*	9.19×10^{-3}*	2.371×10^{-4}*
Haversian Canal Min. Diameter	3.454×10^{-4}*	2.56×10^{-2}*	7.874×10^{-5}*
Haversian Canal Max Diameter	0.010*	1.01×10^{-2}*	3.318×10^{-3}*

* - significant values ($\alpha < 0.05$)

4.7 Summary of Results

4.7.1 Summary of Qualitative Analysis

Carbonization played a large role in the availability of sample areas for observation in all of the burned specimens. Visibility in the samples at 600°C was most affected by the extent of carbonization. The conditions of calcination at 800°C and 1000°C diminished the proliferation of carbonization, although the fogginess caused by melted hydroxyapatite limited the identification of histological structures in certain samples.

Plexiform and Haversian bone were present in all three species at each temperature examined. These two structure types were most often found in combination with each other, although isolated appearances also occurred. Reticular bone was found only in the control samples of deer, and laminar structures present in the burned deer samples. Reticular bone occurred in all of the pig samples except at 1000^{o}C. Non-vascular bone was found in the control samples of cow, but was not visible in any of the burned samples.

4.7.2 Summary of Quantitative Analysis

The histological parameters measured in this study include the areas and minimum and maximum diameters of secondary osteons and Haversian canals. The mean values of each parameter were calculated and presented in tables, while the mean areas of osteons and Haversian canals were displayed in respective graphs. For each species, comparisons were made between the four examined temperatures. Comparisons were made between the three species at each temperature.

The limited visibility due to carbonization impacted the availability of measureable Haversian structures in the pig samples at 600^{o}C. Also, the number of measureable pig osteons

at 800°C and 1000°C were reduced compared to other species, resulting in smaller sample sizes at these two temperatures. Small sample sizes were taken from deer Haversian structures at 600°C.

Data from deer and pig parameters were compared using unpaired *t*-tests except at 600°C. There were no significant differences detected between any of the parameters within deer and pig samples at the two burned temperatures analyzed, although there were significant differences between the control values.

Cow histological parameters were consistently larger than deer and pig values at all temperatures. Significant differences were found for all measurements between deer and cow, and between pig and cow.

Sufficient sample sizes were available at all temperatures for statistical analysis of the cow measurements, allowing an apparent difference to be seen between the mean osteon areas of the controls and 600°C, and those at 800°C and 1000°C. This was verified by unpaired *t*-tests that showed statistically differences between the two pairs of temperatures. Pig samples appeared to follow a similar pattern in that control mean osteon areas were significantly larger than mean osteon areas at 800°C and 1000°C. The lack of Haversian structures measured in pig samples at 600°C precluded any statistical confirmation of a similar pattern to those found in cow samples at 600°C.

Chapter 5 – Discussion

This study set out to determine if qualitative and quantitative analysis of burned mammal remains would be possible using simple light microscopy. The results demonstrate success in identifying various histological structures that can be used for species differentiation and especially for recognizing features that are reported in the literature to be exclusive to non-human individuals. Plexiform structures were found consistently in all three species at each temperature level, indicating that sufficient evidence of this structure remains to be used to determine a non-human origin. Other structure types that can be used to distinguish artiodactyl remains from human remains, like reticular bone and non-vascular bone, were also observed in the three species. Most of the structure types met expectations outlined in previous literature, although a few exceptional cases will be discussed further below in this chapter.

Haversian structures were present in the majority of samples which allowed for histomorphometric analysis under most, but not all, of the cremation conditions. Unfortunately, histomorphometric analysis and statistical analysis was greatly impeded by the abundant presence of carbonization associated with the burning process. The limited visibility of cortical areas restricted the measurement of a representative sample of secondary osteons and Haversian canals. This circumstance led to biased data sets which may not be comparable with prior studies. The underrepresentation of measureable Haversian structures made statistical analysis amongst the pig and deer samples unfeasible at certain temperatures. In light of these biases, the statistical results may not accurately reflect results performed under ideal conditions, but they do provide interesting questions that could be further explored in future research.

5.1 Observations of Histological Structures

Structure types were observed in deer and pig samples that were not consistent with reports on these species in the previous literature, and the lack of visible non-vascular bone in burned cow samples was also unexpected. Carbonization was prevalent at all three cremation temperatures, but was most extensive at 600^{o}C due to residual organic content in the bone. A grey-white cloudiness was apparent in samples burned at 800^{o}C and 1000^{o}C, though this did not prevent the recognition of histological structures. This cloudiness has been described as a result of the melting and recrystallization of hydroxyapatite, a mineral change that has been identified around 700-800^{o}C by Herrmann (1972a; 1977), Shipman et al (1984), and Mayne Correia (1997).

5.1.1 Presence of Laminar Bone in Burnt Deer

The appearance of laminar structures in deer samples at 600^{o}C and 1000^{o}C is inconsistent with previous studies (Foote, 1916; Singh et al, 1974; Owsley et al, 1984; Skedros et al, 2003; Hillier and Bell, 2007; Morris, 2007; Paral et al, 2007) that have not demonstrated any laminar bone in deer. The absence of laminar bone in the control samples and the peculiarity of having this structure type appear in two non-adjacent temperature groups both suggest that laminar bone structure is not actually present in these deer bone sections. It is not realistic to suggest a spontaneous creation of an entirely new structure type present only in burned samples. Rather, alterations caused by heat and the distorted visibility caused by carbonization are more likely culprits for the laminar-like appearance of these sections under light microscopy.

Samples at all cremated temperatures exhibited either limited visibility due to carbonization at the lower temperature or a milky-grey film caused by melted and recrystallized

hydroxyapatite at the higher temperatures. These conditions could potentially have obscured the cement lines of Haversian systems or the brick-like cells of plexiform bone. The loss of these features would result in relatively consistent bands of canals that would appear as primary vascular canals without an encompassing Haversian system, much like the appearance of laminar bone (see Fig. 3.1).

It is important to mention, though, that each thin-sectioned sample does not replicate every possible transverse layer of cortex present in a bone. It is possible that the laminar-like appearance of the burned samples reflect the structure types present at that specific point in the femoral diaphysis, although the complete absence of this structure type in other studies makes this hypothesis unlikely.

5.1.2 Presence of Reticular Bone in Pig Femora

The prevalence of reticular structure in all five pig samples at most temperatures is unexpected, as no other literature has previously cited the presence of reticular bone in pig femora. Only one study cites the appearance of reticular bone in swine (Enlow and Brown, 1958), although this structure type was found in mandible samples of *Sus scrofa* rather than long bones as seen here. The pattern of the structure present in these samples is quite distinctive and matches the examples of reticular bone in Enlow and Brown (1958), leading to a positive identification of reticular structures for this study.

This observation may direct researchers to question how prevalent reticular bone structures actually are in pigs. It is possible that the findings of this study reflect individual variability, and that previous studies simply did not reflect the diversity in pig individuals. Other factors that are not examined in this study such as pathology, age, sex, and activity level could be

explored in other studies in order to gain more insight in the diversity of histological structures in pigs. It is important to note that reticular structures were visible in the controls as well as in the burned samples at 600^{o}C and 800^{o}C. This demonstrates a resilience that makes reticular structures a potential feature in other burned fragments, suggesting that researchers should not rule out swine origin when reticular bone is present in burnt bone samples. It is unknown why there was no reticular bone detected in the 1000^{o}C samples. It could potentially be a matter of sampling selection since the gross morphological appearance of the bone at this temperature is not much different than that at 800^{o}C.

5.1.3 Absence of Non-Vascular Bone in Burnt Cow

The presence of non-vascular structures in the cow control samples was consistent with results published in previous studies (Martiniaková et al, 2006a; 2006b; 2007; Cuijpers, 2006). No non-vascular structure was detected in any of the burned cow specimens, even at 800^{o}C and 1000^{o}C. This finding raises the question of whether non-vascular structure is visible in cremated specimens due to mineral changes undergone by heat-exposed bone, or whether the presence of non-vascular structure is concealed by carbonization.

While it can be assumed that carbonization obscures any sign of non-vascular structures in burned bone, it is necessary to point out that the bulk of the area obscured by carbonization is the mid-cortical region. Other studies (Martiniaková et al, 2006b, 2007) have noted that non-vascular bone does not occur in the mid-cortical region, and results from this study verify these findings (see 4.3.3.1). The most visible areas of burned bone, the periosteal and endosteal edges of the cortex, are also the only areas where non-vascular bone is abundantly present. Why then

are non-vascular structures not observed in burned bones when the areas that house them are visible?

It is possible that carbonization is still responsible for the lack of observable non-vascular structures in burned bone. Despite the periosteal area being the most visible cortical zone, its clarity is not uniform throughout all samples. When considering all 40 digital images taken of the control samples, only 7.5% of these images displayed non-vascular structures. This low frequency, coupled with an impregnable sheet of carbonization across all cortical zones, suggests that observing non-vascular structures in burned bone is unlikely. As well, in many burned cow samples, the identification of structure type was dependent on the presence or absence of either plexiform brick-cells or distinguishable Haversian systems. These features are morphologically distinct, making it easier to classify structure types based solely on these two features rather than inferring a structure type that is characterized by less distinct features (like non-vascular bone which is characterized by the absence of vascular canals). However, the presence of non-vascular bone is not mutually exclusive to the appearance of plexiform and/or Haversian bone. The appearance of non-vascular bone could not be verified under burned conditions. This culmination of factors makes it difficult to positively recognize non-vascular structures in burned material, but it should not be concluded that non-vascular structures do not exist after heat-exposure.

5.1.5 Potential Impact of Age on Haversian Structure

A number of variables were not rigidly controlled for when selecting specimens because the individuals of all three species were generously donated by outside sources. There have been no studies indicating that factors such as sex and sidedness show any histological differences in

non-human mammals, and based on this these factors are not considered to impact the data. Age, however, has been demonstrated to have a direct relationship with the prevalence of plexiform and Haversian bone. Hillier and Bell (2007) indicate that there are differences between mature and immature cervids in the relative proportion of plexiform bone. In mature cervids, dense Haversian structures replace plexiform bone, especially near the endosteal area of the cortex (Hillier and Bell, 2007). Morris (2007) notes that in her study, the limited availability of pig Haversian structures for analysis was most likely related to the young age of her pig specimens. These two studies, along with Enlow and Brown (1956) suggest that plexiform bone is more abundant in immature artiodactyls, while proportions of Haversian structures increase in mature individuals. However, numerous other studies do not account for any age discrepancies in their samples, regardless of whether or not age ranges are acknowledged. This inconsistent account for age in animal individuals makes it difficult to conduct a comparative examination on the relationship between age and Haversian structures.

Age assessment could not be conducted on the pig specimens due to the complete absence of epiphyseal ends when samples were procured. In the individuals used in this study, two out of five specimens each for cows and deer were juveniles (Table 3.1). In the juvenile deer and cow specimens, one individual from each species showed disproportionately higher ratios of plexiform bone versus Haversian structures. However, since this variable was not accounted for during the sampling process, it is difficult to verify a relationship between plexiform prevalence and the age of these individuals, especially when plexiform and Haversian structures were still present in most adult deer and cow specimens.

5.2 Quantitative Analysis

The results of this study show the limitations inherent in using histomorphometric techniques to analyze burned material, especially in the pig and deer individuals. Several factors contributed to the disappointing results, adding up to the conclusion that metric analysis of burned fragments may not be feasible with light microscopy.

In light of all of these unanticipated problems in histomorphometric analysis, the results from this study are limited in their comparative applications. Statistical analysis was performed on the data collected in this study to examine any patterns present in histological changes due to temperature. Ultimately, though, some key assumptions involved in statistical analysis were violated, and this may have biased the results presented.

5.2.1 Impact of Qualitative Appearance on Histomorphometry

The amount of carbonization affected the availability of osteons and Haversian canals that could be measured. This limitation influenced the visibility of Haversian structures, creating a sampling bias that prevented fully random sampling of representative structures.

The carbonization prevalent in the burned samples, especially at 600^{o}C and 800^{o}C, had a great impact on the numbers of osteons available for metric analysis. The abundant spread of the carbon resulted in the majority of the sample areas becoming obscured under the light microscope. The carbon limited visibility to a small number of pockets where light could penetrate. The areas surrounding the periosteal and endosteal edges, as well as mid-cortical regions with dominant fractures, were disproportionately visible in relation to the entire surface area. This affected which histological structures are visible, which in turn influenced the proportion of Haversian structures identifiable for histomorphometric methods. Although

Haversian structures were present in all three zones of cortical bone, the amount of Haversian systems and canals hidden by carbonization cannot be accounted for. This impedes the ability to determine the percentage of Haversian structures lost.

Heat-induced changes also affected the clarity of histological structures. The fogginess caused by melted hydroxyapatite and the black coating from carbonization both resulted in distorted histological appearance under the light microscope. These two factors either partially obscured the range of structures present or resulted in atypical structures that could easily be misdiagnosed as structure types not expected in the given species. The partial obstruction directly affected the ability to measure osteons by making it difficult to visualize the cement line which defines the border of the Haversian system. Therefore, even if a secondary osteon was recognizable in a burned specimen, the extent of carbonization or melted hydroxyapatite made it unfeasible to measure the dimensions of that osteon.

Haversian canals were distorted due to heat, although in a different manner than secondary osteons. Canals appeared either as blackened circles, or as empty pockets through which light penetrated. The inconsistent appearance, along with the possibility of size overestimation in empty canals, led to the exclusion of some potential osteons and Haversian canals for measurement. If the circular shape was disfigured or unverifiable the osteons and Haversian canals were excluded from the study.

5.2.2 Disproportionate Representation of Haversian Structures

A consequence of the disproportional visibility of histological structures is the bias towards using individuals with better visibility and applying these measurements as a representation of the species at each temperature (see Appendix B for more detail on each

specimen). Ideally, representation would be evenly split amongst the samples used per temperature. However, because of carbonization and the difference in Haversian bone prevalence, this was not possible.

5.2.2.1 Disproportionate Representations in Deer

In the controls for deer, D5 was responsible for 40% of the total osteons and Haversian canals measured, while D3 had 9%. In the burned deer samples at 600^{o}C, only individuals D1 and D2 had visible Haversian structures available for analysis. At 800^{o}C, the Haversian structures measured in D1 and D2 made up 70% of the total osteon and Haversian canals measured in deer at this temperature, while D4 had no measured structures. The individual D5 made up nearly half of the osteon and Haversian canals measured at 1000^{o}C, while the cumulative sum of structures in D1, D3 and D4 was less than one-quarter of the total Haversian structures measured at this temperature in deer.

Overall, D5 yielded the most overrepresented deer samples, with 36 out of 98 total osteons and 36 out of 112 Haversian structures measured in deer. Specimen D2 was almost as overrepresented, with only three fewer osteons measured than D5. The least represented specimens were D3 and D4, with eight and seven Haversian structures measured, respectively. For an evenly-split representation, roughly 20 Haversian structures should have been measured from each specimen across the four temperatures.

5.2.2.2 Disproportionate Representations in Pig

The distribution of measured Haversian structures in control pig samples was evenly split between the four specimens analyzed. As stated previously, no histological structures were visible at 600^{o}C, resulting in a uniform underrepresentation of the three samples section at this

temperature. At 800°C, one image from P5 resulted in 60% of the measured osteons and 56% of the measured Haversian canals, while P4 had no Haversian structures measured at this temperature. The specimen P1 only had representation of Haversian measurements at 1000°C, where it had the overrepresentation of roughly half of the measurements taken at this temperature. No Haversian structures were measured in P3 at 1000°C.

The most underrepresented pig specimen was P1 due to its only having Haversian structures measured at 1000°C. P1 represented 10% of the total osteons measured, and 16% of the total Haversian canals measured in pig. Interestingly, the other four specimens had equal representations for osteons measured. Specimens P2 and P5 had disproportionately higher counts of Haversian canals, with 25 and 22 Haversian canals measured respectively out of a collective sum of 83 Haversian canals. The disproportionate distribution of pig specimens therefore was more temperature-dependent.

5.2.2.3 Disproportionate Representations in Cow

Specimen C5 was the least represented in the cow control samples with only 9% of the total Haversian structures measured at this temperature. At 600°C, no Haversian structures were measured in C4 and C5, with C3 contributing 80% of the structures measured at this temperature in cow. Specimen C3 at 800°C, however, had no measureable Haversian structures, with C1 also underrepresented with only two osteons and ten Haversian canals measured out of a sum of 37 and 41, respectively. At 1000°C, C1, C3 and C5 had evenly distributed Haversian structures, while C2 and C4 cumulatively made up less than one-fifth of the total structures measured at this temperature.

The most underrepresented cow specimen was C5, which only contributed a substantive amount of Haversian structures at 1000^{o}C. The contribution of C5 to the total Haversian structures measured was less than 10%. The most overrepresented specimen was C3 with roughly 30% of the total Haversian structures measured coming from this individual. The other three specimens were evenly divided amongst the remaining 60% of measured structures.

5.2.3 Histomorphometric Analysis of Deer Bone

Adequate sampling of osteons and Haversian canals were present in deer samples except at 600^{o}C where only five osteons and 10 Haversian canals could be measured. The low results at this temperature made it impossible to properly conduct statistical analysis comparing the mean values at 600^{o}C with those at other temperatures. There were no significant differences found amongst the other three temperatures analyzed, and the visual representation of the mean areas in Figures 4.21 and 4.22 show that the mean values present at 600^{o}C did not appear much different than those in the other temperatures.

The dimensions for deer osteons and Haversian canals were consistently smaller when compared to pig and cow samples at all temperatures. This outcome follows similar results from previous literature like Urbanová and Novotný (2005) and Morris (2007) in which deer bone was compared to pig and/or cow bone (See Table 2.4). The mean osteon areas of deer in this study were slightly higher than those presented in Morris (2007) but still fell within one standard deviation of them. The mean Haversian canal areas, however, were smaller in this study than those in Morris (2007). The mean areas of osteons were much larger than those presented in the red deer and roe deer samples used in Urbanová and Novotný (2005), but this can be attributed to differences in species. Interestingly, though, the area and the minimum and maximum diameters

of Haversian canals in these two species (Urbanová and Novotný, 2005) matched those found for the white-tailed deer samples in this study. The lack of research done on histomorphometric values on deer species makes it difficult to conclude whether or not the deer samples in this study can be considered consistent with or different from those reported in other deer studies. This suggests further exploration of histological studies on comparative cervid groups should be undertaken.

5.2.4 Histomorphometric Analysis of Pig

The sample sizes of pig at each burned temperature were much smaller than deer and cow samples at the same temperatures. At 600^{o}C, there were no identifiable histological structures present in any of the samples examined, and smaller sample sizes of osteons were available at 800^{o}C and 1000^{o}C. There were significant differences between the control mean osteon areas, versus those found at 800^{o}C and 1000^{o}C, which is discussed below in section 5.2.7. These results showed no significant differences between the mean dimensions of Haversian canals.

Age and sex have not been consistently controlled for across histological studies of pig individuals (Albu et al, 1990; Urbanová and Novotný, 2005; Martikiniakova et al, 2006a; 2006b; 2007; Morris, 2007). Still, there have been examples in the literature (Mulhern and Ubelaker, 2011; Hillier and Bell, 2007) that publish summaries to compare the histomorphometric data from various studies, despite these cited studies lacking uniform age and sex variables.

Despite the inherent biases present in the availability of histological structures in burned samples, the control samples of pig are more representative and thus can be tentatively compared to other studies. These comparisons are still useful in establishing ranges of values to determine whether or not values from this study are anomalous.

The mean osteon dimensions of the pig samples used in this study were smaller than the values presented in Urbanová and Novotný (2005), and Martiniaková et al (2006a; 2006b). The values in Morris (2007) were more similar to the mean values found in this study's control samples, but the burned samples from this experiment were smaller than all of the previous literature (See Table 2.5). The mean values for the Haversian canal area in pig samples were smaller than those seen in other studies (Urbanová and Novotný, 2005; Martiniaková et al, 2006a; 2006b; Morris, 2007), but the large range of minimum and maximum Haversian canal diameters in these same studies cover the range of values present in this study.

The gross disparity in the mean values in the results of this study compared to those displayed in other literature is interesting. The studies performed by Urbanová and Novotný (2005), and Martiniaková and her team (2006a; 2006b) emphasize the similarities between pig and cow histological dimensions, yet in this study there were significant differences between pig and cow values.

An explanation for the disparity could be based on the unknown ages of the pig specimens in this study. Age does play a role in the distribution and prevalence of Haversian structures, and previous research has shown that there are differences in the dimensions of Haversian structures based on age in human samples (Currey, 1964; Hillier and Bell, 2007; Jowsey, 1966). However, as explained above, many histological studies performed using non-human mammals have not accounted for age in their analyses. As well, there has only been one study found by this author that accounts for age determination in non-human mammals (Ruddle, 1997); this research was conducted using SEM analysis. This study did not demonstrate any changes in dimensions correlated to age. With this in mind, it is possible that the age of the pig

individuals used in this study influenced the dimensions of measured osteons and Haversian canals, but there is no way to verify this relationship.

5.2.5 Histomorphometric Analysis of Cow

The physical size of the cow femora used in this experiment when compared to the deer and pig individuals was an advantage in providing a larger surface area for microscopic analysis. Carbonization was as extensive in burned cow samples as in the other two species; however, the wider area of cortical bone and the higher number of fractures increased the availability of visible histological structures. This difference in size between the cow samples and the deer and pig samples made it possible to collect histomorphometric data from adequate sample sizes in the burned cow samples, while insufficient histological structures were measured in the burned deer and pig samples.

5.2.6 Differences between Control and 600^{o}C vs 800^{o}C and 1000^{o}C in Cow and Pig

The graphical representation of the mean osteon areas in cow (Fig. 4.26) showed a striking difference between the mean values in the controls and at 600^{o}C versus the mean values at 800^{o}C and 1000^{o}C. The dimensions of the osteons in the second pair (800^{o}C and 1000^{o}C) are much smaller than those present in the first pair (controls and 600^{o}C). The ability to include statistically sufficient sample sizes at 600^{o}C helped confirm these differences through unpaired *t*-tests. The difference between these two paired temperatures suggests a change in the bone dimensions in conditions present above 600^{o}C.

A difference in osteon dimensions between the controls and 800^{o}C-1000^{o}C was observable in the mean osteon area in pig samples (Fig. 4.24). Statistical analysis showed significant differences between control samples and each of the burned samples, suggesting a

similar pattern to that seen in cow samples. The lack of measured osteons at 600°C precludes the ability to verify whether osteon areas at this temperature would be significantly different than osteons at 800°C and 1000oC. Since pig and cow samples at 600°C have similar gross morphological appearance, it is suggested that pig samples at 600°C would display similar osteon dimensions to control samples.

As outlined in Herrmann (1972a), the critical point at which all of the organic components of bone are destroyed occurs around 700-800°C. This critical point lies in between 600°C and 800°C where the division in the alteration of osteon dimensions lies, suggesting a link between the amount of organic material present and the dimensions of osteons in burned bone.

This relationship has been demonstrated in Herrmann (1977) and Bradtmiller and Buikstra (1984). Herrmann (1977) noted that burned material after the critical point displayed shrunken osteons. He attributed this phenomenon to the "fusion of mineral crystals and the characteristic shrinkage of cremated remains" (Herrmann, 1977:102).

Bradtmiller and Buikstra (1984), on the other hand, found that after 700-800°C, the osteons present in the burned samples appeared inflated compared to samples burned at lower temperatures. They proposed three different scenarios that may be responsible for the changes in osteon dimensions: a) Osteons normally expand first before shrinking, but the cremation process stopped before shrinking could occur. This would then result in expanded osteons being trapped in the burned specimens in this study; b) The bone in its gross morphology may shrink at high temperatures, but the microstructure actually expands; or c) The bone and the associated osteons shrink as a result of melted hydroxyapatite, and the results in this study reflect a sampling error.

Based on the results of this study, the results found in Herrmann (1977) are supported, suggesting that the third scenario (sampling error) occurred in Bradtmiller and Buikstra's experiment (1984).

This pattern was not seen in Haversian canal dimensions, although an increase in Haversian canal dimensions in burned human material at 600-900^{o}C was noted in studies by Squires and her researchers (2011). The different species type and the use of a different methodology (FTIR-AR) in Squires et al (2011) make it difficult to verify whether the results in this study were anomalous.

The distinct lack of a division between 600^{o}C and 800^{o}C in the deer osteon values may either reflect the low sample sizes present at these temperatures, or indicate a difference in bone shrinkage in cervids compared to other mammals.

Another possible explanation for the difference in deer osteons remaining a constant shape may revolve around the condition of the deer samples at cremation versus the conditions of the pig and cow samples. As noted earlier, the pig and cow specimens were classified as greasy because of their residual grease and fat contents, whereas the deer was considered to be dry bone. The increase in organic content present in the pig and cow specimens may contribute to the degree of bone distortion. With a higher content of organic material to burn, the greasy bones may respond more drastically than in dry bones. This would suggest that the contraction of osteons could relate to the amount of organic content present, in addition to reformation caused by melted hydroxyapatite.

In future studies, it would be worthwhile to pursue this question to determine how prevalent contraction of osteon dimensions is in all artiodactyl groups, and whether contraction occurs in relation to organic components of bone material

5.2.7 Significant Differences between Deer and Pig

Significant differences were present in the control samples between deer and pig. However, at 800^{o}C and 1000^{o}C, there were no significant differences. This pattern, as explained above in section 5.2.7, has implications surrounding the ability to correctly identify certain species above the critical point (700-800^{o}C). Since the burned samples of deer and pig were shown to be similar, it shows that any attempt to determine the species of unknown burned material runs the risk of being incorrectly identified when using metric analysis. This is further evidence that performing histomorphometric analysis in burned material is not ideal to pursue, especially if sufficient histological structures cannot be identified for qualitative identification of species origin.

5.3 Applications for Future Research

The consistent difficulties in examining bone samples at 600^{o}C suggest that burned material with a similar morphological appearance as the samples under this condition may not present enough visible histological structures for analysis. The samples at 800^{o}C and 1000^{o}C still showed limitations in histological analysis, but the reduction in carbonization helped in the recognition of histological structures at these temperatures. As a result, it is proposed that histological analysis should only be pursued in material that has lost all of the organic content or has undergone calcination. The extent of carbonization present at any temperature level may be

too much to overcome for metric analysis, and so quantitative analysis of burned material is not recommended.

It is important to note that the levels of carbonization are not solely dependent on the temperature at which material was cremated. As noted in Chapters 2 and 3, heat-induced changes to bone are a cumulative result of the burning temperature and the duration of exposure. Therefore, it is emphasized that the success rate of histomorphometric analysis relies more on the gross morphological appearance of bone (i.e. the degree of residual organic content) rather than explicitly the temperature of cremation. This allows researchers to recognize burned samples that are unlikely to provide sufficient data without having to rely on reconstructing the temperature of initial cremation.

The preservation and size of fragments are other factors that will influence the success of using histological analysis on burned remains. The difference in sample sizes between the cow specimens and the other two smaller species reflects the advantage of having larger fragments to study. The majority of the cow samples used in this study were larger than 2 cm in thickness, while most of the deer and pig samples were less than 1 cm thick. Histological analysis, therefore, should ideally be pursued in burned fragments that are larger than 1 cm in cortical thickness.

Even with the limitations in histomorphometric analysis, light microscopy is still a valid technique for archaeological and police laboratories that may not have adequate access to expensive equipment like SEM or XRD. The ability to identify histological structures in burned material allows researchers to determine a human origin based on the presence or absence of certain structure types. For many unknown cases, this is the first step in determining whether or

not further investigation is needed for forensic relevance (Byers, 2007). In archaeological studies, the differentiation of human from non-human material may lead to further questions that can be explored. If the identification of a specific non-human group is necessary, it is suggested that techniques like SEM or XRD be pursued because of their greater success rate.

Chapter 6 – Conclusions

The aims of this study were to verify whether histological structures are still visible through light microscopy in burned material, and whether histomorphometric analysis can be conducted on visible Haversian structures in burned material. The first hypothesis was that histological structures would still be observable at all three burned temperatures. The results of this experiment showed evidence to support this hypothesis, except unanticipated limitations in examining burned material attributed to different degrees of visibility.

Carbonization and melted hydroxyapatite affected the visibility of burned samples in all three species. Samples burned at 600^{o}C were particularly impacted by the extent of carbonization, limiting the number of histological structures that could be identified. The carbonization also affected the visibility of Haversian structures that could be measured for metric analysis. The sampling bias that occurred because cortical regions were obstructed from microscopic analysis undermines the reliability of representative data.

The second hypothesis was that the dimensions of secondary osteons and Haversian canals would be distorted in the burned samples compared to the control samples. The results of this experiment are based on small sample sizes and biased selection processes, therefore all inherent biases must be considered when interpreting the findings outlined in this thesis. This hypothesis was supported in the burned cow and pig material with osteon dimensions being smaller at 800^{o}C and 1000^{o}C than in the controls and at 600^{o}C (observable in cow only). However, there were no alterations in the osteon dimensions in burned deer samples, and there were no significant changes in the dimensions of Haversian canals at any burned temperature in

any of the species. This indicates that the hypothesis could not be uniformly supported across all three species or in both Haversian structures.

In deer samples at all temperatures, plexiform and Haversian structures were prevalent. Reticular bone was found in the control samples and the samples burned at 600^{o}C of deer, but not in any of the burned material from 800^{o}C and 1000^{o}C. Laminar-like structures were found in deer samples at 600^{o}C and 1000^{o}C, although this appearance is more likely due to carbonization distorting the appearance of plexiform and/or reticular bone rather than laminar bone spontaneously occurring in burned samples.

Plexiform and Haversian structures were prevalent in pig samples at all four temperatures. Reticular bone, which has not been found in previous publications on pig femora, was present in samples at control, 600^{o}C and 800^{o}C. The lack of visible reticular bone in pig samples at 1000^{o}C may be a result of sampling bias. The presence of reticular bone in unburned and burned pig samples at 600^{o}C and 800^{o}C indicates that further investigation must be done to determine the extent of individual variation and other factors (like age, sex, activity level) in the diversity of histological structures in pig.

Cow samples at all temperatures displayed plexiform and Haversian structures. Besides plexiform, no other primary vascular structure types were present in cow samples. Non-vascular bone occurred in all of the control samples, but this structure type was not visible in any of the burned samples. It is suggested that non-vascular bone may be more easily obscured by carbonization or other heat-induced changes due to reliance on absent features (like vascular canals) for the identification of this structure type.

Through metric analysis, it was demonstrated that deer osteons and Haversian canals were consistently smaller than those seen in cow samples and unburned pig samples; these results were similar to previous studies. The dimensions of pig Haversian structures were smaller than other literature has shown, showing no significant difference in burned material when compared to deer osteons and Haversian canals. For all of the histological parameters measured, cow values were consistently the largest and fell within the range found in other publications. These differences were confirmed through unpaired *t*-tests for all of the measured Haversian structures between deer and cow, and between pig and cow specimens.

There were no significant differences found between any of the temperatures for deer samples. A pattern of two distinct groups of mean osteon areas appeared in pig samples: the mean areas at 800^{o}C and 1000^{o}C were found to be smaller than the mean area in the control samples. This same pattern was seen in cow samples, with control and 600^{o}C mean osteon areas having similar values, while osteon areas at 800^{o}C and 1000^{o}C were smaller in size. This relationship was found to be significantly different in pig and cow samples.

Constrictions in the Haversian dimensions of pig samples at 800^{o}C and 1000^{o}C led to unpaired *t*-tests demonstrating no significant difference between deer and pig samples at these two temperatures. This suggests that misdiagnosis of species origin is possible in burned material above 800^{o}C, and further emphasizes the difficulties in using histomorphometric analysis in burned material.

A number of issues arose during the analysis of qualitative and quantitative features. The proportional difference in plexiform and Haversian bone that is based on age is a factor that was not accounted for during analysis. Although other studies have listed the age of the mammalian

specimens used in their analyses, very little has been done to test the quantifiable differences in histological structures between juvenile and adult individuals. Uniform approaches for examining the age of non-human individuals will help establish better representation for the diversity of histological structures found in species which will in turn assist in more accurate identification.

The prevalence of carbonization made visibility difficult in the burned samples, and led to a biased sampling for statistical analysis. The extent of carbonization is possibly linked to the amount of organic material present in bone during initial cremation. In an experimental setting, it is possible that cremating dry bones may result in less carbonization, allowing for better visibility. However, this is impossible to control when examining archaeological or forensic material. In order to still examine burned material in archaeological or forensic cases, it is worthwhile to pursue treatments that could potentially reduce the presence of carbonization in processed samples.

Besides the limitation in visible areas, carbonization and melted hydroxyapatite impacted the identification of visible histological structures. The apparent presence of laminar-like structures in deer, and the absence of non-vascular structures in cow both raise questions in the feasibility of correctly identifying histological structures in burned bone. This study was based on the comparisons between structures present in control (unburned) samples and structures found in burned samples from the same individuals. When examining archaeological or forensic cremated material, there are no comparative unburned individuals. Therefore, the reliability of histological analysis in burned material without comparative unburned samples is challenged.

This study demonstrated the appearance of reticular structures in pig femora. This adds another histological feature that can be included in the identification of pig fragments in archaeological and forensic studies under any condition. The lack of visible non-vascular bone in burned cow, on the other hand, cautions researchers from ruling out bovine identification if non-vascular structures are absent in unknown burned material.

The results of this research show that forensic determination of non-human origin in burned material is possible through qualitative analysis, but any attempt at metric analysis may not be successful. As well, the significant contraction of osteon areas at 800^{o}C and 1000^{o}C in pig and cow specimens indicates that metric analysis of osteon dimensions at higher temperatures may not be reliable in species identification when using standards developed on unburned samples.

Light microscopy has been demonstrated to be limited in its applicability for differentiating human and non-human burned material. Therefore it is suggested that this technique be used only for the most basic determination of non-human material in forensic investigations.

Bibliography

Amprino, R
1947. La structure du tissu osseux envisagée comme expression de différences dans la vitesse de l'accroissement. *Archives de Biologie.* 58: 315-330.

Albu I, Georgia R, and Georoceanu M
1990. The canal system in the diaphysial compacta of the femur in some mammals. *Anatomischer Anzeiger* 170: 181-187.

Beckett, S, Rogers, KH and Clement, JG
2011. Inter-species variation in bone mineral behavior upon heating. *Journal of Forensic Sciences* 56(3): 571-579.

Bhayro, L
2003. *Histological Quantitative and Morphological Analysis of Burned and Unburned Bone.* Unpublished MSc dissertation, Sheffield University.

Bond, JM
1996. Burnt offerings: Animal bone in Anglo-Saxon cremations. *World Archaeology* 28(1): 76-88.

Bradtmiller, B and Buikstra, JE
1984. Effects of burning on human bone microstructure: a preliminary study. *Journal of Forensic Sciences* 29(2): 535-540.

Buikstra, JE and Swegle, M
1989. Bone modification due to burning: experimental evidence. In: Bone Modification. R Bonnischen and MH Sorg, *eds*. Maine: Peopling of the Americas Publications.

Byers, S
2007. Introduction to forensic anthropology, 3rd Edition. London: Allyn & Bacon.

Castillo, RF, Ubelaker, DH, Acosta, JAL and de la Fuente, GAC
2013. Effects of temperature on bone tissue. Histological study of the changes in the bone matrix. *Forensic Science International* 226(1-3): 33-37.

Castrovagianni, P, Imbesi, R, Fisichella, M and Mazzone, V
2011. Osteonic organization of limb bones in mammals, including humans, and birds: a preliminary study. *Italian Journal of Anatomy and Embryology* 116 (1): 30-37

Cattaneo, C, DiMartino, S, Scali, S, Craig, OE, Grandi, M and Sokol, RJ
1999. Determining the human origin of fragments of burnt bone: a comparative study of histological, immunological and DNA techniques. *Forensic Science International* 102: 181-191.

Cattaneo, C, Porta, D, Gibelli, D and Gamba, C
2009. Histological determination of the human origin of bone fragments. *Journal of Forensic Sciences* 54 (3): 531-533

Crescimanno, A and Stout, SD
2012. Differentiating fragmented human and nonhuman long bone using osteon circularity. *Journal of Forensic Sciences* 57 (2): 287-294

Cuijpers, AGFM
1995. Possibilities of histological research on diaphyseal fragments in cremated remains. In: Proceedings of the Symposium *Cremation Studies in Archaeology.* Amsterdam, 26-27 October 1995. Smits, E, Iregren, E and Drusini, AG, *eds*.

Cuijpers, AGFM
2006. Histological identification of bone fragments in archaeology: telling humans apart from horses and cattle. *International Journal of Osteoarchaeology* 16: 465-480

Cuijpers, AGFM
2009. The application of bone histology for species identification in archaeology; with a photo catalogue: a thesis. PhD thesis. Institute for Geo and Bioarchaeology, Vrije, Universiteit.

Cuijpers, S and Lauwerier, RCGM
2008. Differentiating between bone fragments from horses and cattle: a histological identification method for archaeology. *Environmental Archaeology* 13 (2): 165-179

Currey, JD
1964. Some effects of ageing in human Haversian systems. *Journal of Anatomy, London* 98(1): 69-75.

De Winters, JCF
2013. Using the Student's *t*-test with extremely small sample sizes. *Practical Assessment, Research & Evaluation* 18(10): 1-12.

Dixon, KJ, Novak, SA, Robbins, G, Schlablitsky, JM, Scott, GR and Tasa, GL
2010. "Men, women, and children starving": archaeology of the Donner Family Camp. *American Antiquity* 75(3): 627-656.

Enlow D
1963. Principles of bone remodeling. Springfield, IL: Charles C.Thomas.

Enlow DH and Brown SO
1956. A comparative histological study of fossil and recent bone tissues, part I. *The Texas Journal of Science* 7(4):405–443.

Enlow DH, Brown SO
1957. A comparative histological study of fossil and recent bone tissues, part II. *The Texas Journal of Science* 9(2):186-214.

Enlow DH, Brown SO
1958. A comparative histological study of fossil and recent bone tissues, part III. *The Texas Journal of Science* 10(2):187–230.

Foote, JS
1916. A contribution to the comparative histology of the femur. *Smithsonian Contributions to Knowledge* 35(3).

Francillon-Vieillot, H, de Buffrénil, V, Castanet, J, Géraudie, J, Meunier, FJ, Sire, JY, Zylberberg, L and de Ricqlès, A
1989. Microstructure and mineralization of vertebrate skeletal tissues. In: Skeletal biomineralization: patterns, processes and evolutionary trends. JG Carter, *ed*. Washington, DC: American Geophysical Union.

Frost, HM
1966. Bone dynamics in metabolic bone disease. *The Journal of Bone & Joint Surgery* 48(6): 1192-1203.

Gonçalves, D
2012. The micro-analysis of human burned bones: some remarks. *Cadernos do GEEvH* 1(1): 32-40.

Greenlee, DM and Dunnell, RC
2010. Identification of fragmentary bone from the Pacific. *Journal of Archaeological Science* 37: 957-970.

Hanson, M and Cain, CR
2007. Examining histology to identify burned bone. *Journal of Archaeological Science* 34: 1902-1913.

Herrmann, B
1972 Das Combe Capell-Skelet. Eine Untersuchung der Brandreste unter Berucksichtigung thermoinduzierter veranderungen am Knochen. *Ausgrabungen in Berlin* 3: 7-69.

Herrmann, B
1972. Zur Beurteilung von Kohlenstoffverfäbungen bei Leichenbränden. *Ausgrabungen u. Funde* 17(6): 275-277.

Herrmann, B
1977. On histological investigations of cremated human remains. *Journal of Human Evolution* 6: 101-103.

Hiller, JC, Thompson, TJU, Evison, MP, Champerlain, AT and Wess, TJ.
2003. Bone mineral change during experimental heating: an X-ray scattering investigation. *Biomaterials* 24: 5091-5097.

Hillier, ML and Bell, LS
2007. Differentiating human bone from animal bone: a review of histological methods. *Journal of Forensic Sciences* 52 (2): 249-263

Junqueira, LC and Carneiro, J
2005. Basic histology: Eleventh Edition. The McGraw Companies Inc., USA.

Iregren, E
1995. Why animal bones in human graves – an attempt to interpret animals present in Iron Age cremations in Sweden. In: Proceedings of the Symposium *Cremation Studies in Archaeology.* Amsterdam, 26-27 October 1995. Smits, E, Iregren, E and Drusini, AG, *eds*.

Jowsey, J
1966 Studies of Haversian systems in Man and some animals. *Journal of Anatomy* 100(4):857-864.

Kerley, ER
1965. The microscopic determination of age in human bone. *American Journal of Physical Anthropology* 23: 149-164.

Martini, FH, Timmons, MJ and Tallitsch, RB
2009. Human anatomy - 6th edition. Glenview, IL: Pearson Education.

Martiniaková, M, B Grosskopf, R Omelka, K Dammers, M Vondráková, M Bauerova
2006b. Differences among species in compact bone tissue microstructure of mammalian skeleton: use of a discriminant function analysis for species identification. *Journal of Forensic Sciences* 51 (6): 1235-1239

Martiniaková, M, B Grosskopf, R Omelka, K Dammers, M Vondráková, M Bauerova
2007. Histological study of compact bone tissue in some Mammals: a method for species determination. *International Journal of Osteoarchaeology* 17: 82–90

Martiniaková, M, B Grosskopf, M Vondráková, R Omelka, M Fabiš
2006a. Differences in femoral compact bone tissue microscopic structure between adult cows (*Bos taurus*) and pigs (*Sus scrofa domestica*). *Anatomia, Histologia, Embryologia* 35: 167-170

Mayne, PM
1990. The identification of precremation trauma in cremated bone: a thesis. Master of Arts thesis. Department of Anthropology, University of Alberta.

Mayne Correia, PM
1997. Fire modification of bone: a review in literature. In: Forensic taphonomy: the postmortem fate of human remains. Haglund WD, Sorg MH, *eds*. London: CRC Press. pp. 275-293.

Mayne Correia, PM and Beattie, O
2001. A critical look at methods for recovering, evaluating, and interpreting cremated human remains. In: Advances

in forensic taphonomy: Method, theory, and archaeological perspectives. WD Haglund and Sorg MD, *eds*. Boca Raton: CRC Press. pp. 435-450.

McCormick, F
1985/1986. Faunal remains from prehistoric Irish burials. *The Journal of Irish Archaeology* 3: 37-48.

Morris, ZH
2007. Quantitative and spatial analysis of the microscopic bone structures of deer (*Odocoileus virginianus*), dog (*Canis familiaris*), and pig (*Sus scrofa domesticus*): A Thesis. Master of Arts thesis. Department of Geography and Anthropology, University of Toronto.

Mulhern, DM and Ubelaker, DH
2001. Differences in osteon banding between human and nonhuman bone. *Journal of Forensic Sciences* 46(2): 220-222.

Mulhern, DM and Ubelaker, DH
2011. Differentiating human from nonhuman bone microstructure. *In*: Bone Histology: an anthropological perspective. Stout, SD and Crowder, C, eds. London: CRC Press. pp. 109-134.

Nicholson, RA
1993. A morphological investigation of burnt animal bone and an evaluation of its utility in archaeology. *Journal of Archaeological Science* 20: 411-428.

Owsley, DW, Mires, AM and Keith, MS
1985. Case involving differentiation of deer and human bone fragments. *Journal of Forensic Science* 30(2): 572-578.

Paral, V, Witter, K and Tonar, Z
2007. Microscopic examination of ground sections – a simple method for distinguishing between bone and antler? *International Journal of Osteoarchaeology* 17: 627-634.

Piga, G, Malgosa, A, Thompson, TJU and Enzo, S
2008. A new calibration of the XRD technique for the study of archaeological burned human remains. *Journal of Archaeological Science* 35: 2171-2178.

Rasaband, WS
ImageJ, U. S. National Institutes of Health, Bethesda, Maryland, USA, http://imagej.nih.gov/ij/, 1997-2012.

Robbins, G and Gray, K
2011. Bone histology and identification of a starvation diet. In: Archaeology of desperation: Exploring the Donner Party's Alder Creek Camp. Dixon, KJ, Schablitsky, JM, and Novak, SA, *eds*. Norman, OK: University of Oklahoma Press. pp. 163-184.

Ruxton, GD
2006. The unequal variance *t*-test is an underused alternative to Student's *t*-test and the Mann-Whitney *U* test. *Behavioral Ecology* 17(4): 688-690.

Sauer, NJ and Lackey MWL
2000. Anthropology: skeletal analysis. In: Encyclopedia of Forensic Sciences. JA Siegel, PJ Saukko, GC Knupfer, *eds*. New York: Academic Press. pp. 261-270.

Schwartz, JK
1993. What the bones tell us. New York: Henry Holt.

Shipman, P, Foster, G and Schoeninger, M
1984. Burnt bone and teeth: an experimental study of color, morphology, crystal structure and shrinkage. *Journal of Archaelogical Science* 11: 307-325.

Skedros, JG, Sybrowksky, CL, Parry, TR, and Bloebaum, RD
2003. Regional differences in cortical bone of organization and microdamage prevalence in Rocky Mountain Mule Deer. *The Anatomical Record* Part A 274A: 837-850.

Singh, IJ, Tonna, EA and Gandel, CP
2005. A comparative histological study of mammalian bone. *Journal of Morphology* 144 (4): 421-437.

Squires, KE, Thompson, TJU, Islam, M, Chamberlain, A
2011. The application of histomorphometry and Fourier Transform Infrared Spectroscopy to the analysis of early Anglo-Saxon burned bone. *Journal of Archaeological Science* 38 (9): 2399-2409.

Stiner, MC, Kuhn, SL, Weiner, S, and Bar-Yosef, O.
1995. Differential burning, recrystallization, and fragmentation of archaeological bone. *Journal of Archaeological Science* 22: 223-237.

Stout, SD and Crowder, C
2011. Bone remodeling, histomorphology, and histomorphometry. In: Bone Histology: an anthropological perspective. Stout, SD and Crowder, C, *eds.* London: CRC Press. pp. 1-22.

Thompson, TJU
2004. Recent advances in the study of burned bone and their implications for forensic anthropology. *Forensic Science International* 146: 203-205.

Thompson, TJU
2005. Heat-induced dimensional changes in bone and their consequences for forensic anthropology. *Journal of Forensic Science* 50(5): 1-8.

Thompson, TJU, Gauthier, M and Islam, M
2009. The application of a new method of Fourier Transform Infrared Spectroscopy to the analysis of burned bone. *Journal of Archaeological Science* 36(3): 910-914.

Ubelaker, DH
2009. The forensic evaluation of burned skeletal remains: a synthesis. *Forensic Science international* 183: 1-5.

Urbanová, P and Novotný, V
2005. Distinguishing between human and non-human bones: histometric method for forensic anthropology. *Anthropologie* 43(1):77–85.

Weiner, S and Bar-Yosef, O.
1990. States of preservation of bones from prehistoric sites in the Near East: a survey. *Journal of Archaeological Science* 17: 187-196.

White, TD and Folkens, PA
2005. The human bone manual. San Diego: Elsevier Academic Press.

Whyte, T
2001. Distinguishing human cremations from burned animal bones. *Journal of Field Archaeology* 28: 437-448.

Zedda, M, Lepore, G, Manca, P, Chisu, V and Farina, V
2008. Comparative bone histology of adult horses (*Equus callabus*) and cows (*Bos taurus*). *Anatomia Histologia Embryologia* 37: 442-445.

Appendix A – Methodology

Samples that were burned using the Barnstead-Thermolyne Type F62700 Furnace at 600^{o}C and 800^{o}C were monitored by a digital temperature gauge throughout the cremation process. Initial temperatures account for heat loss through open oven doors. Maximum temperatures are the result of combusting grease and fat in the specimens. End temperatures are the final temperatures measured before samples were removed from the oven. The Fisher IsoTemp Muffle Furnace did not have any means of monitoring internal temperatures, and thus samples burned at 1000^{o}C could not be monitored for temperature fluctuations.

Table A1 – Temperatures recorded during cremation process for deer specimens at 600^{o}C and 800^{o}C.

Sample	Set Temperature (^{o}C)	Initial Temperature (^{o}C)	Maximum Temperature (^{o}C)	End Temperature (^{o}C)
D1-1	600	542	608	600
D1-2	800	706	802	802
D2-1	600	540	612	600
D2-2	800	710	801	801
D3-1	600	544	608	601
D3-2	800	713	802	802
D4-1	600	576	607	601
D4-2	800	708	802	802
D5-1	600	545	606	602
D5-2	800	717	802	802

Table A2 – Temperatures recorded during cremation process for pig specimens at 600°C and 800°C.

Sample	Set Temperature (°C)	Initial Temperature (°C)	Maximum Temperature (°C)	End Temperature (°C)
P1-1	600	570	631	599
P1-2	800	749	808	801
P2-1	600	542	631	600
P2-2	800	726	801	801
P3-1	600	523	642	600
P3-2	800	708	804	801
P4-1	600	523	640	597
P4-2	800	710	801	801
P5-1	600	529	626	600
P5-2	800	685	802	802

Table A3 – Temperatures recorded during cremation process for cow specimens at 600°C and 800°C.

Sample	Set Temperature (°C)	Initial Temperature (°C)	Maximum Temperature (°C)	End Temperature (°C)
C1-1	600	540	617	597
C1-2	800	717	807	800
C2-1	600	535	612	599
C2-2	800	718	800	800
C3-1	600	533	631	598
C3-2	800	717	810	800
C4-1	600	547	609	597
C4-2	800	720	806	800
C5-1	600	536	613	598
C5-2	800	715	808	799

Difficulties were encountered in sample embedding, with many samples failing to set properly. This resulted in samples with some unhardened resin blended with hardened resin. There was no clear reason as to why the resin did not set properly. It was originally speculated that the epoxy hardening agent was not reacting appropriately with the burned material, but tests done on small non-analyzed fragments did not support this theory. It is possible that the mixing of the resin was inadequate to blend the catalyst completely. To remedy the issue, the most affected samples (i.e. those with resin still predominantly viscous) were treated with ethanol to strip away the residual unhardened resin. Fresh epoxy chemicals were then used to recast the samples to greater success. There was no observable difference between the various samples due to this problem.

Appendix B – Specimens

Table B1 – Histological structures and cortical regions displayed in digital images taken of deer specimen, D1.

Temperature	Number of Images	Images from Periosteal Area	Images from Mid-Cortical Area	Images from Endosteal Area	Images with Plexiform Bone	Images with Haversian Bone	Images with Primary Vascular Bone
Control	7	2	3	3	7	2	0
600	5	3	1	1	0	5	5
800	7	5	2	2	2	7	0
1000	4	2	0	2	3	1	0

Table B2 – Mean values of the histological parameters measured in secondary osteons in deer specimen, D1.

Temperature (^{o}C)	Number of Osteons	Mean Osteon Area (μm^2)	Mean Min. Diameter of Osteon (μm)	Mean Max. Diameter of Osteon (μm)
Control	5	15680.92 $\pm$ 6937.17	114.25 $\pm$ 23.28	166.18 $\pm$ 43.49
600	2	16686.61 $\pm$ 480.58	138.10 $\pm$ 6.22	162.50 $\pm$ 5.47
800	9	17721.39 $\pm$ 6854.31	129.58 $\pm$ 26.55	164.24 $\pm$ 34.10
1000	3	21393.09 $\pm$ 1271.70	150.40 $\pm$ 4.61	185.70 $\pm$ 16.60

Table B3 - Mean values of the histological parameters measured in Haversian canals in deer specimen, D1.

Temperature (^{o}C)	Number of Haversian Canals	Mean Haversian Canal Area (μm^2)	Mean Min. Diameter of Haversian Canal (μm)	Mean Max Diameter of Haversian Canal (μm)
Control	5	458.17 $\pm$ 142.65	20.08 $\pm$ 3.36	27.00 $\pm$ 6.71
600	3	284.71 $\pm$ 105.17	15.22 $\pm$ 3.69	18.82 $\pm$ 2.31
800	19	317.21 $\pm$ 116.84	16.52 $\pm$ 4.32	22.86 $\pm$ 5.19
1000	3	465.04 $\pm$ 153.02	20.87 $\pm$ 3.40	26.99 $\pm$ 6.10

Table B4 – Histological structures and cortical regions displayed in digital images taken of deer specimen, D2.

Temperature	Number of Images	Images from Periosteal Area	Images from Mid-Cortical Area	Images from Endosteal Area	Images with Plexiform Bone	Images with Haversian Bone	Images with Primary Vascular Bone	Images with Laminar Bone
Control	5	2	1	2	3	3	0	5
600	4	3	0	1	0	4	4	0
800	8	3	6	2	5	8	0	0
1000	5	2	2	2	5	3	0	2

Table B5 – Mean values of the histological parameters measured in secondary osteons in deer specimen, D2.

Temperature (^{o}C)	Number of Osteons	Mean Osteon Area (μm^2)	Mean Min. Diameter of Osteon (μm)	Mean Max. Diameter of Osteon (μm)
Control	9	16029.72 $\pm$ 1995.12	119.64 $\pm$ 10.00	158.02 $\pm$ 18.07
600	3	12966.31 $\pm$ 3882.36	124.66 $\pm$ 20.14	127.80 $\pm$ 27.50
800	12	15012.66 $\pm$ 4581.36	114.83 $\pm$ 21.47	157.13 $\pm$ 27.09
1000	9	14242.28 $\pm$ 7905.92	120.86 $\pm$ 34.79	140.19 $\pm$ 33.99

Table B6 - Mean values of the histological parameters measured in Haversian canals in deer specimen, D2.

Temperature (^{o}C)	Number of Haversian Canals	Mean Haversian Canal Area (μm^2)	Mean Min. Diameter of Haversian Canal (μm)	Mean Max Diameter of Haversian Canal (μm)
Control	9	279.14 $\pm$ 70.36	15.40 $\pm$ 1.87	20.84 $\pm$ 3.12
600	6	255.76 $\pm$ 46.89	14.78 $\pm$ 2.86	19.50 $\pm$ 2.48
800	12	207.82 $\pm$ 72.58	13.56 $\pm$ 3.06	17.64 $\pm$ 3.62
1000	9	276.19 $\pm$ 161.94	15.91 $\pm$ 4.95	21.13 $\pm$ 5.50

Table B7 – Histological structures and cortical regions displayed in digital images taken of deer specimen, D3.

Temperature	Number of Images	Images from Periosteal Area	Images from Mid-Cortical Area	Images from Endosteal Area	Images with Plexiform Bone	Images with Haversian Bone	Images with Primary Vascular Bone
Control	4	1	2	1	1	4	0
600	5	2	3	2	2	1	3
800	6	3	2	3	5	2	0
1000	2	1	2	1	1	2	0

Table B8 – Mean values of the histological parameters measured in secondary osteons in deer specimen, D3.

Temperature (^{o}C)	Number of Osteons	Mean Osteon Area (μm^2)	Mean Min. Diameter of Osteon (μm)	Mean Max. Diameter of Osteon (μm)
Control	3	16567.12 $\pm$ 4643.47	127.45 $\pm$ 13.36	163.50 $\pm$ 19.42
600	0	-	-	-
800	4	20564.60 $\pm$ 8838.76	138.10 $\pm$ 25.08	175.77 $\pm$ 38.55
1000	1	12067.19	112.40	152.12

Table B9 - Mean values of the histological parameters measured in Haversian canals in deer specimen, D3.

Temperature (^{o}C)	Number of Haversian Canals	Mean Haversian Canal Area (μm^2)	Mean Min. Diameter of Haversian Canal (μm)	Mean Max Diameter of Haversian Canal (μm)
Control	3	244.89 $\pm$ 51.99	12.53 $\pm$ 1.67	21.79 $\pm$ 7.36
600	0	-	-	-
800	4	363.72 $\pm$ 215.44	16.14 $\pm$ 4.24	24.36 $\pm$ 8.88
1000	1	360.97	17.15	27.13

Table B10 – Histological structures and cortical regions displayed in digital images taken of deer specimen, D4.

Temperature	Number of Images	Images from Periosteal Area	Images from Mid-Cortical Area	Images from Endosteal Area	Images with Plexiform Bone	Images with Haversian Bone	Images with Reticular Bone	Images with Laminar Bone
Control	5	2	2	1	4	3	2	0
600	3	1	1	1	3	0	1	1
800	4	2	2	2	4	0	0	4
1000	6	2	3	3	5	3	0	6

Table B11 – Mean values of the histological parameters measured in secondary osteons in deer specimen, D4.

Temperature (^{o}C)	Number of Osteons	Mean Osteon Area (μm^2)	Mean Min. Diameter of Osteon (μm)	Mean Max. Diameter of Osteon (μm)
Control	4	16061.22 $\pm$ 4850.19	121.97 $\pm$ 17.68	162.38 $\pm$ 33.40
600	0	-	-	-
800	0	-	-	-
1000	3	13667.29 $\pm$ 5454.60	120.03 $\pm$ 28.66	143.75 $\pm$ 33.36

Table B12 - Mean values of the histological parameters measured in Haversian canals in deer specimen, D4.

Temperature (^{o}C)	Number of Haversian Canals	Mean Haversian Canal Area (μm^2)	Mean Min. Diameter of Haversian Canal (μm)	Mean Max Diameter of Haversian Canal (μm)
Control	4	206.49 $\pm$ 35.73	14.11 $\pm$ 0.75	18.29 $\pm$ 1.99
600	0	-	-	-
800	0	-	-	-
1000	3	396.71 $\pm$ 186.21	20.27 $\pm$ 4.38	24.72 $\pm$ 5.20

Table B13 – Histological structures and cortical regions displayed in digital images taken of deer specimen, D5.

Temperature	Number of Images	Images from Periosteal Area	Images from Mid-Cortical Area	Images from Endosteal Area	Images with Plexiform Bone	Images with Haversian Bone	Images with Primary Vascular Bone	Images with Laminar Bone
Control	7	2	3	2	3	7	0	0
600	7	3	0	4	6	1	1	1
800	7	4	0	3	4	3	0	0
1000	9	2	5	3	5	5	0	0

Table B14 – Mean values of the histological parameters measured in secondary osteons in deer specimen, D5.

Temperature (^{o}C)	Number of Osteons	Mean Osteon Area (μm^2)	Mean Min. Diameter of Osteon (μm)	Mean Max. Diameter of Osteon (μm)
Control	14	15162.52 $\pm$ 4445.64	124.95 $\pm$ 20.26	150.42 $\pm$ 24.89
600	0	-	-	-
800	6	16024.59 $\pm$ 6044.17	124.69 27.80	158.70 $\pm$ 38.87
1000	15	12054.85 $\pm$ 3356.09	100.59 $\pm$ 15.90	146.56 $\pm$ 25.17

Table B15 - Mean values of the histological parameters measured in Haversian canals in deer specimen, D5.

Temperature (^{o}C)	Number of Haversian Canals	Mean Haversian Canal Area (μm^2)	Mean Min. Diameter of Haversian Canal (μm)	Mean Max Diameter of Haversian Canal (μm)
Control	14	376.83 $\pm$ 165.53	18.14 $\pm$ 4.21	24.39 $\pm$ 6.05
600	1	193.64	14.42	19.06
800	5	420.88 $\pm$ 241.94	19.27 $\pm$ 6.13	28.09 $\pm$ 10.40
1000	15	375.50 $\pm$ 199.74	17.72 $\pm$ 5.02	24.88 $\pm$ 7.11

Table B16 – Histological structures and cortical regions displayed in digital images taken of pig specimen, P1.

Temperature	Number of Images	Images from Periosteal Area	Images from Mid-Cortical Area	Images from Endosteal Area	Images with Plexiform Bone	Images with Haversian Bone
Control	0	-	-	-	-	-
600	2	2	0	0	0	2
800	0	-	-	-	-	-
1000	7	3	4	3	3	6

Table B17 – Mean values of the histological parameters measured in secondary osteons in pig specimen, P1.

Temperature (^{o}C)	Number of Osteons	Mean Osteon Area (μm^2)	Mean Min. Diameter of Osteon (μm)	Mean Max. Diameter of Osteon (μm)
Control	0	-	-	-
600	0	-	-	-
800	0	-	-	-
1000	5	17399.88 $\pm$ 5753.41	126.68 $\pm$ 22.18	180.14 $\pm$ 39.81

Table B18 - Mean values of the histological parameters measured in Haversian canals in pig specimen, P1.

Temperature (^{o}C)	Number of Haversian Canals	Mean Haversian Canal Area (μm^2)	Mean Min. Diameter of Haversian Canal (μm)	Mean Max Diameter of Haversian Canal (μm)
Control	0	-	-	-
600	0	-	-	-
800	0	-	-	-
1000	13	435.30 $\pm$ 361.52	19.42 $\pm$ 6.59	27.57 $\pm$ 10.07

Table B19 – Histological structures and cortical regions displayed in digital images taken of pig specimen, P2.

Temperature	Number of Images	Images from Periosteal Area	Images from Mid-Cortical Area	Images from Endosteal Area	Images with Plexiform Bone	Images with Haversian Bone	Images with Reticular Bone
Control	8	3	3	2	7	5	2
600	2	0	0	2	0	1	2
800	5	3	3	3	3	4	2
1000	10	4	6	3	7	8	0

Table B20 – Mean values of the histological parameters measured in secondary osteons in pig specimen, P2.

Temperature (^{o}C)	Number of Osteons	Mean Osteon Area (μm^2)	Mean Min. Diameter of Osteon (μm)	Mean Max. Diameter of Osteon (μm)
Control	11	21519.69 ± 7516.17	138.36 ± 26.73	179.35 ± 39.27
600	0	-	-	-
800	0	-	-	-
1000	1	9	15197.86	118.68

Table B21 - Mean values of the histological parameters measured in Haversian canals in pig specimen, P2.

Temperature (^{o}C)	Number of Haversian Canals	Mean Haversian Canal Area (μm^2)	Mean Min. Diameter of Haversian Canal (μm)	Mean Max Diameter of Haversian Canal (μm)
Control	11	347.28 ± 147.41	16.59 ± 2.79	25.85 ± 7.58
600	0	-	-	-
800	5	357.93 ± 198.71	16.87 ± 6.26	24.04 ± 8.44
1000	9	178.77 ± 198.49	419.18 ± 4.37	17.45 ± 6.71

Table B22 – Histological structures and cortical regions displayed in digital images taken of pig specimen, P3.

Temperature	Number of Images	Images from Periosteal Area	Images from Mid-Cortical Area	Images from Endosteal Area	Images with Plexiform Bone	Images with Haversian Bone	Images with Reticular Bone
Control	8	2	3	2	4	7	0
600	-	-	-	-	-	-	-
800	5	2	1	2	1	3	1
1000	8	4	7	2	7	4	0

Note: Trabecular bone also present in one image at control, but not included in qualitative analysis

Table B23 – Mean values of the histological parameters measured in secondary osteons in pig specimen, P3.

Temperature (^{o}C)	Number of Osteons	Mean Osteon Area (μm^2)	Mean Min. Diameter of Osteon (μm)	Mean Max. Diameter of Osteon (μm)
Control	10	26263.43 $\pm$ 11564.52	155.90 $\pm$ 34.05	197.09 $\pm$ 46.52
600	-	-	-	-
800	2	19044.75 $\pm$ 534.37	141.08 $\pm$ 1.25	160.99 $\pm$ 13.70
1000	0	-	-	-

Table B24 - Mean values of the histological parameters measured in Haversian canals in pig specimen, P3.

Temperature (^{o}C)	Number of Haversian Canals	Mean Haversian Canal Area (μm^2)	Mean Min. Diameter of Haversian Canal (μm)	Mean Max Diameter of Haversian Canal (μm)
Control	9	851.82 $\pm$ 520.54	24.11 $\pm$ 8.00	31.45 $\pm$ 12.14
600	-	-	-	-
800	1	550.44	25.47	26.40
1000	0	-	-	-

Table B25 – Histological structures and cortical regions displayed in digital images taken of pig specimen, P4.

Temperature	Number of Images	Images from Periosteal Area	Images from Mid-Cortical Area	Images from Endosteal Area	Images with Plexiform Bone	Images with Haversian Bone	Images with Reticular Bone
Control	7	3	2	1	6	2	4
600	-	-	-	-	-	-	-
800	6	3	2	2	0	4?	2?
1000	9	4	7	2	8	8	0

Note: Trabecular bone also present in one image at control, but not included in qualitative analysis

Table B26 – Mean values of the histological parameters measured in secondary osteons in pig specimen, P4.

Temperature (^{o}C)	Number of Osteons	Mean Osteon Area (μm^2)	Mean Min. Diameter of Osteon (μm)	Mean Max. Diameter of Osteon (μm)
Control	8	19055.76 $\pm$ 5362.40	145.44 $\pm$ 25.48	187.07 $\pm$ 29.54
600	-	-	-	-
800	0	-	-	-
1000	2	10564.57 $\pm$ 680.23	95.96 $\pm$ 3.97	135.94 $\pm$ 5.30

Table B27 - Mean values of the histological parameters measured in Haversian canals in pig specimen, P4.

Temperature (^{o}C)	Number of Haversian Canals	Mean Haversian Canal Area (μm^2)	Mean Min. Diameter of Haversian Canal (μm)	Mean Max Diameter of Haversian Canal (μm)
Control	8	590.15 $\pm$ 262.17	22.67 $\pm$ 5.62	29.38 $\pm$ 6.72
600	-	-	-	-
800	0	-	-	-
1000	4	348.17 $\pm$ 141.54	18.40 $\pm$ 4.50	25.70 $\pm$ 5.06

Table B28 – Histological structures and cortical regions displayed in digital images taken of pig specimen, P5.

Temperature	Number of Images	Images from Periosteal Area	Images from Mid-Cortical Area	Images from Endosteal Area	Images with Plexiform Bone	Images with Haversian Bone	Images with Reticular Bone
Control	8	3	2	3	6	7	1
600	5	0	2	3	?	?	1
800	7	4	4	3	4	5	2
1000	8	4	7	3	3	8	0

Table B29 – Mean values of the histological parameters measured in secondary osteons in pig specimen, P5.

Temperature (^{o}C)	Number of Osteons	Mean Osteon Area (μm^2)	Mean Min. Diameter of Osteon (μm)	Mean Max. Diameter of Osteon (μm)
Control	8	17124.09 ± 3426.028	131.3013 ± 13.9158	165.5475 ± 19.0353
600	-	-	-	-
800	3	13689.72 ± 3636.729	112.1733 ± 11.89228	154.3967 ± 26.01985
1000	1	19516.89	137.36	161.78

Table B30 - Mean values of the histological parameters measured in Haversian canals in pig specimen, P5.

Temperature (^{o}C)	Number of Haversian Canals	Mean Haversian Canal Area (μm^2)	Mean Min. Diameter of Haversian Canal (μm)	Mean Max Diameter of Haversian Canal (μm)
Control	8	346.4575 ± 188.722	16.39125 ± 4.860239	25.30375 ± 6.494551
600	-	-	-	-
800	9	459.1783 ± 161.4107	19.83667 ± 7.5102	26.39111 ± 4.720777
1000	4	357.2158 ± 159.0417	17.225 ± 3.320434	26.135 ± 3.838798

Table B31 – Histological structures and cortical regions displayed in digital images taken of cow specimen, C1.

Temperature	Number of Images	Images from Periosteal Area	Images from Mid-Cortical Area	Images from Endosteal Area	Images with Plexiform Bone	Images with Haversian Bone	Images with Non-Vascular Bone
Control	10	4	3	3	2	8	3
600	7	4	2	1	7	7	0
800	8	3	3	2	7	6	0
1000	7	1	2	4	1	6	0

Table B32 – Mean values of the histological parameters measured in secondary osteons in cow specimen, C1.

Temperature (^{o}C)	Number of Osteons	Mean Osteon Area (μm^2)	Mean Min. Diameter of Osteon (μm)	Mean Max. Diameter of Osteon (μm)
Control	13	24384.59 ± 6136.36	159.23 ± 25.52	187.66 ± 23.79
600	1	25244.00	161.82	202.89
800	2	15017.34 ± 2577.43	122.93 ± 12.03	150.84 ± 13.30
1000	13	19566.04 ± 5273.54	140.50 ± 21.29	176.65 ± 28.68

Table B33 - Mean values of the histological parameters measured in Haversian canals in cow specimen, C1.

Temperature (^{o}C)	Number of Haversian Canals	Mean Haversian Canal Area (μm^2)	Mean Min. Diameter of Haversian Canal (μm)	Mean Max Diameter of Haversian Canal (μm)
Control	13	626.51 ± 256.04	22.97 ± 4.40	33.55 ± 11.31
600	1	995.73	30.60	42.81
800	10	225.94 ± 76.09	14.11 ± 2.56	20.32 ± 3.74
1000	13	588.17 ± 405.34	21.38 ± 7.58	30.63 ± 9.08

Table B34 – Histological structures and cortical regions displayed in digital images taken of cow specimen, C2.

Temperature	Number of Images	Images from Periosteal Area	Images from Mid-Cortical Area	Images from Endosteal Area	Images with Plexiform Bone	Images with Haversian Bone
Control	6	2	2	2	3	6
600	6	2	4	2	2	6
800	5	2	3	1	1	5
1000	6	3	1	2	4	4

Table B35 – Mean values of the histological parameters measured in secondary osteons in cow specimen, C2.

Temperature (^{o}C)	Number of Osteons	Mean Osteon Area (μm^2)	Mean Min. Diameter of Osteon (μm)	Mean Max. Diameter of Osteon (μm)
Control	8	37382.86 $\pm$ 16609.44	180.18 $\pm$ 36.77	241.21 $\pm$ 55.87
600	6	27557.25 $\pm$ 7938.72	172.40 $\pm$ 31.25	205.78 $\pm$ 28.50
800	17	19244.95 $\pm$ 5333.50	142.26 $\pm$ 21.45	166.87 $\pm$ 27.26
1000	4	16955.13 $\pm$ 3318.17	253.04 $\pm$ 16.50	172.63 $\pm$ 23.32

Table B36 - Mean values of the histological parameters measured in Haversian canals in cow specimen, C2.

Temperature (^{o}C)	Number of Haversian Canals	Mean Haversian Canal Area (μm^2)	Mean Min. Diameter of Haversian Canal (μm)	Mean Max Diameter of Haversian Canal (μm)
Control	8	1022.84 $\pm$ 669.37	28.46 $\pm$ 8.72	40.05 $\pm$ 14.20
600	18	528.93 $\pm$ 195.19	22.47 $\pm$ 4.09	31.24 $\pm$ 6.18
800	17	823.10 $\pm$ 401.80	28.75 $\pm$ 7.31	35.77 $\pm$ 9.56
1000	4	438.41 $\pm$ 179.40	17.51 $\pm$ 3.68	30.23 $\pm$ 5.59

Table B37 – Histological structures and cortical regions displayed in digital images taken of cow specimen, C3.

Temperature	Number of Images	Images from Periosteal Area	Images from Mid-Cortical Area	Images from Endosteal Area	Images with Plexiform Bone	Images with Haversian Bone	Images with Non-Vascular Bone
Control	8	3	3	2	2	6	2
600	9	3	5	4	2	7	0
800	4	3	1	0	4	0	0
1000	6	2	2	2	0	6	0

Table B38 – Mean values of the histological parameters measured in secondary osteons in cow specimen, C3.

Temperature (^{o}C)	Number of Osteons	Mean Osteon Area (μm^2)	Mean Min. Diameter of Osteon (μm)	Mean Max. Diameter of Osteon (μm)
Control	12	34662.46 ± 17332.52	194.03 ± 42.31	219.23 ± 57.18
600	18	32515.61 ± 12556.74	174.72 ± 37.28	229.63 ± 40.14
800	0	-	-	-
1000	16	30848.59 ± 13377.46	182.78 ± 49.61	211.11 ± 49.00

Table B39 - Mean values of the histological parameters measured in Haversian canals in cow specimen, C3.

Temperature (^{o}C)	Number of Haversian Canals	Mean Haversian Canal Area (μm^2)	Mean Min. Diameter of Haversian Canal (μm)	Mean Max Diameter of Haversian Canal (μm)
Control	12	724.67 ± 486.98	26.04 ± 9.25	31.28 ± 10.33
600	18	957.42 ± 284.50	30.06 ± 5.47	40.79 ± 7.86
800	0	-	-	-
1000	16	706.63 ± 320.08	26.64 ± 7.18	32.85 ± 9.19

Table B40 – Histological structures and cortical regions displayed in digital images taken of cow specimen, C4.

Temperature	Number of Images	Images from Periosteal Area	Images from Mid-Cortical Area	Images from Endosteal Area	Images with Plexiform Bone	Images with Haversian Bone	Images with Non-Vascular Bone
Control	8	2	3	3	0	8	1
600	2	1	1	0	1	1?	0
800	5	3	2	0	0	5	0
1000	5	3	1	1	0	5	0

Table B41 – Mean values of the histological parameters measured in secondary osteons in cow specimen, C4.

Temperature (^{o}C)	Number of Osteons	Mean Osteon Area (μm^2)	Mean Min. Diameter of Osteon (μm)	Mean Max. Diameter of Osteon (μm)
Control	6	38691.69 $\pm$ 9453.03	196.23 $\pm$ 23.41	235.71 $\pm$ 42.20
600	0	-	-	-
800	18	34442.83 $\pm$ 8619.98	181.84 $\pm$ 30.05	237.39 $\pm$ 34.87
1000	5	28599.18 $\pm$ 7605.51	162.68 $\pm$ 25.93	220.73 $\pm$ 38.72

Table B42 - Mean values of the histological parameters measured in Haversian canals in cow specimen, C4.

Temperature (^{o}C)	Number of Haversian Canals	Mean Haversian Canal Area (μm^2)	Mean Min. Diameter of Haversian Canal (μm)	Mean Max Diameter of Haversian Canal (μm)
Control	6	667.17 $\pm$ 373.91	27.26 $\pm$ 7.04	32.12 $\pm$ 8.01
600	0	-	-	-
800	14	693.98 $\pm$ 266.60	26.57 $\pm$ 5.59	34.00 $\pm$ 6.57
1000	5	612.55 $\pm$ 153.21	22.41 $\pm$ 3.67	32.55 $\pm$ 5.89

Table B43 – Histological structures and cortical regions displayed in digital images taken of cow specimen, C5.

Temperature	Number of Images	Images from Periosteal Area	Images from Mid-Cortical Area	Images from Endosteal Area	Images with Plexiform Bone	Images with Haversian Bone
Control	8	3	3	2	4	5
600	1	1	0	0	0	1
800	-	-	-	-	-	-
1000	8	3	3	2	3	7

Table B44 – Mean values of the histological parameters measured in secondary osteons in cow specimen, C5.

Temperature (^{o}C)	Number of Osteons	Mean Osteon Area (μm^2)	Mean Min. Diameter of Osteon (μm)	Mean Max. Diameter of Osteon (μm)
Control	4	32844.86 ± 7074.50	190.56 ± 36.55	216.04 ± 17.45
600	0	-	-	-
800	-	-	-	-
1000	11	29245.10 ± 12142.09	168.36 ± 35.77	207.49 ± 40.75

Table B45 - Mean values of the histological parameters measured in Haversian canals in cow specimen, C5.

Temperature (^{o}C)	Number of Haversian Canals	Mean Haversian Canal Area (μm^2)	Mean Min. Diameter of Haversian Canal (μm)	Mean Max Diameter of Haversian Canal (μm)
Control	4	604.77 ± 239.97	23.66 ± 4.45	32.13 ± 5.15
600	0	-	-	-
800	-	-	-	-
1000	11	878.49 ± 390.32	27.78 ± 6.65	39.93 ± 10.27

Appendix C – Quantitative Analysis per Temperature

Table C1 – Measurements of all osteon parameters for deer control samples.

Specimen	Image Number	Cortical Region	Area (μm^2)	Min. Diameter (µm)	Max. Diameter (µm)
D1-C	6	MC	13457.35	105.34	171.00
D1-C	6	MC	12733.51	104.49	146.79
D1-C	6	MC	14930.36	118.59	153.17
D1-C	6	MC	27607.46	152.02	237.50
D1-C	6	MC	9675.92	90.83	122.46
D2-C	1	E	18874.06	130.74	189.27
D2-C	1	E	16195.05	121.84	157.33
D2-C	1	E	14374.92	121.35	146.91
D2-C	1	E	15263.58	111.04	149.79
D2-C	1	E	15198.45	114.28	137.03
D2-C	1	E	17491.29	126.21	162.01
D2-C	2	E	13969.57	115.88	137.68
D2-C	2	E	13903.17	101.87	160.27
D2-C	2	E	18997.43	133.54	181.85
D3-C	2	MC	21893.83	142.79	180.76
D3-C	2	MC	14434.30	121.21	167.27
D3-C	3	MC	13373.22	118.35	142.48
D4-C	3	MC	20711.17	142.14	175.32
D4-C	3	MC	18984.08	113.10	202.26
D4-C	4	E	14697.00	130.25	145.79
D4-C	4	E	9852.61	102.39	126.15
D5-C	1	P	15773.34	112.77	152.70
D5-C	1	P	15947.11	124.91	182.53
D5-C	1	P	8817.80	94.91	118.27
D5-C	2	P	18918.71	138.29	182.50
D5-C	2	P	10824.34	108.41	122.11
D5-C	4	MC	9249.82	101.28	109.94
D5-C	4	MC	12972.02	120.81	128.27
D5-C	5	MC	10711.93	105.89	133.06
D5-C	5	MC	11507.09	111.28	138.24
D5-C	5	MC	21140.79	157.18	167.38
D5-C	6	E	19648.64	131.49	166.73
D5-C	6	E	16228.84	140.90	161.56
D5-C	6	E	20861.52	155.79	167.85
D5-C	7	E	19673.29	145.36	174.71

P = Periosteal Region MC = Mid-Cortical Region Endo = Endosteal Region

Table C2 – Measurements of all Haversian canal parameters for deer control samples.

Specimen	Image Number	Cortical Region	Area (μm^2)	Min. Diameter (µm)	Max. Diameter (µm)
D1-C	6	MC	477.26	20.73	28.35
D1-C	6	MC	524.99	23.03	24.75
D1-C	6	MC	231.40	14.68	20.82
D1-C	6	MC	615.84	19.34	37.96
D1-C	6	MC	441.37	22.62	23.14
D2-C	1	E	424.32	18.30	27.67
D2-C	1	E	262.41	14.05	21.26
D2-C	1	E	209.37	14.51	17.3
D2-C	1	E	361.05	17.70	20.00
D2-C	1	E	267.99	15.25	18.44
D2-C	1	E	242.87	15.70	18.63
D2-C	2	E	217.64	14.40	19.79
D2-C	2	E	241.62	12.30	23.30
D2-C	2	E	284.96	16.35	21.20
D3-C	2	MC	230.63	14.27	18.84
D3-C	2	MC	201.52	12.36	16.36
D3-C	3	MC	302.52	10.95	30.17
D4-C	3	MC	206.06	14.76	16.95
D4-C	3	MC	201.70	13.18	20.29
D4-C	4	E	165.56	13.80	16.25
D4-C	4	E	252.65	14.68	19.66
D5-C	1	P	376.22	17.04	24.62
D5-C	1	P	338.60	16.76	24.02
D5-C	1	P	222.15	14.69	17.99
D5-C	2	P	226.02	12.81	18.21
D5-C	2	P	286.16	17.13	17.61
D5-C	4	MC	453.29	21.25	24.44
D5-C	4	MC	184.10	14.32	18.02
D5-C	5	MC	378.28	16.17	28.46
D5-C	5	MC	360.27	17.40	25.97
D5-C	5	MC	180.13	13.10	19.50
D5-C	6	E	617.28	23.98	33.12
D5-C	6	E	755.60	26.42	38.05
D5-C	6	E	504.76	23.37	26.47
D5-C	7	E	392.84	19.55	24.96

P = Periosteal Region MC = Mid-Cortical Region E = Endosteal Region

Table C3 – Measurements of all osteon parameters for deer samples at 600°C.

Specimen	Image Number	Cortical Region	Area (μm^2)	Min. Diameter (μm)	Max. Diameter (μm)
D1-1	2	P	17026.43	142.5	158.63
D1-1	2	P	16346.79	133.7	166.36
D2-1	1	P	17425.09	139.51	156.07
D2-1	1	P	11139.6	101.73	126.19
D2-1	3	P	10334.23	132.73	101.14

P = Periosteal Region

Table C4 – Measurements of all Haversian canal parameters for deer samples at 600°C.

Specimen	Image Number	Cortical Region	Area (μm^2)	Min. Diameter (μm)	Max. Diameter (μm)
D1-1	2	P	165.95	11.41	16.22
D1-1	2	P	366.06	18.78	19.62
D1-1	2	P	322.13	15.47	20.62
D2-1	1	P	207.00	14.24	17.8
D2-1	1	P	310.50	19.33	21.62
D2-1	3	P	242.64	12.41	20.58
D2-1	3	P	305.32	17.09	22.63
D2-1	3	P	202.20	13.47	16.26
D2-1	3	P	266.90	12.11	18.13
D5-1	5	E	193.64	14.42	19.06

P = Periosteal Region E = Endosteal Region

Table C5 – Measurements of all osteon parameters for deer samples at 800°C.

Specimen	Image Number	Cortical Region	Area (μm^2)	Min. Diameter (μm)	Max. Diameter (μm)
D1-2	1	P	32719.43	181.58	228.64
D1-2	1	P	10899.12	104.68	129.87
D1-2	2	P	15491.46	128.33	155.69
D1-2	2	P	13105.50	95.47	150.87
D1-2	2	P	12776.84	117.93	136.24
D1-2	3	P	14946.93	121.96	134.51
D1-2	3	P	15724.00	125.65	152.94
D1-2	6	P	20072.43	130.40	200.81
D1-2	6	P	23756.79	160.22	188.56
D2-2	4	MC/E	15255.69	119.25	151.97
D2-2	4	MC/E	12127.70	100.38	143.17
D2-2	4	MC/E	8168.569	92.89	109.05
D2-2	4	MC/E	9899.281	91.60	122.13
D2-2	4	MC/E	14944.75	111.90	171.44
D2-2	4	MC/E	16751.73	115.00	189.66
D2-2	5	MC	16547.26	111.10	161.12
D2-2	5	MC	10008.60	95.71	135.14

D2-2	5	MC	15407.19	111.98	183.16
D2-2	7	MC/E	19667.14	134.05	177.32
D2-2	7	MC/E	16633.26	124.92	147.26
D2-2	7	MC/E	24740.77	169.18	194.16
D3-2	3	MC/E	14757.52	127.87	165.71
D3-2	3	MC/E	11464.38	110.42	125.77
D3-2	5	P	29851.44	169.25	210.95
D3-2	5	P	26185.07	144.85	200.66
D5-2	3	P	12372.90	106.13	126.84
D5-2	3	P	18679.26	126.29	187.55
D5-2	4	E	6462.473	81.12	103.52
D5-2	4	E	22461.43	160.63	179.82
D5-2	4	E	14852.00	133.54	149.59
D5-2	4	E	21319.51	140.45	204.87

P = Periosteal Region MC = Mid-Cortical Region E = Endosteal Region
MC/E = Image displaying section of Mid-Cortical/Endosteal Regions

Table C6 – Measurements of all Haversian canal parameters for deer samples at 800^{o}C.

Specimen	**Image Number**	**Cortical Region**	**Area (μm^2)**	**Min. Diameter (µm)**	**Max. Diameter (µm)**
D1-2	1	P	203.84	12.34	21.52
D1-2	1	P	341.48	13.36	23.58
D1-2	1	P	286.85	21.36	13.87
D1-2	1	P	360.40	16.69	30.82
D1-2	1	P	315.22	19.58	20.48
D1-2	1	P	332.03	15.10	23.60
D1-2	1	P	353.04	14.57	27.06
D1-2	1	P	184.93	11.04	17.84
D1-2	1	P	420.29	22.13	26.73
D1-2	1	P	290.00	17.80	26.08
D1-2	2	P	359.33	21.22	26.23
D1-2	2	P	102.53	7.97	15.69
D1-2	2	P	414.91	19.28	27.54
D1-2	3	P	316.74	17.50	20.36
D1-2	3	P	568.02	19.84	29.14
D1-2	3	P	401.20	21.16	25.30
D1-2	3	P	456.11	20.27	26.52
D1-2	6	P	198.96	12.40	19.17
D1-2	6	P	121.06	10.31	12.83
D2-2	4	MC/E	294.32	13.74	17.31
D2-2	4	MC/E	133.96	9.12	15.43
D2-2	4	MC/E	138.85	10.18	15.48
D2-2	4	MC/E	142.76	12.85	12.97
D2-2	4	MC/E	114.40	8.18	15.91
D2-2	4	MC/E	324.63	17.52	23.82

D2-2	5	MC	222.00	16.35	17.47
D2-2	5	MC	158.41	12.31	16.21
D2-2	5	MC	301.78	15.66	25.73
D2-2	7	MC/E	229.50	15.57	16.18
D2-2	7	MC/E	188.75	15.90	18.43
D2-2	7	MC/E	244.51	15.38	16.70
D3-2	3	MC/E	643.54	21.49	34.83
D3-2	3	MC/E	404.84	16.94	27.36
D3-2	5	P	265.54	14.78	21.31
D3-2	5	P	140.98	11.36	13.94
D5-2	3	P	425.24	21.07	26.69
D5-2	3	P	109.92	9.50	17.73
D5-2	4	E	258.02	17.57	19.07
D5-2	4	E	636.98	25.12	34.86
D5-2	4	E	674.27	23.09	42.10

P = Periosteal Region MC = Mid-Cortical Region E = Endosteal Region
MC/E = Image displaying section of Mid-Cortical/Endosteal Regions

Table C7 – Measurements of all osteon parameters for deer samples at 1000^{o}C.

Specimen	**Image Number**	**Cortical Region**	**Area (μm^2)**	**Min. Diameter (µm)**	**Max. Diameter (µm)**
D1-3	1	E	22612.29	145.38	204.44
D1-3	1	E	20074.70	154.44	172.86
D1-3	1	E	21492.27	151.37	179.79
D2-3	1	MC	19806.56	136.15	183.35
D2-3	1	MC	31754.46	197.71	183.88
D2-3	1	MC	10822.90	113.92	116.45
D2-3	1	MC	6820.80	88.41	99.32
D2-3	5	E	8235.23	100.97	108.23
D2-3	5	E	10870.98	105.22	130.32
D2-3	5	E	14627.06	111.91	164.54
D2-3	5	E	7997.09	87.70	110.31
D2-3	5	E	17245.49	145.75	165.29
D3-3	2	MC/E	12067.19	112.4	152.12
D4-3	5	MC/E	18120.17	146.76	167.99
D4-3	5	MC/E	15298.5	123.57	157.55
D4-3	5	MC/E	7583.19	89.76	105.70
D5-3	3	MC	7246.41	72.21	118.09
D5-3	3	MC	12886.8	103.4	157.60
D5-3	3	MC	11100.19	101.18	129.26
D5-3	3	MC	9784.42	85.70	115.61
D5-3	3	MC	9517.83	84.70	142.20

D5-3	4	MC	10148.33	97.76	127.91
D5-3	4	MC	12138.91	99.71	135.44
D5-3	4	MC	20412.91	125.80	215.03
D5-3	4	MC	12556.57	96.22	167.57
D5-3	4	MC	17975.87	132.16	173.27
D5-3	5	MC	12254.28	110.99	141.60
D5-3	5	MC	10204.34	84.03	148.25
D5-3	5	MC	9388.60	95.44	133.89
D5-3	5	MC	13436.05	106.96	155.32
D5-3	5	MC	11771.29	112.54	137.37

P = Periosteal Region MC = Mid-Cortical Region E = Endosteal Region
MC/E = Image displaying section of Mid-Cortical/Endosteal Regions

Table C8 – Measurements of all Haversian canal parameters for deer samples at 1000^{o}C.

Specimen	**Image Number**	**Cortical Region**	**Area (μm^2)**	**Min. Diameter (µm)**	**Max. Diameter (µm)**
D1-3	1	E	641.41	24.79	34.03
D1-3	1	E	367.73	18.73	23.71
D1-3	1	E	385.97	19.10	23.24
D2-3	1	MC	287.23	17.61	23.86
D2-3	1	MC	670.21	26.73	32.45
D2-3	1	MC	110.11	11.74	12.91
D2-3	1	MC	164.68	11.76	17.61
D2-3	5	E	191.59	14.60	17.55
D2-3	5	E	290.10	12.18	23.98
D2-3	5	E	202.42	12.13	18.87
D2-3	5	E	257.62	17.69	20.99
D2-3	5	E	311.74	18.74	21.95
D3-3	2	MC/E	360.97	17.15	27.13
D4-3	5	MC/E	595.58	25.27	29.85
D4-3	5	MC/E	368.05	18.46	24.85
D4-3	5	MC/E	226.49	17.08	19.46
D5-3	3	MC	271.97	16.75	22.26
D5-3	3	MC	160.17	11.82	16.11
D5-3	3	MC	492.34	19.56	26.98
D5-3	3	MC	268.74	14.44	22.37
D5-3	3	MC	216.07	14.96	19.02
D5-3	4	MC	198.54	12.99	15.70
D5-3	4	MC	191.34	13.36	16.32
D5-3	4	MC	427.95	16.38	31.30
D5-3	4	MC	401.20	15.21	30.41
D5-3	4	MC	682.04	24.11	36.26

D5-3	5	MC	465.85	24.86	27.88
D5-3	5	MC	411.40	18.42	26.88
D5-3	5	MC	311.58	18.04	21.96
D5-3	5	MC	884.31	29.82	38.48
D5-3	5	MC	249.06	15.10	21.26

P = Periosteal Region MC = Mid-Cortical Region E = Endosteal Region

MC/E = Image displaying section of Mid-Cortical/Endosteal Regions

Table C9 - Measurements of all osteon parameters for pig control samples.

Specimen	Image Number	Cortical Region	Area (μm^2)	Min. Diameter (µm)	Max. Diameter (µm)
P2-C	4	MC	8895.84	96.13	107.83
P2-C	4	MC	16521.46	134.48	147.88
P2-C	5	MC	22427.60	129.64	201.32
P2-C	5	MC	20157.66	143.62	173.15
P2-C	5	MC	28463.49	183.44	188.79
P2-C	6	MC	28724.74	170.36	213.89
P2-C	7	E	32795.70	152.04	240.41
P2-C	7	E	28267.56	153.52	223.19
P2-C	8	E	16748.43	111.26	163.46
P2-C	8	E	12449.79	106.34	139.71
P2-C	8	E	21264.28	141.17	173.23
P3-C	1	P	17014.14	104.46	155.57
P3-C	1	P	17406.66	137.94	167.64
P3-C	3	MC	23707.24	163.21	199.21
P3-C	3	MC	34234.67	184.10	232.18
P3-C	3	MC	50410.30	219.35	287.57
P3-C	4	MC	33545.08	173.65	205.84
P3-C	4	MC	33096.94	170.96	237.42
P3-C	4	MC	16574.69	139.73	151.56
P3-C	5	MC	12543.40	113.85	136.34
P3-C	5	MC	24101.23	151.73	197.56
P4-C	2	P	16202.95	120.13	154.32
P4-C	2	P	20259.52	147.79	187.84
P4-C	3	P	18449.97	158.47	170.97
P4-C	3	P	9859.18	108.84	117.88
P4-C	3	P	14806.50	122.11	124.99
P4-C	5	MC	25709.50	179.17	191.10
P4-C	5	MC	24902.86	168.72	176.93
P4-C	5	MC	22255.58	158.26	193.17
P5-C	2	P	18936.16	142.14	156.61
P5-C	2	P	18887.40	128.25	177.68

P5-C	6	MC	22018.54	161.47	170.07
P5-C	7	E	17890.81	126.69	174.13
P5-C	7	E	12800.18	123.26	149.10
P5-C	7	E	12215.24	124.14	136.98
P5-C	8	E	19175.76	125.13	198.83
P5-C	8	E	15068.60	119.33	160.98

P = Periosteal Region MC = Mid-Cortical Region E = Endosteal Region

Table C10 - Measurements of all Haversian canal parameters for pig control samples.

Specimen	**Image Number**	**Cortical Region**	**Area (μm^2)**	**Min. Diameter (µm)**	**Max. Diameter (µm)**
P2-C	4	MC	304.10	14.79	24.66
P2-C	4	MC	177.68	14.82	15.02
P2-C	5	MC	237.58	13.67	22.57
P2-C	5	MC	200.23	11.92	23.27
P2-C	5	MC	500.05	17.32	37.08
P2-C	6	MC	488.23	22.52	25.49
P2-C	7	E	634.12	17.72	39.64
P2-C	7	E	452.74	17.56	31.33
P2-C	8	E	286.85	17.46	21.93
P2-C	8	E	286.16	18.14	26.26
P2-C	8	E	252.38	16.61	17.10
P3-C	1	P	507.23	24.32	29.42
P3-C	1	P	269.40	17.83	19.06
P3-C	3	MC	1677.74	37.30	52.36
P3-C	3	MC	1435.61	34.24	51.33
P3-C	3	MC	335.79	16.27	22.95
P3-C	4	MC	317.06	16.50	24.39
P3-C	4	MC	586.69	29.05	28.42
P3-C	4	MC	315.38	16.91	23.83
P3-C	5	MC	569.66	24.58	31.30
P4-C	2	P	676.68	22.79	33.75
P4-C	2	P	558.84	21.87	28.94
P4-C	3	P	953.79	27.16	39.94
P4-C	3	P	282.48	16.37	18.73
P4-C	3	P	347.84	14.88	26.42
P4-C	5	MC	962.28	32.59	34.27
P4-C	5	MC	568.44	23.56	29.81
P4-C	5	MC	370.84	22.10	23.16
P5-C	2	P	766.93	24.30	39.68
P5-C	2	P	303.67	15.65	23.08

P5-C	6	MC	225.26	15.16	17.89
P5-C	7	E	262.08	10.50	25.76
P5-C	7	E	464.34	22.43	26.24
P5-C	7	E	307.66	17.57	26.32
P5-C	8	E	189.86	11.81	21.02
P5-C	8	E	251.85	13.71	22.44

P = Periosteal Region MC = Mid-Cortical Region E = Endosteal Region

Table C11 - Measurements of all osteon parameters for pig samples at 800^{o}C.

Specimen	Image Number	Cortical Region	Area (μm^2)	Min. Diameter (μm)	Max. Diameter (μm)
P3-2	2	E	19422.61	140.19	170.68
P3-2	2	E	18666.90	141.96	151.30
P5-2	4	P/MC	11650.28	110.95	139.66
P5-2	4	P/MC	11530.39	100.94	139.09
P5-2	4	P/MC	17888.48	124.63	184.44

E = Endosteal Region

P/MC = Image displaying section of Periosteal/Mid-Cortical Regions

Table C12 - Measurements of all Haversian canal parameters for pig samples at 800^{o}C.

Specimen	Image Number	Cortical Region	Area (μm^2)	Min. Diameter (μm)	Max. Diameter (μm)
P2-2	2	P/M/E	598.85	26.50	26.63
P2-2	2	P/M/E	295.28	17.62	19.46
P2-2	2	P/M/E	190.42	10.80	20.07
P2-2	2	P/M/E	536.75	17.66	37.60
P2-2	2	P/M/E	168.34	11.75	16.46
P3-2	2	E	550.44	25.47	26.40
P5-2	4	P/MC	562.16	23.04	30.93
P5-2	4	P/MC	377.80	17.93	25.81
P5-2	4	P/MC	594.40	14.30	32.06
P5-2	4	P/MC	205.52	14.06	17.87
P5-2	4	P/MC	312.31	12.42	24.42
P5-2	4	P/MC	738.47	37.19	21.63
P5-2	4	P/MC	482.57	20.69	31.30
P5-2	4	P/MC	371.75	16.61	25.83
P5-2	4	P/MC	487.61	22.29	27.67

E = Endosteal Region

P/MC = Image displaying section of Periosteal/Mid-Cortical Regions

P/M/E = Image displaying section Periosteal/Mid-Cortical/Endosteal Regions

Table C13 - Measurements of all osteon parameters for pig samples at 1000°C.

Specimen	Image Number	Cortical Region	Area (μm^2)	Min. Diameter (µm)	Max. Diameter (µm)
P1-3	7	E	16203.37	114.90	187.35
P1-3	7	E	19661.26	135.07	193.35
P1-3	7	E	14748.92	130.14	155.52
P1-3	7	E	25860.26	156.21	234.67
P1-3	7	E	10525.59	97.10	129.81
P2-3	10	MC/E	15197.86	118.68	178.77

E = Endosteal Region
MC/E = Image displaying section of Mid-Cortical/Endosteal Regions

Table C14 - Measurements of all Haversian canal parameters for pig samples at 1000°C.

Specimen	Image Number	Cortical Region	Area (μm^2)	Min. Diameter (µm)	Max. Diameter (µm)
P1-3	1	P	230.09	15.67	19.97
P1-3	1	P	658.62	28.93	32.49
P1-3	1	P	287.61	17.65	21.15
P1-3	5	MC/E	365.85	24.75	26.00
P1-3	5	MC/E	199.13	12.30	19.02
P1-3	5	MC/E	346.17	17.91	24.89
P1-3	5	MC/E	295.22	18.32	20.09
P1-3	7	E	389.18	15.75	25.54
P1-3	7	E	264.08	12.16	28.10
P1-3	7	E	231.32	12.16	19.24
P1-3	7	E	1571.59	33.18	56.31
P1-3	7	E	388.18	19.58	32.58
P1-3	7	E	431.87	24.10	33.04
P2-3	6	MC	568.15	22.38	33.07
P2-3	6	MC	817.56	25.94	38.45
P2-3	6	MC	441.90	17.32	33.59
P2-3	6	MC	373.59	16.68	31.21
P2-3	8	MC/E	210.46	12.72	19.54
P2-3	8	MC/E	339.48	14.04	29.35
P2-3	8	MC/E	270.74	14.54	24.74
P2-3	8	MC/E	542.53	19.21	35.21
P2-3	10	MC/E	208.20	14.22	19.87

P = Periosteal Region MC = Mid-Cortical Region E = Endosteal Region
MC/E = Image displaying section of Mid-Cortical/Endosteal Regions

Table C15 - Measurements of all osteon parameters for cow control samples.

Specimen	Image Number	Cortical Region	Area (μm^2)	Min. Diameter (µm)	Max. Diameter (µm)
C1-C	3	P	25893.42	179.42	180.59
C1-C	3	P	33302.72	196.61	204.35
C1-C	4	MC	17489.43	136.15	181.52
C1-C	4	MC	26111.41	177.15	188.6
C1-C	5	MC	22888.08	154.18	182.61
C1-C	5	MC	23031.89	159.3	186.05
C1-C	5	MC	23927.54	165.08	169.21
C1-C	5	MC	14428.61	130.57	146.56
C1-C	6	MC	31134.59	156.89	219.66
C1-C	6	MC	22548.48	148.82	188.22
C1-C	6	MC	33883.43	197.39	224.08
C1-C	7	MC	26491.55	161.15	215.57
C1-C	7	MC	15868.56	107.28	152.50
C2-C	1	P	25275.11	144.15	196.91
C2-C	3	MC	34543.03	162.36	243.04
C2-C	3	MC	27378.9	162.01	200.78
C2-C	3	MC	23012.73	152.08	174.11
C2-C	4	MC	30757.22	165.70	233.07
C2-C	4	MC	38801.84	185.62	263.58
C2-C	4	MC	74353.71	251.06	353.60
C2-C	5	E	44940.39	218.45	264.62
C3-C	3	P	34516.39	214.68	223.26
C3-C	3	P	34027.91	186.97	247.20
C3-C	3	P	25980.13	179.78	196.53
C3-C	4	P	25311.68	165.25	196.35
C3-C	4	P	18890.22	153.59	158.14
C3-C	5	MC	19384.35	158.48	162.16
C3-C	5	MC	21908.72	159.33	170.28
C3-C	7	E	75123.94	276.28	351.75
C3-C	7	E	48032.57	224.75	267.82
C3-C	7	E	26390.99	157.23	177.84
C3-C	8	E	58467.11	264.58	273.34
C3-C	8	E	27915.54	187.44	206.07
C4-C	1	P	42217.41	204.20	261.48
C4-C	1	P	45908.47	213.53	270.94
C4-C	4	MC	50201.86	216.71	276.78
C4-C	4	MC	25750.98	162.59	166.67
C4-C	7	E	38450.72	209.56	218.22

C4-C	7	E	29620.72	170.77	220.19
C5-C	3	P	32194.95	197.72	216.61
C5-C	3	P	43037.44	235.62	236.11
C5-C	8	E	27684.1	147.66	217.90
C5-C	8	E	28462.96	181.25	193.53

P = Periosteal Region MC = Mid-Cortical Region E = Endosteal Region

Table C16 - Measurements of all Haversian canal parameters for cow control samples.

Specimen	**Image Number**	**Cortical Region**	**Area (μm^2)**	**Min. Diameter (µm)**	**Max. Diameter (µm)**
C1-C	3	P	517.45	22.7	32.07
C1-C	3	P	849.71	23.01	39.83
C1-C	4	MC	574.46	32.39	23.32
C1-C	4	MC	607.46	25.89	33.25
C1-C	5	MC	521.55	18.23	34.58
C1-C	5	MC	562.51	18.33	30.43
C1-C	5	MC	407.77	20.76	21.96
C1-C	5	MC	249.40	16.38	17.17
C1-C	6	MC	580.29	26.97	27.73
C1-C	6	MC	425.54	20.84	28.42
C1-C	6	MC	659.81	21.79	38.98
C1-C	7	MC	1227.25	23.90	58.12
C1-C	7	MC	961.44	27.43	50.35
C2-C	1	P	774.33	27.68	33.97
C2-C	3	MC	1239.99	27.22	53.12
C2-C	3	MC	259.85	16.43	19.38
C2-C	3	MC	753.34	27.76	33.65
C2-C	4	MC	705.40	25.19	36.9
C2-C	4	MC	442.33	21.28	29.00
C2-C	4	MC	2076.63	39.21	54.31
C2-C	5	E	1930.86	42.87	60.05
C3-C	3	P	788.11	24.5	34.57
C3-C	3	P	375.59	19.76	24.35
C3-C	3	P	649.90	26.71	28.76
C3-C	4	P	485.67	23.33	20.91
C3-C	4	P	578.27	25.44	28.7
C3-C	5	MC	1067.26	37.21	37.44
C3-C	5	MC	229.66	14.12	17.18
C3-C	7	E	2104.46	48.66	56.38
C3-C	7	E	717.71	20.34	41.17
C3-C	7	E	406.22	18.64	26.58

C3-C	8	E	743.35	30.28	31.02
C3-C	8	E	549.89	23.45	28.33
C4-C	1	P	1433.32	39.68	48.87
C4-C	1	P	546.24	21.05	29.68
C4-C	4	MC	521.48	26.26	27.34
C4-C	4	MC	376.76	20.24	20.81
C4-C	7	E	744.72	29.37	31.75
C4-C	7	E	671.89	26.97	34.29
C5-C	3	P	589.01	22.36	33.33
C5-C	3	P	938.77	30.22	38.01
C5-C	8	E	488.88	20.34	27.47
C5-C	8	E	386.64	21.73	27.30

P = Periosteal Region MC = Mid-Cortical Region E = Endosteal Region

Table C17 - Measurements of all osteon parameters for cow samples at 600^{o}C.

Specimen	**Image Number**	**Cortical Region**	**Area (μm^2)**	**Min. Diameter (µm)**	**Max. Diameter (µm)**
C1-1	2	P	25244.00	161.82	202.89
C2-1	2	MC/E	30533.17	175.22	206.41
C2-1	3	MC/E	22384.31	148.06	210.52
C2-1	3	MC/E	29020.44	184.35	203.59
C2-1	3	MC/E	36688.63	208.6	232.95
C2-1	4	MC/E	32266.84	194.25	228.24
C2-1	6	P	14450.09	123.89	152.95
C3-1	5	MC	17877.85	149.37	161.08
C3-1	5	MC	42679.32	190.33	252.21
C3-1	5	MC	18891.69	120.56	198.67
C3-1	6	MC/E	64551.71	286.38	300.69
C3-1	6	MC/E	27936.64	180.00	192.53
C3-1	6	MC/E	31294.85	162.39	240.75
C3-1	6	MC/E	22392.61	154.43	190.22
C3-1	6	MC/E	24716.48	155.72	210.17
C3-1	6	MC/E	23020.12	151.96	197.52
C3-1	7	MC/E	41884.36	206.40	285.12
C3-1	7	MC/E	23884.84	151.49	205.22
C3-1	7	MC/E	21573.37	138.55	200.57
C3-1	7	MC/E	22783.86	142.65	218.65
C3-1	7	MC/E	46847.39	191.12	247.08
C3-1	7	MC/E	30976.05	199.85	209.30
C3-1	7	MC/E	41229.53	184.63	287.50
C3-1	7	MC/E	46745.94	206.22	272.83

C3-1	7	MC/E	35994.42	172.88	263.26
C3-1	9	E	36245.78	185.19	242.22
C3-1	9	E	38785.46	197.22	276.38
C3-1	9	E	54471.48	249.67	302.46
C3-1	9	E	37833.22	190.77	235.31
C3-1	9	E	33512.42	181.65	239.82
C3-1	9	E	42702.63	220.44	257.98
C3-1	9	E	24195.6	155.91	204.21

P = Periosteal Region MC = Mid-Cortical Region E = Endosteal Region
MC/E = Image displaying section of Mid-Cortical/Endosteal Regions

Table C18 - Measurements of all Haversian canal parameters for cow samples at 600^{o}C.

Specimen	**Image Number**	**Cortical Region**	**Area (μm^2)**	**Min. Diameter (μm)**	**Max. Diameter (μm)**
C1-1	2	P	995.73	29.01	42.81
C2-1	2	MC/E	585.80	23.98	31.61
C2-1	2	MC/E	723.28	29.96	30.06
C2-1	2	MC/E	477.21	19.97	31.97
C2-1	2	MC/E	937.47	26.63	44.04
C2-1	2	MC/E	549.93	23.46	29.94
C2-1	3	MC/E	558.87	22.90	38.60
C2-1	3	MC/E	1016.71	34.93	41.65
C2-1	3	MC/E	590.84	21.25	37.97
C2-1	3	MC/E	423.31	20.23	32.13
C2-1	4	MC/E	397.84	21.00	27.00
C2-1	4	MC/E	379.75	17.58	21.79
C2-1	4	MC/E	479.81	25.47	27.80
C2-1	4	MC/E	578.67	21.41	34.20
C2-1	4	MC/E	323.09	17.58	27.09
C2-1	4	MC/E	353.23	21.32	21.44
C2-1	6	P	373.91	17.47	29.96
C2-1	6	P	379.70	19.95	26.39
C2-1	6	P	391.28	19.29	28.73
C3-1	5	MC	1198.46	37.37	45.14
C3-1	5	MC	1418.14	36.06	53.93
C3-1	5	MC	608.51	25.23	30.25
C3-1	6	MC/E	1265.47	34.36	43.81
C3-1	6	MC/E	1183.90	34.50	45.89
C3-1	6	MC/E	984.14	32.55	42.72
C3-1	6	MC/E	787.52	29.45	37.36
C3-1	6	MC/E	836.68	27.52	39.62

C3-1	6	MC/E	676.66	25.89	35.45
C3-1	7	MC/E	1383.43	33.30	53.20
C3-1	7	MC/E	973.01	29.91	42.34
C3-1	7	MC/E	715.92	25.27	36.54
C3-1	7	MC/E	666.35	21.39	28.70
C3-1	7	MC/E	620.24	22.04	33.32
C3-1	7	MC/E	956.87	36.01	37.22
C3-1	7	MC/E	1185.13	32.18	49.26
C3-1	7	MC/E	559.13	21.50	29.66
C3-1	7	MC/E	1213.96	36.52	49.84
C3-1	9	E	611.38	24.76	32.25
C3-1	9	E	863.51	27.46	42.54
C3-1	9	E	971.72	27.01	44.44
C3-1	9	E	640.60	26.70	28.97
C3-1	9	E	717.43	29.15	37.89
C3-1	9	E	1034.48	33.06	41.60

P = Periosteal Region MC = Mid-Cortical Region E = Endosteal Region
MC/E = Image displaying section of Mid-Cortical/Endosteal Regions

Table C19 - Measurements of all osteon parameters for cow samples at 800^{o}C.

Specimen	**Image Number**	**Cortical Region**	**Area (μm^2)**	**Min. Diameter (μm)**	**Max. Diameter (μm)**
C1-2	7	E	13194.82	114.42	141.43
C1-2	8	E	16839.86	131.44	160.24
C2-2	3	MC	19302.34	151.94	165.57
C2-2	3	MC	19591.71	147.19	186.64
C2-2	3	MC	12192.32	119.50	123.53
C2-2	3	MC	10378.37	104.90	125.39
C2-2	3	MC	24814.37	158.02	191.49
C2-2	3	MC	9941.08	99.19	122.78
C2-2	3	MC	25299.17	170.77	176.90
C2-2	3	MC	18347.86	146.61	165.58
C2-2	3	MC	23960.30	149.84	194.97
C2-2	3	MC	18809.99	140.51	156.43
C2-2	3	MC	13153.28	134.41	135.28
C2-2	3	MC	18808.91	137.22	158.05
C2-2	4	MC	24233.60	154.83	192.65
C2-2	4	MC	16210.57	124.18	161.21
C2-2	4	MC	25584.09	170.75	204.31
C2-2	4	MC	24887.99	172.50	176.32
C2-2	4	MC	21648.26	136.00	199.77

C4-2	1	P	33194.42	195.97	223.59
C4-2	1	P	46803.31	222.29	242.95
C4-2	1	P	19550.30	136.12	178.72
C4-2	1	P	44787.61	232.81	240.00
C4-2	3	P	37982.39	203.36	245.82
C4-2	3	P	33715.79	176.83	242.13
C4-2	3	P	29074.77	137.98	257.85
C4-2	3	P	24351.91	151.05	196.44
C4-2	4	MC	44075.16	212.84	259.33
C4-2	4	MC	32374.14	198.95	219.49
C4-2	4	MC	53104.37	227.57	334.37
C4-2	4	MC	25591.19	159.93	222.40
C4-2	4	MC	29273.55	161.86	226.73
C4-2	4	MC	33210.16	186.17	219.19
C4-2	4	MC	29742.16	165.40	212.54
C4-2	5	MC	37052.98	160.13	293.04
C4-2	5	MC	27964.28	160.05	222.69
C4-2	5	MC	38122.44	183.86	235.65

P = Periosteal Region MC = Mid-Cortical Region E = Endosteal Region

Table C20 - Measurements of all Haversian canal parameters for cow samples at 800^{o}C.

Specimen	Image Number	Cortical Region	Area (μm^2)	Min. Diameter (μm)	Max. Diameter (μm)
C1-2	6	MC	226.53	15.88	20.84
C1-2	6	MC	158.57	10.96	19.11
C1-2	6	MC	134.93	14.07	14.23
C1-2	6	MC	193.04	14.31	17.89
C1-2	7	E	237.40	13.39	23.83
C1-2	7	E	285.52	16.55	21.33
C1-2	7	E	236.33	10.80	25.58
C1-2	7	E	221.36	13.13	18.31
C1-2	8	E	401.03	19.20	25.20
C1-2	8	E	164.75	12.77	16.85
C2-2	3	MC	1166.11	37.42	38.45
C2-2	3	MC	574.42	24.96	29.79
C2-2	3	MC	767.69	32.21	33.95
C2-2	3	MC	570.10	22.24	29.59
C2-2	3	MC	921.01	25.98	41.86
C2-2	3	MC	714.78	28.59	33.77
C2-2	3	MC	1740.53	42.40	56.35
C2-2	3	MC	1258.97	34.42	50.07

C2-2	3	MC	1067.85	34.60	43.02
C2-2	3	MC	1455.48	42.20	45.73
C2-2	3	MC	376.83	21.69	23.24
C2-2	3	MC	323.92	19.32	24.54
C2-2	4	MC	698.49	23.68	36.18
C2-2	4	MC	381.43	20.31	25.50
C2-2	4	MC	562.60	24.12	27.76
C2-2	4	MC	519.69	25.13	27.16
C2-2	4	MC	892.77	29.56	41.21
C4-2	3	P	1071.70	36.06	39.30
C4-2	3	P	382.27	19.47	28.33
C4-2	3	P	367.69	18.76	26.92
C4-2	3	P	588.54	23.22	36.57
C4-2	4	MC	810.16	34.37	35.35
C4-2	4	MC	837.10	28.35	39.92
C4-2	4	MC	528.98	23.21	30.38
C4-2	4	MC	506.35	23.87	25.69
C4-2	4	MC	780.00	28.55	37.92
C4-2	4	MC	893.12	28.91	41.07
C4-2	4	MC	479.49	25.37	25.81
C4-2	5	MC	979.48	31.84	40.06
C4-2	5	MC	364.46	19.21	25.46
C4-2	5	MC	1126.41	30.78	43.16

P = Periosteal Region MC = Mid-Cortical Region E = Endosteal Region

Table C21 - Measurements of all osteon parameters for cow samples at 1000^{o}C.

Specimen	**Image Number**	**Cortical Region**	**Area (μm^2)**	**Min. Diameter (μm)**	**Max. Diameter (μm)**
C1-3	3	MC	17186.54	150.62	151.18
C1-3	3	MC	16343.07	132.92	163.16
C1-3	5	E	25315.91	156.20	204.18
C1-3	5	E	22691.98	160.76	191.58
C1-3	5	E	28338.30	180.11	208.39
C1-3	5	E	22644.92	145.09	187.67
C1-3	6	E	24161.07	162.03	187.81
C1-3	6	E	22041.18	140.16	209.54
C1-3	7	E	22161.32	122.59	212.71
C1-3	7	E	12717.00	132.77	135.79
C1-3	7	E	13929.17	122.79	136.09
C1-3	7	E	13247.84	114.59	147.08
C1-3	7	E	13580.24	105.84	161.24

C2-3	1	P	18455.93	129.37	171.47
C2-3	1	P	14529.89	100.31	203.22
C2-3	3	P/MC	13919.56	121.68	146.48
C2-3	3	P/MC	20915.16	139.14	169.36
C3-3	1	P	47822.09	248.59	258.02
C3-3	1	P	49223.69	243.14	262.43
C3-3	1	P	64639.80	300.50	322.48
C3-3	2	P	19689.68	147.20	183.61
C3-3	2	P	11736.90	120.81	129.89
C3-3	2	P	18475.76	154.46	167.03
C3-3	2	P	33117.97	159.41	247.06
C3-3	2	P	22670.12	156.26	184.72
C3-3	2	P	17244.04	135.45	162.23
C3-3	3	MC	30228.47	170.90	207.36
C3-3	3	MC	40112.38	191.14	267.37
C3-3	3	MC	33685.63	237.59	192.20
C3-3	3	MC	22283.10	163.77	180.41
C3-3	5	E	29672.89	182.50	202.59
C3-3	5	E	30801.04	175.48	220.61
C3-3	5	E	22173.98	137.35	189.71
C4-3	1	P	31604.37	149.31	258.77
C4-3	1	P	26035.89	156.20	221.84
C4-3	2	P	21800.14	145.10	181.10
C4-3	2	P	23136.57	154.38	182.38
C4-3	4	MC	40418.93	208.41	259.55
C5-3	2	MC	49154.24	217.28	290.35
C5-3	2	MC	47414.03	233.81	239.36
C5-3	2	MC	29941.94	165.96	192.86
C5-3	3	P	41700.17	201.14	263.28
C5-3	4	MC	16085.04	128.12	167.56
C5-3	4	MC	22366.27	148.24	196.43
C5-3	4	MC	16667.97	121.48	173.60
C5-3	5	E	20424.33	156.96	168.83
C5-3	5	E	33705.76	170.95	216.57
C5-3	5	E	24785.21	165.56	193.68
C5-3	7	E	19451.15	142.44	179.82

P = Periosteal Region MC = Mid-Cortical Region E = Endosteal Region

P/MC = Image displaying section of Periosteal/Mid-Cortical Regions

Table C22 - Measurements of all Haversian canal parameters for cow samples at 1000^{o}C.

Specimen	Image Number	Cortical Region	Area (μm^2)	Min. Diameter (μm)	Max. Diameter (μm)
C1-3	3	MC	372.81	20.30	24.85
C1-3	3	MC	366.94	17.02	20.94
C1-3	5	E	1752.78	39.78	52.43
C1-3	5	E	455.97	23.19	26.10
C1-3	5	E	793.77	25.40	36.98
C1-3	5	E	726.84	28.41	34.29
C1-3	6	E	708.03	24.17	32.50
C1-3	6	E	636.70	23.58	34.51
C1-3	7	E	735.90	21.96	40.18
C1-3	7	E	275.34	13.91	22.91
C1-3	7	E	332.40	14.23	27.30
C1-3	7	E	207.54	14.23	21.29
C1-3	7	E	281.13	11.82	23.93
C2-3	1	P	695.77	22.77	36.63
C2-3	1	P	346.42	14.40	28.83
C2-3	3	P/MC	291.75	15.76	23.35
C2-3	3	P/MC	419.71	17.12	32.11
C3-3	1	P	1268.18	41.94	45.94
C3-3	1	P	420.34	17.19	20.40
C3-3	1	P	814.85	29.94	34.33
C3-3	2	P	375.64	20.90	27.84
C3-3	2	P	284.70	18.92	20.14
C3-3	2	P	775.01	30.50	34.58
C3-3	2	P	688.02	25.15	31.43
C3-3	2	P	373.67	19.50	22.26
C3-3	2	P	360.82	18.86	25.74
C3-3	3	MC	1221.12	33.42	45.66
C3-3	3	MC	1072.91	30.07	45.51
C3-3	3	MC	656.21	26.94	30.50
C3-3	3	MC	839.86	33.18	34.55
C3-3	5	E	816.45	33.33	32.60
C3-3	5	E	961.24	28.15	47.48
C3-3	5	E	377.06	18.30	26.68
C4-3	1	P	741.79	23.97	41.63
C4-3	1	P	666.14	23.38	28.96
C4-3	2	P	362.27	18.04	26.39
C4-3	2	P	507.59	19.47	31.22
C4-3	4	MC	670.01	27.18	34.53

C5-3	2	MC	1240.41	36.85	46.14
C5-3	2	MC	1104.61	35.50	40.26
C5-3	2	MC	817.60	28.89	36.89
C5-3	3	P	928.15	30.11	41.70
C5-3	4	MC	811.77	26.74	38.86
C5-3	4	MC	503.23	20.52	33.23
C5-3	4	MC	605.69	24.02	34.99
C5-3	5	E	862.24	27.07	43.87
C5-3	5	E	1697.89	35.36	62.33
C5-3	5	E	879.57	25.49	41.33
C5-3	7	E	212.28	15.04	19.58

P = Periosteal Region MC = Mid-Cortical Region E = Endosteal Region

P/MC = Image displaying section of Periosteal/Mid-Cortical Regions